CZECH TECHNICAL UNIVERSITY IN PRAGUE

FACULTY OF MECHANICAL ENGINEERING

12105 – DEPARTMENT OF MECHANICS, BIOMECHANICS AND MECHATRONICS

MASTER'S THESIS

2020

MEAN STRESS EFFECT ON THE S-N CURVE

VLIV STŘEDNÍHO NAPĚTÍ NA WÖHLEROVU KŘIVKU

AUTHOR: Bc. Matěj Mžourek

SUPERVISOR: Ing. Jan Papuga, Ph.D.

ZADÁNÍ DIPLOMOVÉ PRÁCE

I. OSOBNÍ A STUDIJNÍ ÚDAJE

Příjmení: **Mžourek** Jméno: **Matěj** Osobní číslo: **457579**

Fakulta/ústav: **Fakulta strojní**

Zadávající katedra/ústav: **Ústav mechaniky, biomechaniky a mechatroniky**

Studijní program: **Strojní inženýrství**

Studijní obor: **Aplikovaná mechanika**

II. ÚDAJE K DIPLOMOVÉ PRÁCI

Název diplomové práce:

VLIV STŘEDNÍHO NAPĚTÍ NA WÖHLEROVU KŘIVKU

Název diplomové práce anglicky:

MEAN STRESS EFFECT ON THE S-N CURVE

Pokyny pro vypracování:

Zahrnutí vlivu střední hodnoty napětí do odhadu životnosti má klíčový efekt, přesto se často vychází z metod definovaných před více jak stoletím.
* Provedení rešerše matematických modelů popisujících Wöhlerovu křivku materiálu se zohledněním střední hodnoty napětí cyklu. Popis jak celé křivky, tak změny polohy meze únavy. Vliv střední hodnoty napětí cyklu na počet kmitů na mezi únavy.
* Sběr experimentálních dat pro validaci jak z www.matigue.cz tak odjinud a jejich umístění do této databáze.
* Analýza vhodnosti jednotlivých metod se zohledněním kategorizace materiálů.
* Závěry

Seznam doporučené literatury:

[1] Dowling, N. E., Calhoun, C. A., Arcari, A.: Mean stress effects in stress-life fatigue and the Walker equation. Fat Fract Eng Mater Struct 32(3), 163-179 (2009).
[2] Papuga, J., Vízková, I., Lutovinov, M., Nesládek, M.: Mean stress effect in stress-life fa-tigue prediction re-evaluated. In: Hénaff, G. (ed.) MATEC Web of Conferences, Vol. 165.
[3] Anon. 2006. FEMFAT 4.4 Basic Theory Manual. Magna Steyr Engineering.

Jméno a pracoviště vedoucí(ho) diplomové práce:

Ing. Jan Papuga, Ph.D., odbor pružnosti a pevnosti FS

Jméno a pracoviště druhé(ho) vedoucí(ho) nebo konzultanta(ky) diplomové práce:

Datum zadání diplomové práce: **22.04.2020** Termín odevzdání diplomové práce: **07.08.2020**

Platnost zadání diplomové práce: _____

Ing. Jan Papuga, Ph.D.	doc. Ing. Miroslav Španiel, CSc.	prof. Ing. Michael Valášek, DrSc.
podpis vedoucí(ho) práce	podpis vedoucí(ho) ústavu/katedry	podpis děkana(ky)

III. PŘEVZETÍ ZADÁNÍ

Diplomant bere na vědomí, že je povinen vypracovat diplomovou práci samostatně, bez cizí pomoci, s výjimkou poskytnutých konzultací. Seznam použité literatury, jiných pramenů a jmen konzultantů je třeba uvést v diplomové práci.

Datum převzetí zadání _____ Podpis studenta _____

ANNOTATION LIST

Author:	Bc. Matěj Mžourek
Title of the thesis:	MEAN STRESS EFFECT ON THE S-N CURVE
Title of the thesis (Czech):	VLIV STŘEDNÍHO NAPĚTÍ NA WÖHLEROVU KŘIVKU
Year:	2019/2020
Field of study:	Applied Mechanics
Department:	Department of Mechanics, Biomechanics and Mechatronics
Master's thesis Supervisor:	Ing. Jan Papuga, Ph.D.

Bibliographic data:	number of pages	93
	number of figures	44
	number of tables	36

Keywords
material fatigue, mean stress effect, equivalent stress amplitude, reduced fatigue limit

Keywords (in Czech)
únava materiálu, vliv středního napětí, ekvivalentní amplituda napětí, redukovaná mez únavy

Abstract
The goal of this thesis is to analyze the accuracy of different approaches of fatigue life prediction that incorporate the influence of the mean stress effect. These approaches can be split into two categories - the equivalent stress amplitude approach and the reduced fatigue limit approach. Fatigue life prediction procedures are described in the theoretical part of the thesis, and their results for numerous experimental data sets are analyzed in the practical part.

Abstract (in Czech)
Cílem práce je zanalyzovat přesnost různých přístupů k predikci únavového života zahrnujících vliv středního napětí. Tyto přístupy lze rozdělit na dvě kategorie – přístup přes ekvivalentní amplitudu napětí a přístup přes redukovanou mez únavy. Aparáty pro predikci únavového života jsou popsány v teoretické části práce, a jejich výsledky pro řadu datových setů jsou analyzovány v praktické části.

DECLARATION

I declare that this thesis is my own work supervised by Ing. Jan Papuga, Ph.D. and supported by the sources listed as references.

In Prague 9. 8. 2020 …….

Matěj Mžourek

ACKNOWLEDGEMENT

I would like to thank my entire family, all my close friends, girlfriend Gabriela, supervisor Jan Papuga and Richard D. James for all the support that made the time spent writing this thesis so much more bearable.

Table of contents

NOMENCLATURE

A	[MPa]	Coefficient of the Kohout-Věchet S-N curve model
b	[-]	Fatigue strength exponent of the Basquin S-N curve model
B	[-]	Coefficient of the Kohout-Věchet S-N curve model
C	[-]	Coefficient of the Kohout-Věchet S-N curve model
C_0	[MPa^W]	Coefficient of the (R = 0) curve according to the power law model
C_{-1}	[MPa^W]	Coefficient of the (R = -1) curve according to the power law model
k_B	[-]	Coefficient of the Bergmann model
M	[MPa]	Coefficient used in many optimized equivalent stress amplitude and reduced fatigue limit models
N	[-]	Fatigue life
N_{FL}	[-]	Fatigue life corresponding to the fatigue limit
p	[-]	Coefficient of the Klubberg model
R	[-]	Stress ratio
R^2	[-]	Coefficient of determination
s	[-]	Standard deviation
W_0	[-]	Exponent of the (R = 0) curve according to the power law model
W_{-1}	[-]	Exponent of the (R = -1) curve according to the power law model
α	[-]	coefficient of the Kwofie model
β	[-]	Coefficient of the Kohout-Věchet S-N curve model
γ	[-]	Coefficient of the Walker model
Δ_{FL}	[-]	Relative fatigue life error
$\Delta\sigma$	[MPa]	Stress range
σ_a	[MPa]	Stress amplitude
$\sigma_{a,eq}$	[MPa]	Equivalent stress amplitude
σ_f'	[MPa]	Fatigue strength coefficient of the Basquin S-N curve model
$\sigma_{FL,red}$	[MPa]	Reduced fatigue limit
σ_{FL0}	[MPa]	Fatigue limit of the (R = 0) curve
σ_{FL-1}	[MPa]	Fatigue limit of the (R = -1) curve
σ_{FS}	[MPa]	Fatigue strength corresponding to a certain fatigue life
σ_m	[MPa]	Mean stress
σ_m^*	[MPa]	Value of mean stress used to define intervals in the reduced fatigue limit model according to FEMFAT
σ_m^+	[MPa]	Value of mean stress used to define intervals in the reduced fatigue limit model according to Haibach
σ_{max}	[MPa]	Maximum stress
σ_{min}	[MPa]	Minimum stress
R_e	[MPa]	Yield strength
R_m	[MPa]	Ultimate tensile strength

1. THEORETICAL PART

1.1 Introduction to fatigue

Fatigue of materials is the process of gradual degradation of the material when exposed to a load that varies in time, and is lower than the static strength of the material [17]. This happens due to cracks that initialize and propagate through the component during loading. An accurate description of the loading process is necessary as a foundation to life prediction, or in other words, to the duration the component is able to withstand loading without failing. Accurate predictions of the fatigue life of a component or of a structure are the main goals of fatigue analysis.

The area of concern of this thesis is restricted to harmonic loading with uniaxial stress, where the stress amplitude and mean stress remain constant throughout time – see Figure 1. This kind of loading is quite simple to describe, and the common notation has been established and widely adopted.

σ_m – Mean stress

σ_a – Stress amplitude

σ_{min} – Maximum stress

σ_{max} – Minimum stress

$\Delta\sigma$ – Stress range

R – Stress ratio (= $\sigma_{min}/\sigma_{max}$) - see Figure 2

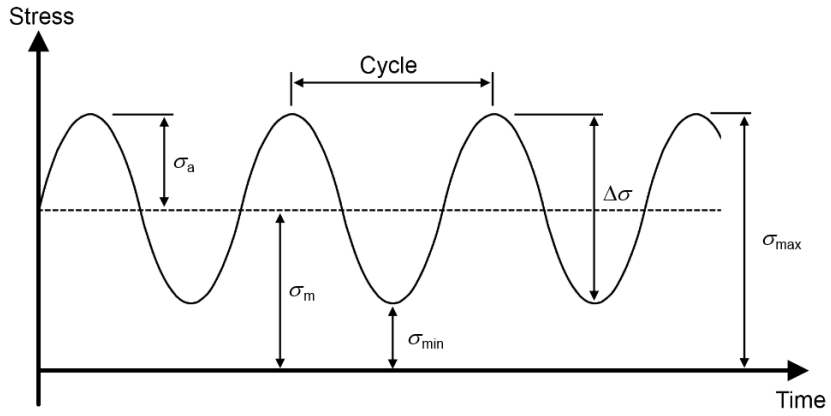

Figure 1 – Key features of harmonic loading [23]

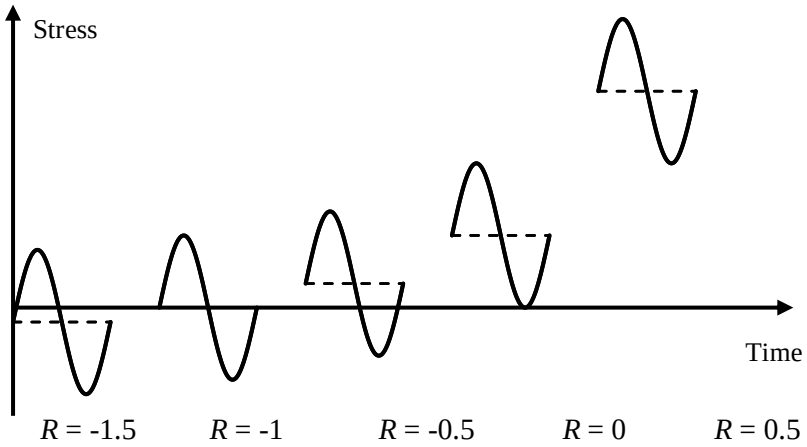

Figure 2 – The effect of stress ratio R on the position of the load cycle. σ_a is constant.

The stress cycle can be described using a combination of any two of the previously described parameters. Here are some useful relations between these:

$$\begin{aligned} &\text{a)} \quad \sigma_{max} = \sigma_m + \sigma_a \\ &\text{b)} \quad \sigma_{min} = \sigma_m - \sigma_a \\ &\text{c)} \quad \Delta\sigma = \sigma_{max} - \sigma_{min} \\ &\text{d)} \quad \frac{\sigma_a}{\sigma_m} = \frac{1-R}{1+R} \end{aligned} \tag{1}$$

In this thesis, compressive (push) stress will be regarded as negative, and tensile (pull) stress as positive.

1.2 S-N Curves

S-N (= stress - life) curves, also known as Wöhler curves, after August Wöhler (1819-1914), are widely used as a method of representation of experimental fatigue data. They are visually easy to read, which is quite useful, as they allow quick (although subjective) judgement of the usability, area of validity and potential shortcomings of the presented data.

An S-N curve is a type of graph, where the vertical axis is related to the magnitude of the cyclic load carried by a specimen. In this thesis, because all the experimental data used contains constant amplitude loading, the vertical axis of the S-N curves will be related to σ_a [MPa], though other metrics, such as σ_{max} are often used as well. Both logarithmic and linear scales are used for the vertical axis. Other units such as ksi (kilopounds per square inch) or psi (pounds per square inch) can sometimes be encountered, especially in older articles.

The horizontal axis is related to the fatigue life, typically in the number of unitless cycles N [-] before some type of end criterion has been met. This criterion may be e.g. a complete failure of the specimen (the crack propagates through the entire cross-section of the specimen), a crack of certain length being formed or a drop of the natural frequency of the specimen below some threshold due to loss of stiffness because of crack growth. A load cycle consists of two stress half cycles, which are symmetrical in regard to mean stress σ_m. This is quite well-established today, though historically, a cycle was often understood to consist of a single stress half cycle. It is quite important therefore, when dealing with adapted data, to pay attention to how the fatigue life N was measured/calculated, in order to avoid doubling or halving the values.

A logarithmic scale is used for this axis, as the experimental values of N are typically spread across several orders of magnitude. Using a linear scale causes the points in the graph to be "squished", making the graph difficult to read. Another reason for the logarithmic scale is that the experimental data tend to show that the relation between the magnitude of the load stress and fatigue life has a linear trend, when $\log_{10}(N)$ is used as the dependent variable instead of just N.

Because fatigue life N is spread out across more orders of magnitude than stress metrics, and because reading the errors in life prediction N visually from the graph is often more desirable than reading the errors in stress magnitude, the independent variable, stress magnitude, is displayed on the vertical axis, while the dependent variable, fatigue life N, is displayed on the horizontal axis. This means the axis are swapped as opposed to the usual, unwritten norm of displaying experimental data in most fields.
The following graphs show an example of data that form an S-N curve. The mean stress is equal to zero, the data is taken from the BaB data set (data sets are described in 2.3) The graphs display the same data, the upper one uses a logarithmic scale for the horizontal axis, while the lower one uses a linear one. Both vertical scales of the axis are linear. The failure criterion in this case is a complete break of the specimen.

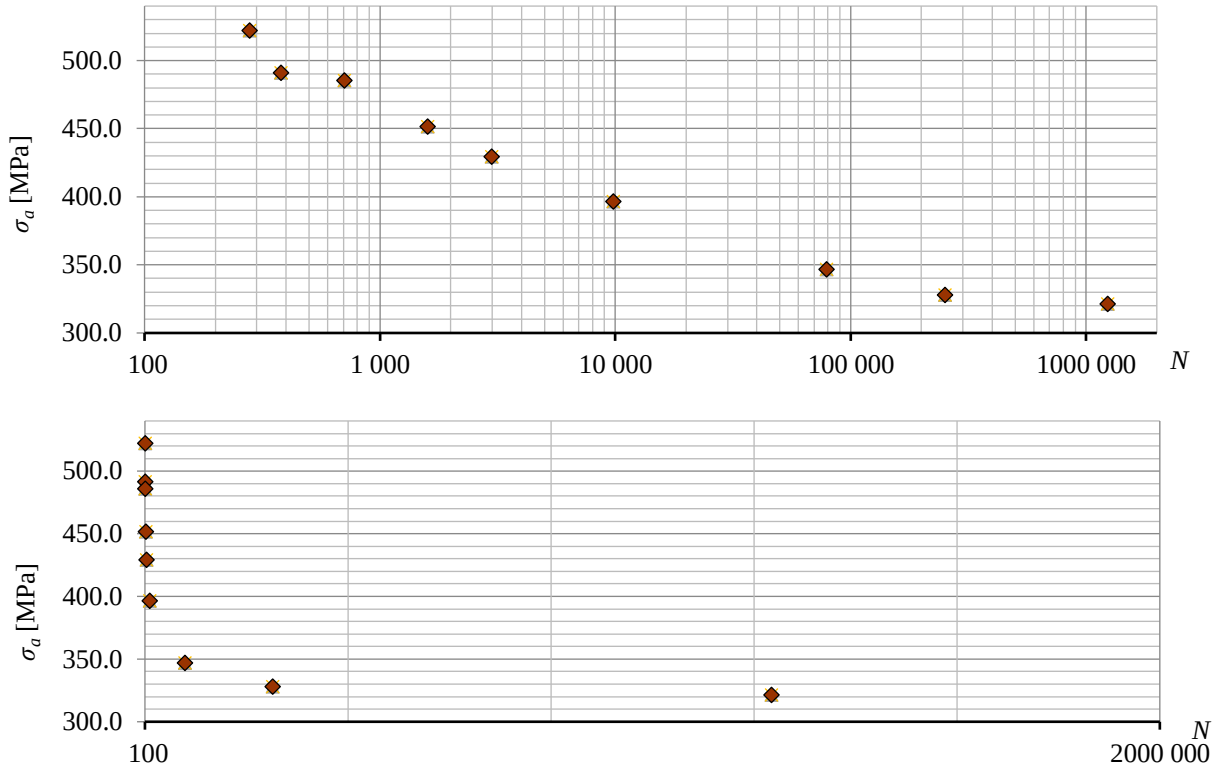

Figure 3 – An example of data forming an S-N curve, taken from the BaB dataset [3]

In order to predict life for different stress levels using experimental data such as shown above, mathematical descriptions of the S-N curves are utilized. These descriptions usually contain some parameters, which are optimized using software tools in order to best fit the supplied experimental data. The fit function is usually minimizing the sum of square errors of $\log_{10}(N)$. A typical example of such model is the Basquin curve [18]:

$$\sigma_a = \sigma_f' \cdot (2N)^b. \quad (2)$$

It conveniently becomes linear in regard to the logarithms of the stress and life quantities when logarithms are applied:

$$\log_{10}(\sigma_a) = \log_{10}(\sigma_f') + b \cdot \log_{10}(2N). \quad (3)$$

σ_f' and b are the constants acquired via fitting the function onto experimental data.

Another typical curve model [18] is the power law model (4), which is equivalent to the Basquin curve.

$$N \cdot \sigma^W = C \quad (4)$$

The power law model will often be used to describe S-N curves in this thesis, and the lower index of the fitting constants C and W will mark the stress ratio of the S-N curve corresponding to these constants, for example, W_0 corresponds to the power law model fit of the (R = 0) curve.

The Wöhler curve can be divided into several domains. Figure 4 shows an established idea of the form of the S-N curve for metals.

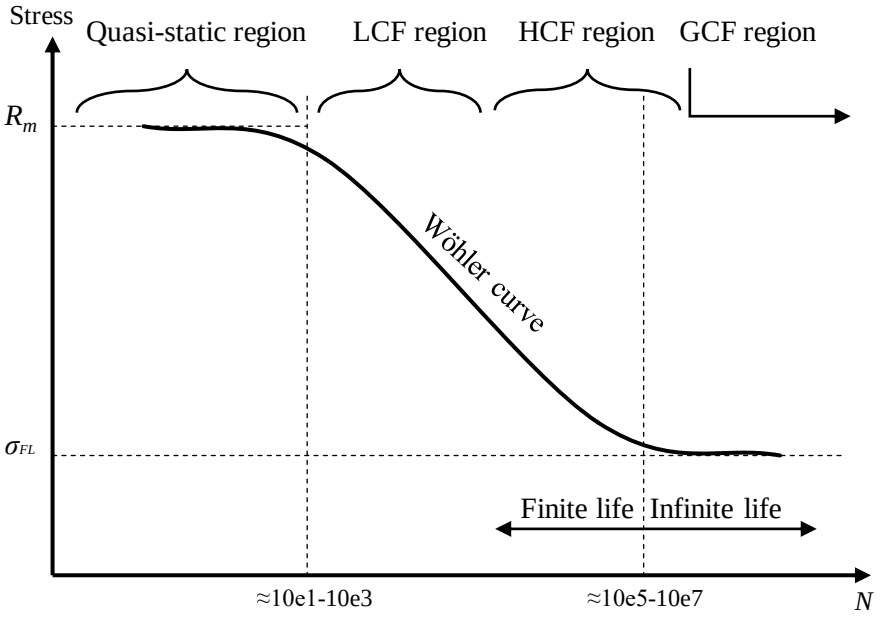

Figure 4 – Wöhler curve

In the lower life domain lies the quasi-static region, where the S-N curve is formed by a nearly horizontal line. It can be argued that in this domain, fatigue of material in the traditional sense does not take place, as the fundamental principle of fatigue, gradual degradation due to cyclic loading of lower magnitude than the static strength of the material [17], is not present. Instead, the rate of the crack growth is quite rapid, causing the specimen to fail completely in the first single or the next several loading cycles [18]. The crack surface of the broken specimen usually shows signs of ductile rather than brittle fracturing, the latter being typical for fatigue. This is due to the propagation mechanism of the crack during cyclic loading. The crack tip acts as a kind of notch, which causes stress to locally concentrate, which means the stress near the notch tip is greater than the nominal stress in the cross-section of the macroscopically smooth specimen. This concentrated stress, when greater than the materials yield strength R_e, causes local plastic deformation at the notch tip. This plastic deformation eventually spreads through the specimen through crack propagation. This part of the S-N curve is usually vertically constrained by the ultimate tensile strength R_m.

After the nearly horizontal part of the S-N curve, $\log_{10}(N)$ starts to increase approximately linearly with the decrease of stress magnitude. This part of the curve is the most well described, as it is of large importance for practical applications. Experiments have shown that this part of the curve is not necessarily continuous, which is why it is often further divided into two regions – the low cycle fatigue (LCF) region, and the high cycle fatigue (HCF) region. The border between these two regions is usually not clearly distinguishable, which is why it is not strictly given. The cause of the discontinuity is due to the fact that in LCF, the fatigue life is crack propagation-dominated, which is a largely deterministic process, while HCF is crack initialization-dominated, which is a process that is more stochastic [17]. This is also why experimental data in the lower stress levels tend to show much more scatter, as opposed to the data from experiments in the higher stress levels. Due to undetectable defects of the test specimen and other, quite random and unobservable factors, some experiments on specimens being tested on a certain stress level might fall into the LCF category, while the same experiments on other specimen on the same stress level may fall in the HCF category. Thus, the discontinuity is introduced. Nevertheless, LCF and HCF regions can be very often indistinguishable, and the entire midsection curve may be quite smooth.

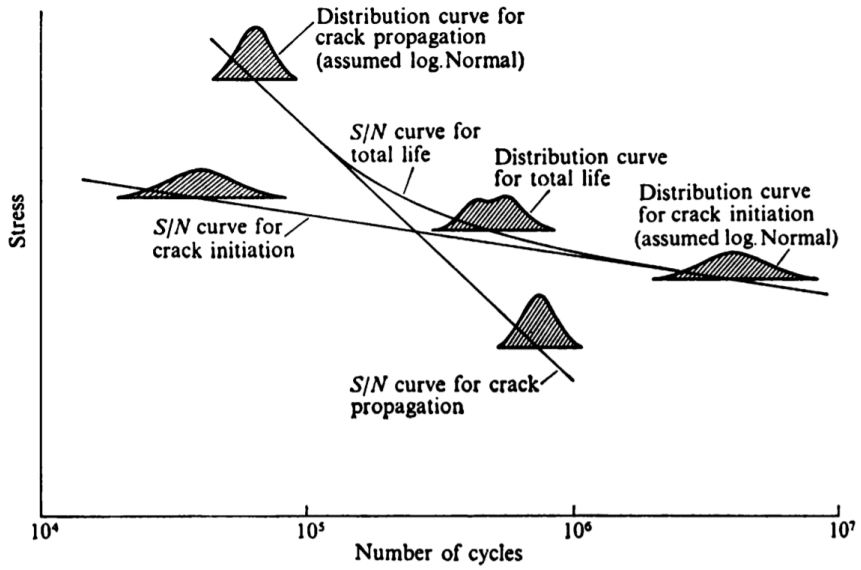

Figure 5 - Distributions of experimental data [17]

A second, nearly horizontal part of the S-N curve follows after the HCF region, which transitions into the gigacycle fatigue region (GCF). Failure due to fatigue still occurs in this region, but the lifetimes often exceed realistic use time of the component. Thus, for many applications, the idea of infinite life of components under cyclic loads beneath σ_{FL} can be acceptable.

1.3 Mean stress effect

When the harmonic cyclic load is not symmetrical with regard to the horizontal axis, in other words, the stress ratio $R \neq$ -1, mean stress is present. This results in the mean stress effect (MSE) affecting the fatigue life of the specimen (or component, structure…).

When R = -1, the crack is forced to close during the compressive half of the load cycle, and residual stresses introduced during the tensile half of the load cycle are lowered, which causes the crack to propagate less rapidly. Introducing positive mean stress to the load cycle causes this mitigating factor of the compressive load to become less pronounced, which causes a decrease in fatigue life. Conversely, negative mean stress can under certain circumstances cause an increase in fatigue life, but this phenomenon, along with negative mean stress in general, is outside the scope of this thesis. Due to an insufficient amount of acquired data, this thesis will not delve into the effects of negative mean stress, in other words, only the $R \in < -1; 1)$ region will be analyzed.

How much influence mean stress effect has on fatigue life differ across various materials, component geometries, etc. In this thesis, experiments on plain, unnotched specimens of different materials will be analyzed.

In order to visualize this influence, the Haigh diagram is often used. The vertical axis of a Haigh diagram corresponds to the stress amplitude σ_a, while the horizontal axis to mean stress σ_m. Lines of constant fatigue life are plotted. The lower the slope is (= the closer the line is to being parallel with the horizontal axis), the less is the specimen/component/structure sensitive to mean stress. As different cases show a different response to the presence of mean stress, a large quantity of theoretical models of these lines in the Haigh diagram have been proposed. For an illustration of the large variety, the following figure shows a Haigh diagram with a number of these models plotted. All of these models either utilize material constants, parameters acquired via fitting, empirical constants, or their combinations. Perhaps the only connecting trend between all these different methods, is that mean stress does cause fatigue life to decrease for identical stress amplitude.

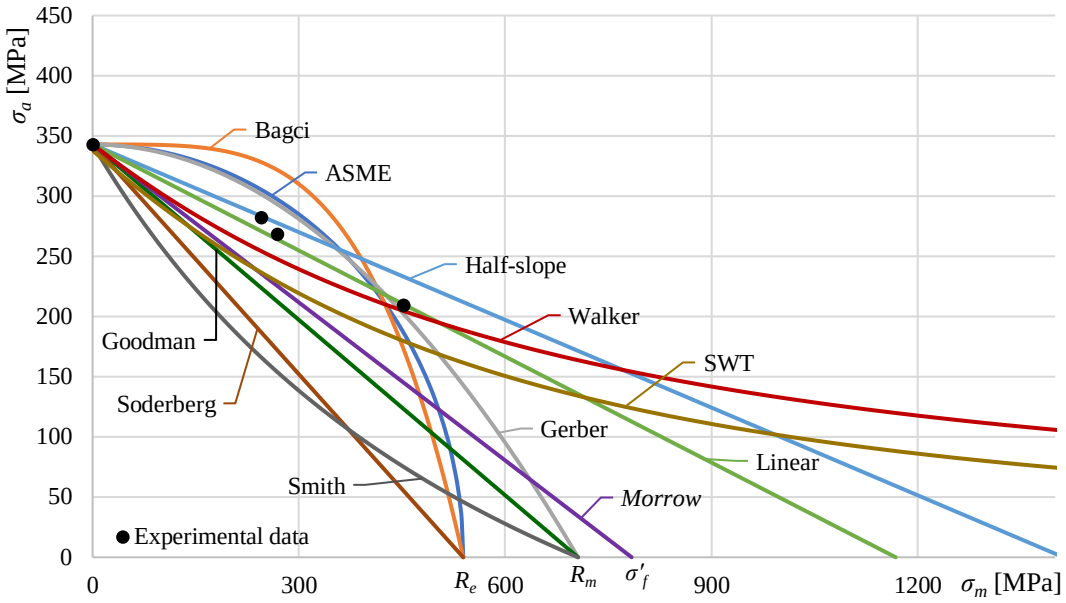

Figure 6 - visualization of some of the different mean stress effect quantifying methods in the Haigh diagram [20]

Equivalent stress amplitude approach

Historically, fatigue testing equipment has not been always able to introduce mean stress into the tested specimens. For a long time, and even today, uniaxial fatigue tests with no mean stress present on polished, unnotched specimens have been understood as the most "basic" form of fatigue experiment, thus, they have been used to map fatigue properties of many materials. These kinds of tests result in the creation of an S-N curve for a particular batch of specimens, thus generating some form of the following function:

$$N = N(\sigma_a) \tag{5}$$

A typical and quite commonly utilized method of life prediction while taking mean stress effect into account is the equivalent stress amplitude (ESA) approach. It introduces the equivalent stress amplitude $\sigma_{a,eq}$, which is calculated from the mean stress and amplitude of the load cycle. The idea of the equivalent stress approach is, that a single load cycle with zero mean stress and $\sigma_{a,eq}$ stress amplitude will cause the same amount of damage, as a single load cycle of mean stress σ_m and stress amplitude σ_a.

$$\sigma_{a,eq} = \sigma_{a,eq}(\sigma_a, \sigma_m) \tag{6}$$

Thus, the zero mean stress curve can be rewritten in the form (7), to incorporate mean stress effect into the life prediction

$$N = N(\sigma_a) \xrightarrow{ESA\ approach} N = N(\sigma_{a,eq}) \tag{7}$$

Many hypotheses for calculating the equivalent stress amplitude $\sigma_{a,eq}$ exist, and one of the goals of this thesis is to evaluate their ability to predict fatigue life while taking the mean stress effect into account using a large amount of experimental data. The experimental data used for these analyses is not a product of the author and are outsourced from prior available works. More on data acquisition in chapter 2.1.

Reduced fatigue limit approach

The reduced fatigue limit approach (RFL), similarly to ESA, can be employed in order to utilize the basic fatigue curve, meaning a curve where zero mean stress is present, in order to perform fatigue life

predictions for load cases with non-zero mean stress. The RFL approach is based on the idea that the fatigue limit of curves of mean stress greater than zero is lower than the fatigue limit of the curve with zero mean stress σ_{FL-1}. This new fatigue limit is called the reduced fatigue limit $\sigma_{FL,red}$, and as with the equivalent stress approach, many models for calculating it exist.

$$\sigma_{FL,red} = \sigma_{FL,red}(\sigma_{FL-1}, \sigma_m) \quad (8)$$

To predict fatigue life, the basic fatigue curve is shifted accordingly to the calculated $\sigma_{FL,red}$. Thus, the RFL approach allows to construct a new fatigue curve for each level of mean stress. From these curves, fatigue life can be predicted for the corresponding stress amplitudes.

In order to utilize the RFL approach, the user needs to extract more information from the basic zero stress curve in comparison with the ESA approach. The ESA approach really only requires the two coefficients of the S-N curve model, C and W of the power law model, for example. The reduced fatigue limit approach requires the same, as well as the fatigue limit of the (R = -1) curve σ_{FL-1} and the fatigue life N_{FL} corresponding to this stress value (though, one can be calculated from the other). The acquisition of these two new required values often lays more weight on the user, as their determination tends to be more subjective compared to identification of the coefficients of the Basquin curve. Overall, the RFL approach tends to be more convoluted and more difficult to grasp and realize compared to the ESA approach. The RFL approach is also not documented as well as the ESA approach, and is definitely less run-in, meaning some of the steps of the calculations can be adopted in different way by different users.

The approach in this thesis is based on information found in [21] and is visualized in Figure 7. Note that both axes are logarithmic, and intercept is located at [1;1]. Two points have to be defined to obtain the basic curve (σ_m = 0), the fatigue limit σ_{FL-1} and the corresponding fatigue life N_{FL}, as well as the fatigue life $N(R_m)$ that theoretically corresponds to a load amplitude equal to the ultimate tensile strength R_m. The latter can be obtained simply by calculating the fatigue life from the Basquin curve model (2) or the power law model (4), where $\sigma_a = R_m$.

In this thesis, the [N_{FL}; σ_{FL-1}] point is found through a visual inspection of plotted experimental data, where an approximate value of the fatigue life N_{FL} corresponding to the fatigue limit is chosen. The fatigue limit σ_{FL-1} itself is then found, again, from the Basquin or power law curve model, where $N = N_{FL}$.

Note that ideally, a bend resulting in a nearly horizontal part of the S-N curve (as shown in the transition region from the high cycle to giga cycle fatigue region in Figure 4) is not necessarily captured by the available experimental data. In such cases, the value of N_{FL} is chosen slightly higher than the largest measured fatigue life of the valid points forming the linear part of the curve. One could argue that this fatigue life N_{FL} and its corresponding stress amplitude σ_{FL-1} do not actually represent the fatigue limit. In such cases, it would be correct to refer to the stress amplitude as a fatigue strength corresponding to a certain fatigue life value rather than fatigue limit. However, to keep the nomenclature as simple and unified as possible, the N_{FL} and σ_{FL-1} notation will be kept, even if this is not strictly correct in said cases.

In order to obtain a curve for a load case where positive mean stress is present (σ_m > 0), two points on the original curve are shifted – see the two arrows in Figure 7. The fatigue life $N(R_m)$ gets shifted down along a straight line connecting [$N(R_m)$; R_m] and [1; 1] to a new stress amplitude level $\sigma_a = R_m - \sigma_m$, while the point [$N_{FL}$; σ_{FL-1}] is moved vertically to [N_{FL}; $\sigma_{FL,red}$]. Different models for calculating $\sigma_{FL,red}$ used in this thesis are shown in 1.7. Note that some of these models can impose further requirements on the input data in order to perform life predictions, such as the Linear model which also requires a defined (R = 0) curve before life predictions can be made.

Now that the curve for the corresponding mean stress level is defined, a life prediction can be made by finding the fatigue life $N(\sigma_a, \sigma_m)$ that corresponds to the stress amplitude level σ_a on this new curve.

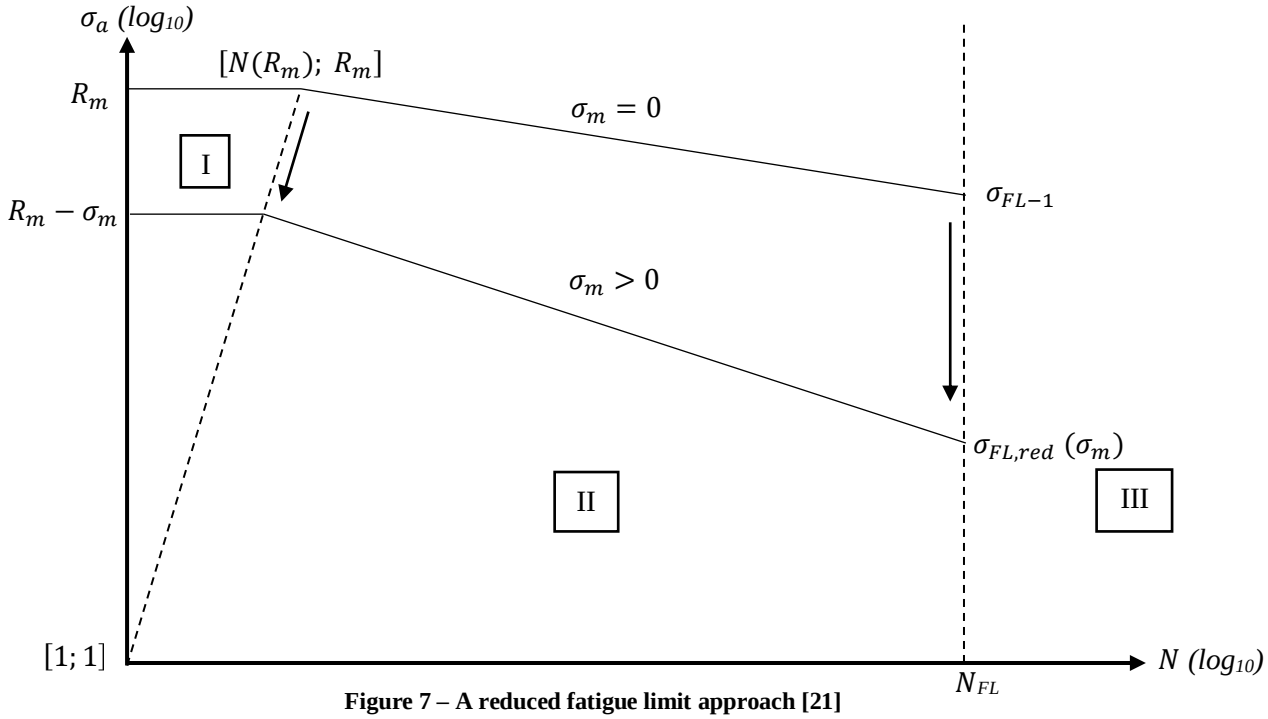

Figure 7 – A reduced fatigue limit approach [21]
I – quasi-static region, II – low to high cycle region, III – theoretical infinite life region

In [21], the predicted fatigue life is further decreased through reduction of the fatigue life N_{FL}. This reduction is based on the ratio of the original and reduced fatigue limits of the ($\sigma_m = 0$) and corresponding ($\sigma_m > 0$) curves. This is described in 1.8 - FEMFAT shift.

1.4 Statistical aspects of fatigue

There are many factors affecting fatigue life, many of which are not quantified or measured in any accurate way, thus making them ineliminable. These factors bring certain degree of randomness to the material fatigue process. This is even more pronounced when fatigue is taken out of laboratory conditions and is observed in real components and structures.

Experimental fatigue data is generally subject to a certain amount of scatter, and experimentally acquired values will never completely conform to an ideal S-N curve, such as the one shown in Figure 4 (unless the experiment was performed on too few specimens, which makes the usability of such data questionable). For this reason, some basic statistical knowledge should be utilized when asserting predictions based on experimental fatigue data. Not doing so may result in the predictions being based on insufficiently informative data.

In practice, the results may then be too conservative, meaning, for example, that components produced based on these predictions are oversized. On the other end of the spectrum, the results can be unconservative, meaning the strength of the produced components is insufficient for the application, which can result in anything from a financial loss to lethal injuries.

For illustration of this typical phenomenon in material fatigue, observe Figure 8. It shows stress – life data obtained experimentally. The end criterion in this case is for the specimen to break completely. The stress ratio R is 0.02, in other words, the mean stress $\sigma_m = 1.041 \cdot \sigma_a$. For the 5 specimens which were subjected to a stress amplitude σ_a of roughly 128 MPa, the fatigue life values are spread across nearly two orders of magnitude, which demonstrates that using a sparse dataset to make fatigue life predictions may be quite unsubstantiated.

Also, say that only the data points of $\sigma_a < 160$ MPa are available. This would drastically change the line obtained via fitting the, for example, power law model (4).

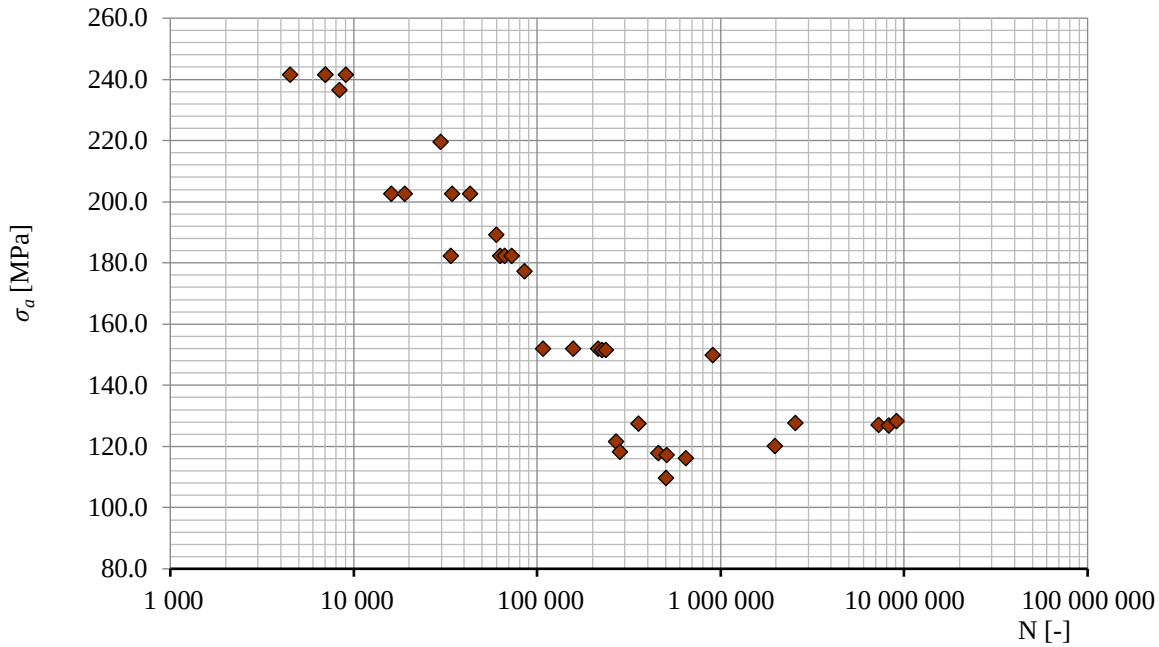

Figure 8 – An example of experimental fatigue data with visible scatter, taken from the GBA set.

In order to quantify the amount of data scatter, standard deviation *s* will be used:

$$s = \sqrt{\frac{1}{N-1}\sum_{i=1}^{N}(x_i - \bar{x})^2}\,, \tag{9}$$

where N is the total number of values, x_i is the i-th value, and $\bar{x}$ is the mean value. For illustration, figure 9 shows the Gauss distribution of several values of s. The higher *s* gets, the more spread out the probability density function *f(x)* becomes.

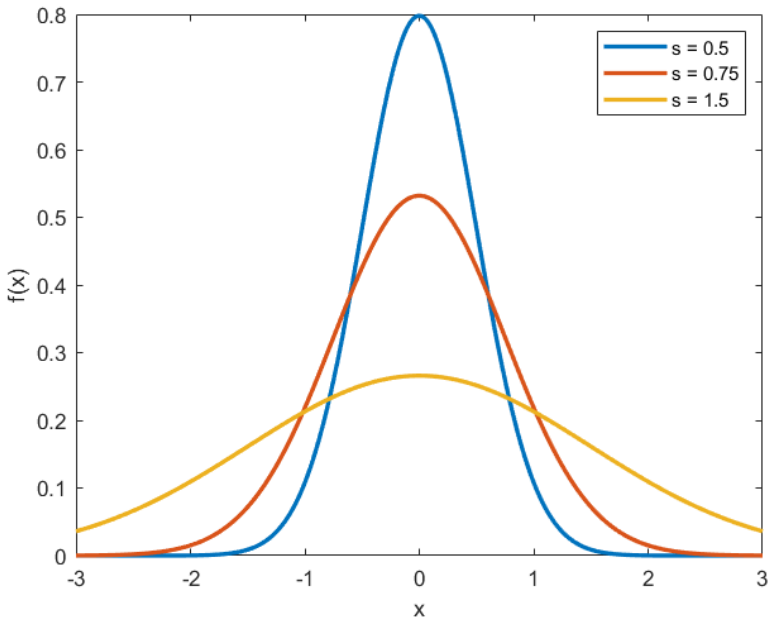

Figure 9 – Effect of standard deviation *s* on the Gauss distribution.

1.5 Transforming models between the equivalent stress and reduced fatigue limit approaches

Most equivalent stress amplitude approach models can be simply transformed into a reduced fatigue limit approach model and vice versa. This can be done by substituting two variables in an equivalent stress / reduced fatigue limit expression with their respective counterparts and solving the new equation for the required variable.

Since the fatigue limits σ_{FL} are in this thesis defined for the same fatigue life N_{FL}, an equivalent stress amplitude (with zero mean stress) to a stress amplitude (with non-zero mean stress) the size of fatigue limit of any curve is the fatigue limit of the (R = -1) curve $\sigma_{FL\text{-}1}$. The fatigue life N_{FL} on any curve generated through the reduced fatigue limit approach corresponds to the stress amplitude σ_a of the size $\sigma_{FL,red}$ (which corresponds to the mean stress of the curve). Thus, substitutions (10) can be performed in order to transform models designed for one approach for use with the other.

$$\sigma_{FL,red} == \sigma_a$$

$$\sigma_{FL-1} == \sigma_{a,eq} \quad \textbf{(10)}$$

An example is given in (11), where the Goodman method is transformed from its equivalent stress amplitude form to the reduced fatigue limit form.

$$\sigma_{a,eq} = \frac{\sigma_a}{1-\frac{\sigma_m}{R_m}} \xrightarrow{substitution} \sigma_{FL-1} = \frac{\sigma_{FL,red}}{1-\frac{\sigma_m}{R_m}} \xrightarrow{solve\ for\ \sigma_{FL,red}} \sigma_{FL,red} = \sigma_{FL-1} \cdot \left(1-\frac{\sigma_m}{R_m}\right) \quad \textbf{(11)}$$

1.6 Equivalent stress amplitude models

In this chapter, the used equivalent stress amplitude models will be described. They are divided into two groups, based on whether they feature a parameter (or parameters) that need to be obtained through optimization. This list does not contain all the existing models.

Unoptimized models

Goodman

The Goodman method [22] utilizes the ultimate tensile strength R_m, though modified versions have been proposed to, for example, provide less conservative results [18].

$$\sigma_{a,eq} = \frac{\sigma_a}{1-\frac{\sigma_m}{R_m}} \quad \textbf{(12)}$$

It is one of the first proposed equivalent stress amplitude models and is still widely used today.

Gerber

Similar to the Goodman method is the approach of Gerber [23]. The Gerber parabola provides less conservative results than the Goodman method. The real material response often lies between these two methods, thus they are sometimes used to gain the upper and lower bound of the problem.

$$\sigma_{a,eq} = \frac{\sigma_a}{1-\left(\frac{\sigma_m}{R_m}\right)^2} \quad \textbf{(13)}$$

Dietmann

For tensile stresses, this method [24] forms a similar curve to the Gerber parabola in the Haigh diagram. Like the Gerber method, it is also less conservative than the approach of Goodman.

$$\sigma_{a,eq} = \frac{\sigma_a}{\sqrt{1 - \frac{\sigma_m}{R_m}}}$$

(14)

SWT

The SWT method, abbreviated from Smith, Watson and Topper [22], is interesting thanks to the fact that it features no material parameters, making it very simple to use.

$$\sigma_{a,eq} = \sqrt{(\sigma_a + \sigma_m) \cdot \sigma_a}$$

(15)

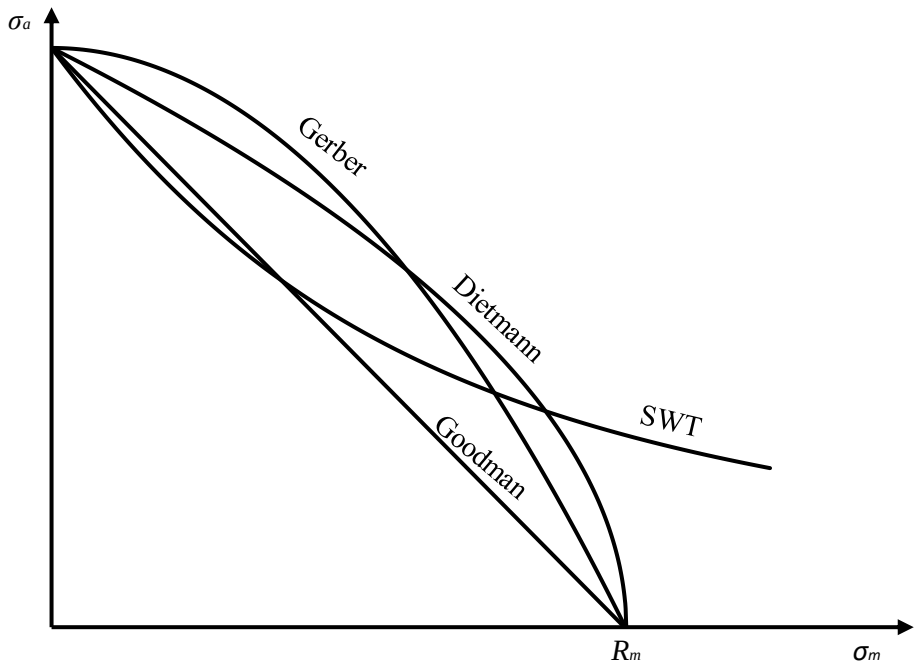

Figure 10 – Various Haigh diagrams according to the unoptimized equivalent stress amplitude models

Walker (unoptimized)

This method is based on the Walker method (16), which features an optimizable parameter γ. The original Walker method is described in 1.6 - Optimized models. The unoptimized version of the Walker method is based on determining γ from the (R = -1) and (R = 0) curves rather than from an optimization algorithm.

$$\sigma_{a,eq} = (\sigma_a + \sigma_m)^{1-\gamma} \cdot {\sigma_a}^{\gamma}$$

(16)

First, write the Walker equivalent stress amplitude $\sigma_{a,eq}$ equation (16) for an (R = 0) curve, in other words, for a ($\sigma_a = \sigma_m$) curve.

$$\sigma_{a,eq} = (\sigma_a + \sigma_m)^{1-\gamma} \cdot {\sigma_a}^{\gamma} \overset{R=0}{\longrightarrow} \sigma_{a,eq} = (\sigma_a + \sigma_a)^{1-\gamma} \cdot {\sigma_a}^{\gamma} = 2^{1-\gamma} \cdot \sigma_a$$

(17)

Now, define fatigue strengths for the (R = -1) and for the (R = 0) curves as stress amplitudes $\sigma_{FS,-1}$ and $\sigma_{FS,0}$ that correspond to the same fatigue life N, so that (16) can be rewritten as (17).

$$\sigma_{FS,-1} = 2^{1-\gamma} \cdot \sigma_{FS,0}$$

(18)

Solving (18) for γ yields (19).

$$\gamma = 1 - \frac{\log_{10} \frac{\sigma_{FS,-1}}{\sigma_{FS,0}}}{\log_{10} 2}$$

(19)

Using the power law model (4), we can write equations (20).

$$\sigma_{FS,-1} = \left(\frac{C_{-1}}{N}\right)^{W_{-1}}$$

$$\sigma_{FS,0} = \left(\frac{C_0}{N}\right)^{W_0}$$

(20)

Equations (19) and (20) yield (21), which shows that the coefficient γ for the unoptimized Walker method is actually a function of fatigue life N.

$$\gamma = 1 - \frac{\log_{10}\left(\left(\frac{C_{-1}}{N}\right)^{W_{-1}}\right) - \log_{10}\left(\left(\frac{C_0}{N}\right)^{W_0}\right)}{\log_{10} 2}$$

(21)

Equation (21) can be rewritten into (22), which shows that the coefficient γ is actually a linear function in regard to $\log_{10} N$ and the C and W power law model coefficients.

$$\gamma = \gamma_a + \gamma_b \cdot \log_{10} N$$

$$where$$

$$\gamma_a = 1 - \frac{\log_{10} C_{-1}}{W_{-1} \cdot \log_{10} 2} + \frac{\log_{10} C_0}{W_0 \cdot \log_{10} 2}$$

$$and$$

$$\gamma_b = \frac{1}{W_{-1} \cdot \log_{10} 2} - \frac{1}{W_0 \cdot \log_{10} 2}$$

(22)

Now, rewrite the power law model (4) for the (R = -1) curve, and instead of a generic stress amplitude σ_a, use the equivalent stress amplitude $\sigma_{a,eq}$ according to Walker (16). This yields (23).

$$\left(\frac{C_{-1}}{N}\right)^{\frac{1}{W_{-1}}} = (\sigma_a + \sigma_m)^{1-\gamma} \cdot {\sigma_a}^{\gamma}$$

(23)

Using γ from (22) in (23), we get (24).

$$\left(\frac{C_{-1}}{N}\right)^{\frac{1}{W_{-1}}} = (\sigma_a + \sigma_m)^{1-\gamma_a+\gamma_b \cdot \log_{10} N} \cdot {\sigma_a}^{\gamma_a+\gamma_b \cdot \log_{10} N}$$

(24)

Equation (24) can be solved for $\log_{10} N$, as shown in (25). Thus, given that the power law model constants *C* and *W* for the (*R* = -1) and (*R* = 0) are known, a prediction of fatigue life *N* can be calculated for a given combination σ_a and σ_m. Note that if $\sigma_m = 0$ in (25), the equation becomes the power law model equation of the (*R* = -1) curve, and if $\sigma_m = \sigma_a$, it becomes the power law model equation of the (*R* = 0) curve.

$$\log_{10} N = \frac{\frac{\log_{10} C_{-1}}{W_{-1}} - \log_{10}(\sigma_a + \sigma_m) + \gamma_a \cdot \log_{10}(\sigma_a + \sigma_m) - \gamma_a \cdot \log_{10}(\sigma_a)}{\frac{1}{W_{-1}} - \gamma_b \cdot log(\sigma_a + \sigma_m) + \gamma_b \cdot log(\sigma_a)}$$

(25)

It is worth noting that equations analogical to (25) can be derived for combinations of other curves than just the (*R* = -1) and (*R* = 0) curves, however, this has been not explored in this thesis.

As γ is no longer a constant but rather a linear function of $\log_{10} N$, the unoptimized Walker model no longer necessarily creates a plane like the original Walker model does, see 1.6 - Optimized models, unless $W_{-1} = W_0$ (which means γ_b would become 0). Only if the value of γ_b, which depends on the power law model constants W_{-1} and W_0 of the (*R* = -1) and (*R* = 0), is equal to zero, the model is able to form a plane.

Linear (unoptimized)

In a similar fashion to the unoptimized Walker model, the unoptimized Linear model is based on its optimizable counterpart (26), see 1.6 - Optimized models, which is in turn based on the Goodman model from this chapter.

$$\sigma_{a,eq} = \frac{\sigma_a}{1 - \frac{\sigma_m}{M}}$$

(26)

Like in (19), the coefficient *M* of the optimized Linear model can be expressed from fatigue strengths from the (*R* = -1) and (*R* = 0) curves, see (27).

$$M = \frac{\sigma_{FS,0}}{1 - \frac{\sigma_{FS,0}}{\sigma_{FS,-1}}}$$

(27)

However, an expression similar to (25) cannot be written for the unoptimized Linear model, as $\log_{10} N$ can not be expressed from the final equation. Instead, an implicit equation (28) must be solved for a combination of σ_a and σ_m in order to gain a fatigue life prediction *N*. This can be done numerically, for example, using the *fzero()* function in MATLAB.

Other optimized models have been modified in a similar fashion in order to utilize the (*R* = -1) and (*R* = 0) curves, namely the Bergmann and Haibach models, which are also described in 1.6 - Optimized models. However, these also required an implicit equation to be solved in order to gain a fatigue life prediction *N*. Furthermore, these models were deemed more problematic for the numerical solver, as optimal solutions were often very difficult to find, and thus will not be discussed in this thesis.

$$0 = \left(\frac{C_{-1}}{N}\right)^{\frac{1}{W_{-1}}} - \frac{\sigma_a}{1 - \frac{\sigma_m}{L}}$$

$$where$$

$$L = \frac{\left(\frac{C_0}{N}\right)^{\frac{1}{W_0}}}{1 - \frac{\left(\frac{C_0}{N}\right)^{\frac{1}{W_0}}}{\left(\frac{C_{-1}}{N}\right)^{\frac{1}{W_{-1}}}}}$$

(28)

Optimized models

Walker

The Walker model (16) can be viewed as a generalization of the SWT model [22]. It includes the γ parameter, the value of which is obtained through optimization. The Walker model can form a plane [22] when employed with an S-N curve model like (2), thus, the coefficient γ can be obtained through a multiple linear regression. The lower the γ parameter is, the more sensitive the material is to mean stress.

Kwofie

Kwofie [23] utilizes an exponential function in order to calculate the equivalent stress amplitude $\sigma_{a,eq}$. The function relates the influence of mean stress to the ratio of the mean stress component of the load to the ultimate tensile strength R_m.

$$\sigma_{a,eq} = \sigma_a \cdot \exp\left(\alpha \frac{\sigma_m}{R_m}\right)$$

(29)

Coefficient α is acquired through fitting of experimental data. Kwofie notes [23] that $\alpha = 1$ provides a good fit for experimental data available in his work. Sensitivity to mean stress grows with α. Is is possible to rewrite (29) to not incorporate R_m, as it is not needed while performing the regression, see (30).

$$\sigma_{a,eq} = \sigma_a \cdot \exp(\tilde{\alpha} \cdot \sigma_m)$$

(30)

Bergmann

Similarly to the model proposed by Walker, the Bergmann [25] model can be viewed as a generalized SWT method. Equation (31) will become equation (15), if the fitting constant $k_B = 1$. The higher the k_B parameter is, the more sensitive the component is to mean stress.

$$\sigma_{a,eq} = \sqrt{(\sigma_a + k_B \cdot \sigma_m) \cdot \sigma_a}$$

(31)

Linear

The Linear model [20] is a straightforward generalization of the Goodman model. Numerous authors have proposed models that tweak the Goodman line, usually by replacing the ultimate tensile strength R_m in (12) with some other material or empirical constant in order to provide more accurate or less conservative results. The Linear model simply replaces the material constant R_m with the fitting constant M.

Gerber (optimized)

The Goodman model has been tweaked to be optimizable in the Linear method. The same principle, replacing the material parameter R_m with the fitting parameter M, can be applied in order to optimize the Gerber parabola.

$$\sigma_{a,eq} = \frac{\sigma_a}{1 - \left(\frac{\sigma_m}{M}\right)^2}$$

(32)

Dietmann (optimized)

An optimizable method that has been derived from (14) analogically to the optimized equivalent stress amplitude Linear and Gerber models.

$$\sigma_{a,eq} = \frac{\sigma_a}{\sqrt{1 - \frac{\sigma_m}{M}}}$$

(33)

Exponential

This model, based on [26], represents a further optimization of the Gerber method (13), allowing for the power law law in the expression to be fine-tuned. It is the only method on this list that has 2 optimizable parameters, which should result in more accurate results. This has a downside though, as the coefficients can become less predictable from other parameters, e.g. from ultimate tensile strength R_m or yield strength R_e.

$$\sigma_{a,eq} = \frac{\sigma_a}{1 - \left(\frac{\sigma_m}{M}\right)^p}$$

(34)

Klubberg

As experimental data often lies between the unoptimized Gerber and Goodman methods, it makes sense to devise an optimizable method that weighs these two methods, in this case, using the p parameter. Originally, this model [27] has been devised to calculate the reduced fatigue limit rather than the equivalent stress amplitude.

$$\sigma_{a,eq} = \frac{\sigma_a}{1 - p \cdot \left(\frac{\sigma_m}{R_m}\right) - (1 - p) \cdot \left(\frac{\sigma_m}{R_m}\right)^2}$$

(35)

Haibach

Similar to the method of Klubberg, the Haibach model [28] has been originally designed for calculating the reduced fatigue limit. A visual definition of the original model can be seen in 1.7. Nevertheless, it can be transformed into an equivalent stress amplitude model (36), see 1.5.

$$\begin{aligned}
\sigma_{a,eq} &= \sigma_a + \sigma_m \cdot M && \text{for} \quad R < 0 \\
\sigma_{a,eq} &= \left(\sigma_a + \sigma_m \cdot \frac{M}{3}\right) \cdot \frac{1 + M}{1 + \frac{M}{3}} && \text{for} \quad 0 \leq R < 0.5 \\
\sigma_{a,eq} &= \sigma_a \cdot \frac{(1 + M)^2}{1 + \frac{M}{3}} && \text{for} \quad R \geq 0.5
\end{aligned}$$

(36)

1.7 Reduced fatigue limit models

In this chapter, a list of reduced fatigue limit models used in this thesis is presented. As with 1.6, the models are divided into two groups – optimized and unoptimized models. Also, it is in no way a complete list of all available models, only of those used in this thesis.

All of these models share a common trait, for zero mean stress, $\sigma_{FL,red} = \sigma_{FL-1}$, which is of course a logical feature.

Unoptimized models

Goodman

The model is based on the idea that the fatigue limit is reduced linearly with the increase of σ_m [22], the slope being given by R_m. When the mean stress $\sigma_m = R_m$, the reduced fatigue limit $\sigma_{FL,red} = 0$, which can be interpreted in the following way: any stress amplitude present with such mean stress will exceed the strength of the component, which will cause said specimen to immediately fail.

$$\sigma_{FL,red} = \sigma_{FL-1} \cdot \left(1 - \frac{\sigma_m}{R_m}\right)$$

(37)

Gerber

Similar to Goodman's model, with the difference being that the reduction of fatigue limit with the increase of σ_m is no longer linear, but parabolical [23]. The reduced fatigue limit $\sigma_{FL,red}$ also becomes zero with $\sigma_m = R_m$. The Gerber method is less conservative than the Goodman method, as it results in greater reduced fatigue limits $\sigma_{FL,red}$ than the Goodman method would for identical mean stresses σ_m.

$$\sigma_{FL,red} = \sigma_{FL-1} \cdot \left(1 - \left(\frac{\sigma_m}{R_m}\right)^2\right)$$

(38)

Smith

This model [29], again like the Goodman and Gerber methods, yields zero reduced fatigue limit $\sigma_{FL,red}$ for mean stress $\sigma_m = R_m$, and is the most conservative out of the three, as it gives the lowest $\sigma_{FL,red}$ for any given σ_m (except for $\sigma_m = 0$ or R_m).

$$\sigma_{FL,red} = \sigma_{FL-1} \cdot \frac{1 - \frac{\sigma_m}{R_m}}{1 + \frac{\sigma_m}{R_m}}$$

(39)

Examples of the Haigh diagrams (or, the relation between $\sigma_{FL,red}$ and σ_m) according to the Goodman, Gerber and Smith methods are shown in Figure 11.

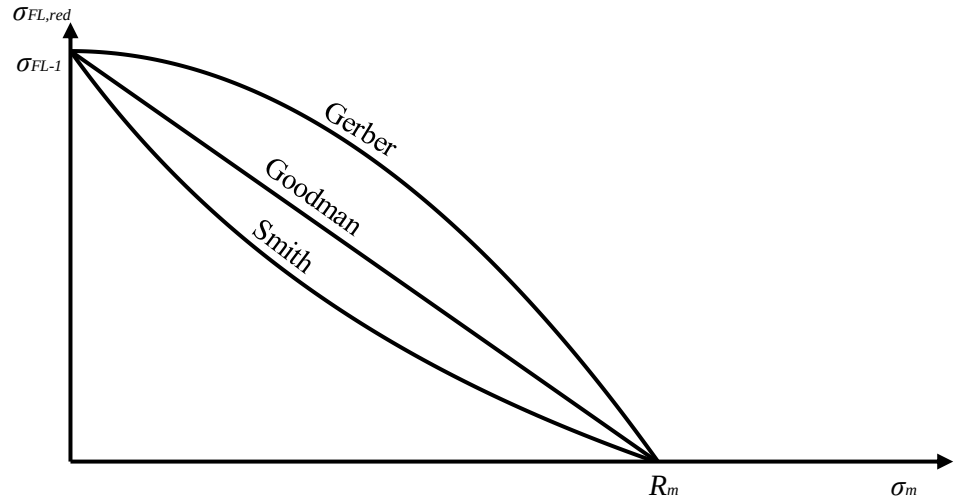

Figure 11 – examples of Haigh diagrams according to different reduced fatigue limit models

FEMFAT

More complex than the previously shown models is the method by FEMFAT [21]. The reduced fatigue limit $\sigma_{FL,red}$ function (40) is defined for positive as well as negative mean stresses, though only the former part will be shown here. The Haigh diagram is shown in Figure 12. This model not only requires the knowledge of the (R = -1) curve in order to calculate $\sigma_{FL,red}$, but also the (R = 0) curve, as it utilizes its corresponding fatigue limit σ_{FL0}. Unlike previously shown models, this one also requires a second material parameter, the yield strength R_e, as well as the common ultimate tensile strength R_m.

$$for\ \sigma_m\ \in < 0; \sigma_m^*)$$

$$\sigma_{FL,red} = \sigma_{FL-1} - \sigma_m \cdot \frac{\sigma_{FL-1} - \sigma_{FL0}}{\sigma_{FL0}}$$

$$for\ \sigma_m\ \in < \sigma_m^*; R_m >$$

$$\sigma_{FL,red} = (R_e - \sigma_m^*) - (\sigma_m - \sigma_m^*) \cdot \frac{R_e - \sigma_m^*}{R_m - \sigma_m^*}$$

$$where$$

$$\sigma_m^* = (\sigma_{FL-1} - R_e) \cdot \left(\frac{\sigma_{FL-1} - 2 \cdot \sigma_{FL0}}{\sigma_{FL0}}\right)^{-1}$$

(40)

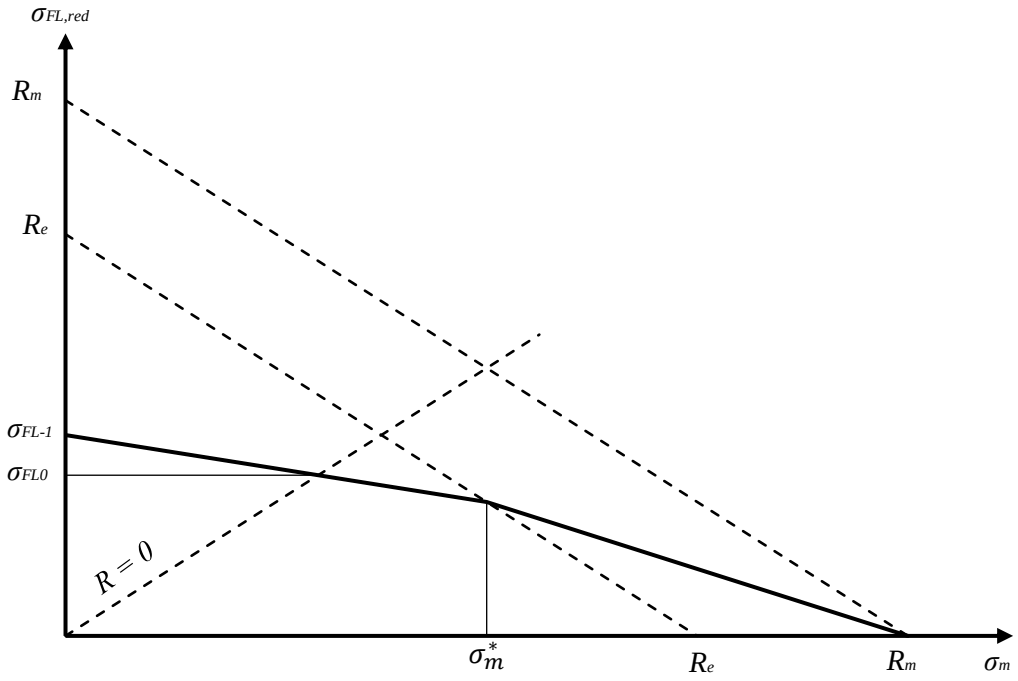

Figure 12 – Haigh diagram constructed using the FEMFAT method

Linear

The Linear method can be viewed as a modified Goodman model. It is again, a straight line, though the slope is defined using the fatigue limit σ_{FL0} instead of the ultimate tensile strength R_m. In this regard, it is similar to the FEMFAT model, it will however, in common cases, tend to yield less conservative life predictions, as it does not introduce the breaking point σ_m^* like the aforementioned method.

$$\sigma_{FL,red} = \sigma_{FL-1} - \sigma_m \cdot \frac{\sigma_{FL-1} - \sigma_{FL0}}{\sigma_{FL0}}$$

(41)

Haibach

This approach [28] does not utilize any static material parameters but requires the (R = -1) and (R = 0) curves to be known, as the Haigh diagram (Figure 13) is defined by their corresponding fatigue limits, σ_{FL-1} and σ_{FL0}. For mean stresses σ_m lower than the fatigue limit σ_{FL0}, the calculated reduced fatigue limit $\sigma_{FL,red}$ is the same as for the Linear and FEMFAT methods. For mean stresses higher than σ_{FL0} and lower than σ_m^+, the slope of the line is decreased to one third of the original slope M. For mean stresses outside of this region, $\sigma_{FL,red}$ remains constant.

$$for\ \sigma_m\ \in < 0; \sigma_{FL0}\ )$$

$$\sigma_{FL,red} = \sigma_{FL-1} - \sigma_m \cdot M$$

$$for\ \sigma_m\ \in < \sigma_{FL0}; \sigma_m^+ >$$

$$\sigma_{FL,red} = \sigma_{FL0} - (\sigma_m - \sigma_{FL0}) \cdot \frac{M}{3}$$

$$for\ \sigma_m > \sigma_m^+$$

$$\sigma_{FL,red} = \sigma_{FL0} - (\sigma_m^+ - \sigma_{FL0}) \cdot \frac{M}{3} = const.$$

$$where$$

$$M = \frac{\sigma_{FL-1} - \sigma_{FL0}}{\sigma_{FL0}}$$

$$\sigma_m^+ = \sigma_{FL0} \cdot \frac{M+3}{M+1}$$

(42)

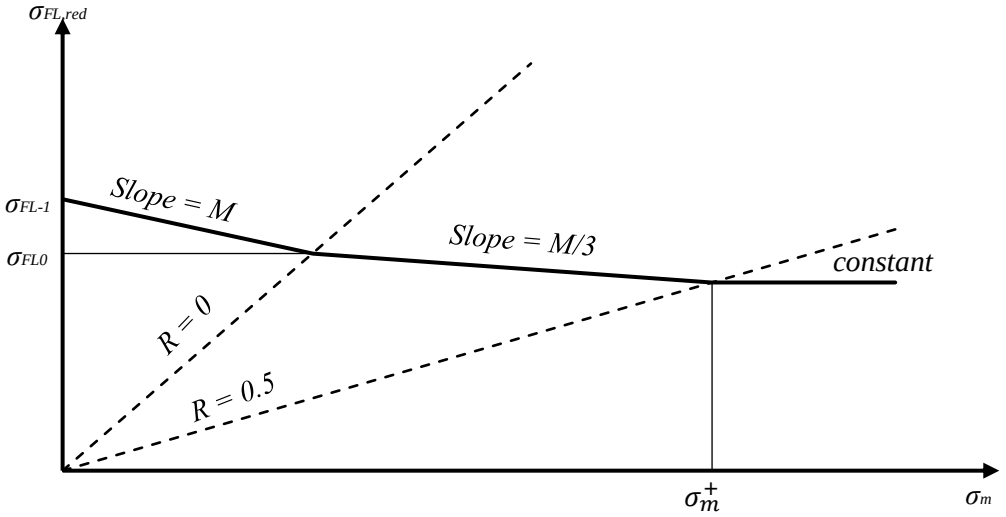

Figure 13 – Haigh diagram according to the Haibach method

Optimized models

Goodman, Gerber, Smith (Optimized)

Analogically to what has been show in chapter 1.6, the optimized Goodman (43), Gerber (44) and Smith (45) models are derived by simply replacing the ultimate tensile strength R_m with a parameter that is found through optimizations.

$$\sigma_{FL,red} = \sigma_{FL-1} \cdot \left(1 - \frac{\sigma_m}{M}\right)$$

(43)

$$\sigma_{FL,red} = \sigma_{FL-1} \cdot \left(1 - \left(\frac{\sigma_m}{M}\right)^2\right)$$

(44)

$$\sigma_{FL,red} = \sigma_{FL-1} \cdot \frac{1 - \frac{\sigma_m}{M}}{1 + \frac{\sigma_m}{M}}$$

(45)

Bergmann, Kwofie

Both optimized reduced fatigue limit methods, Bergmann [25] and Kwofie [23], have been derived from their respective equivalent stress amplitude approach counterparts using the procedure described in 1.5. It is worth noting that the optimized Walker model (16) cannot be transformed this way. For Kwofie's model (47), this is quite straight forward, for Bergmann however, a quadratic formula needs to be

solved. Out of the two possible solutions, only one gives sensible results (46), as the other produces negative values of the reduced fatigue limit $\sigma_{FL,red}$.

$$\sigma_{FL,red} = \frac{-k \cdot \sigma_m + \sqrt{k^2 \cdot {\sigma_m}^2 + 4 \cdot {\sigma_{FL-1}}^2}}{2}$$

(46)

$$\sigma_{FL,red} = \sigma_{FL-1} \cdot \exp\left(-M \cdot \frac{\sigma_m}{R_m}\right)$$

(47)

Klubberg

As has been noted in 1.6, the Klubberg model [27] features the *p* parameter. Obtainable through regression, the *p* parameter allows weighing between the Goodman and Gerber models. This is true when $p \in < 0; 1 >$. However, for many datasets used in this thesis, an optimal value of *p* tends to be found outside of these bounds. This means that imposing these constraints on the value of this parameter into the solver causes it (in most cases) to find the optimal solution to be either $p = 0$ or $p = 1$, which produces results that are either identical to that of the unoptimized reduced fatigue limit Gerber method for the former solution, or Goodman method for the latter. For this reason, no constraints on the *p* have been set in the solver.

$$\sigma_{FL,red} = \sigma_{FL-1} \cdot \left(1 - p \cdot \frac{\sigma_m}{R_m} - (1-p) \cdot \left(\frac{\sigma_m}{R_m}\right)^2\right)$$

(48)

Haibach

The unoptimized reduced fatigue limit Haibach method [28] can be altered in several ways in order to become optimizable, for example, through optimizing the horizontal position of the breaking points, or the slope reduction in the midsection of the Haigh diagram. In this thesis, optimization has been performed on the parameter *p* that has replaced the fatigue limit $\sigma_{FL0,}$ see (49).

$$for\ \sigma_m \in < 0; p)$$

$$\sigma_{FL,red} = \sigma_{FL-1} - \sigma_m \cdot M$$

$$for\ \sigma_m \in < p; \sigma_m^+ >$$

$$\sigma_{FL,red} = p - (\sigma_m - p) \cdot \frac{M}{3}$$

$$for\ \sigma_m > \sigma_m^+$$

$$\sigma_{FL,red} = p - (\sigma_m^+ - p) \cdot \frac{M}{3} = const.$$

$$where$$

$$M = \frac{\sigma_{FL-1} - p}{p}$$

$$\sigma_m^+ = p \cdot \frac{M+3}{M+1}$$

(49)

1.8 Categorization of life prediction procedures

Numerous life prediction methods have been tested for this thesis. They can be divided into several groups of comparable results. The reasoning for the creation of individual categories is provided in this chapter.

Equivalent stress amplitude – unoptimized

The unoptimized Goodman, Gerber, Dietmann and SWT provide a simple, straightforward calculation procedure for determining the fatigue life of components subjected to a load with non-zero mean stress. The equivalent stress approach requires the knowledge of the basic zero mean stress curve, while the individual mentioned methods only require minimal extra input data, namely the stress amplitude and mean stress of the load cycle, and except for the SWT method, the ultimate tensile strength R_m, which is generally available or at least easy to obtain through tensile testing. The equivalent stress amplitude $\sigma_{a,eq}$ is calculated and then substituted for the stress amplitude σ_a in the power law model (4) S-N curve, where the constants C_{-1} and W_{-1} of the (R = -1) curve are employed.

The unoptimized equivalent stress amplitude Walker and Linear models have been placed in this group as well, though comparison of achieved results with the previously mentioned methods in this group is not quite fair, as these two models require the knowledge of the (R = 0) curve, which means they are objectively more demanding in terms of input data.

Equivalent stress amplitude – 1(2) degrees of freedom

This category is based on the methods in 1.6 – Optimized models. They are used in the same way as Goodman, Gerber, Dietmann and SWT models from the equivalent stress amplitude – unoptimized category, but they are separated due to the fact that they feature one (or two in the case of the Exponential model) optimization parameters. These are obtained through fitting corresponding life prediction functions onto experimental data, where the objective function (50) is to minimize the sum of squares of errors of $\log_{10}(N)$.

$$Objective\ function = \sum_i \left(\log_{10}\left(N_{i,experiment}\right) - \log_{10}\left(N_{i,predicted}\right)\right)^2 \quad \textbf{(50)}$$

Equivalent stress amplitude – 3 degrees of freedom

Here, the solver not only attempts to find the best-fit equivalent stress amplitude model parameter to minimize (50), but at the same time, the coefficients of the basic S-N curve, which would otherwise be those of the (R = -1) curve. This means that these two coefficients no longer have to describe the trend of the data in the (R = -1) curve. Instead, such values are found through optimization, so that they minimize the sum of squares of fatigue life errors (50) across the entire dataset.

The coefficients acquired through this way have less potential practical use compared to those of the 1(2) degrees of freedom category. Instead, the results of these regressions allow judgement of whether a selected combination of S-N curve model and equivalent stress amplitude model is actually able to describe fatigue data trends well.

All the equivalent stress amplitude models used in the 1(2) degrees of freedom have been used this way, except for the Exponential model, which features two coefficients rather than one. This brings the total amount of optimization parameters up to four, which can often result in a large number of local minima of the objective function. As finding a combination of four parameters for each dataset that would result in the global minimum of the objective function would require increased effort, the exponential model has been omitted from this category of life prediction procedures.

Reduced fatigue limit – unoptimized

The core procedure is described in 1.3 - Reduced fatigue limit approach. The reduced fatigue limit models used here are described in 1.7 - Unoptimized models. This group of models has mostly similar

requirements (input data-wise) as the unoptimized equivalent stress amplitude category: a well mapped (R = -1) curve and some material parameters, like the ultimate tensile strength R_m. As has been noted in 1.3 though, additional information has to be extracted from the available experimental fatigue data with zero mean stress loads, as the reduced fatigue limit approach also requires the fatigue limit σ_{FL-1} and fatigue life corresponding to this fatigue limit N_{FL}. The value of these two extra parameters can be more affected by subjective opinion compared to other needed values.

Out of all the reduced fatigue limit models used in this group, three also require that the fatigue limit σ_{FL0} of the (R = 0) curve is known (Linear, FEMFAT, Haibach), which is done through the use of the Basquin (2) or power law (4) curve model, where $N = N_{FL}$ and the curve constants correspond to the (R = 0) curve (for example, W_0 and C_0).

Reduced fatigue limit – optimized

The life prediction procedure is the same as with the reduced fatigue limit – unoptimized category, but each of the reduced fatigue limit models feature one optimization parameter. The individual models are described in 1.7 - Optimized models. The parameters are found through optimization, while using the same objective function (50) that was used for the equivalent stress amplitude approach optimizations. Even though the ultimate tensile strength R_m does not explicitly appear in the reduced fatigue limit model equations, it is still needed, as it is used to construct one of the two points that define the non-zero mean stress curves, see Figure 7.

Reduced fatigue limit – optimized, modified

Modified versions of the original reduced fatigue limit approach defined in 1.3 in conjunction with some optimized reduced fatigue limit models have been tested. These models feature a regression coefficient that replaced the ultimate tensile strength R_m in their original unoptimized counterparts, and since the definition of the subsequent non-zero mean stress fatigue curves relies on R_m in the original approach from [21], a new approach based on shifting the [$N(R_m)$; R_m] point in Figure 7 has been devised. This leads to a change of slope of the original (R = -1) curve.

A total of three variants of this approach have been tested, each of them shifting the point [$N(R_m)$, R_m] vertically to a new value. They differ in the way the point is shifted horizontally – see Figure 15. For variant *a)*, the horizontal (N) coordinate is always 1. For variant *b)*, the point stays over the original $N(R_m)$ coordinate. In variant c), the point follows the original trend of the [1; 1] – [$N(R_m)$; R_m] line.

As the different variants produced similar results, variants *b)* and *c)* have been cut from the thesis, and when referring to reduced fatigue limit – optimized, modified outside of this chapter, it is being referred to variant *a).*

This adaptation of the reduced fatigue limit has been used in conjunction with the optimized reduced fatigue limit models Goodman, Gerber, Smith and Haibach – see 1.7. For the first three, the shifted point has the vertical coordinate equal to optimization parameter M in equations (43),(44) and (45), as the coefficient replaced original ultimate tensile strength R_m. As for the optimized Haibach model, where the optimization parameter replaced the fatigue limit σ_{FL0} of the (R = 0) curve from the unoptimized version, the vertical coordinate has been replaced by the value of σ_m, where in the Haigh diagram, Figure 13, the line with slope = M intercepts the horizontal axis, which is $\frac{\sigma_{FL-1}}{M}$.

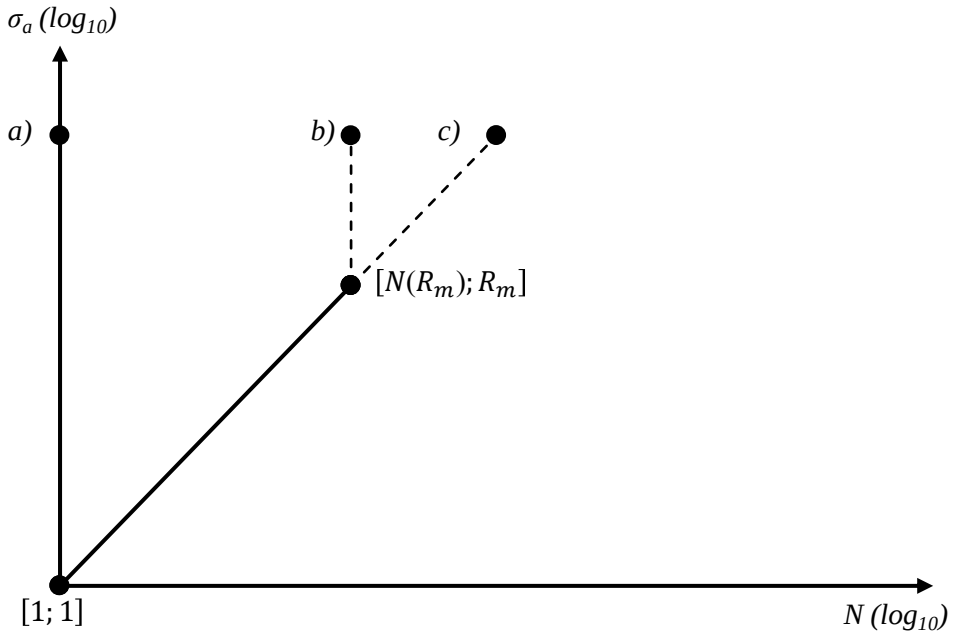

Figure 14 – different variants (*a) b) c)*) of the [*N; N*(R_m)] point horizontal shift of the optimized, modified reduced fatigue limit approach

The optimization is, again, performed while minimizing the objective function (50). During the regression, changing the value of the optimization parameter alters both, the shape of the Haigh diagram of the corresponding reduced fatigue limit method, and vertical position of the slope-defining left point of the (R = -1) curve. Thus, the values of the coefficients gained through this optimization will be (in most cases) different to those obtained through the original reduced fatigue limit optimized version. The process of deriving a fatigue curve where the mean stress σ_m is greater than zero is visualized in Figure 15.

The main reason for the creation of this modified variant was to provide more flexibility in terms of the optimization of the slope of the ($\sigma_m > 0$) curves, which was thought to possible increase the quality of fatigue life predictions for bending type loads.

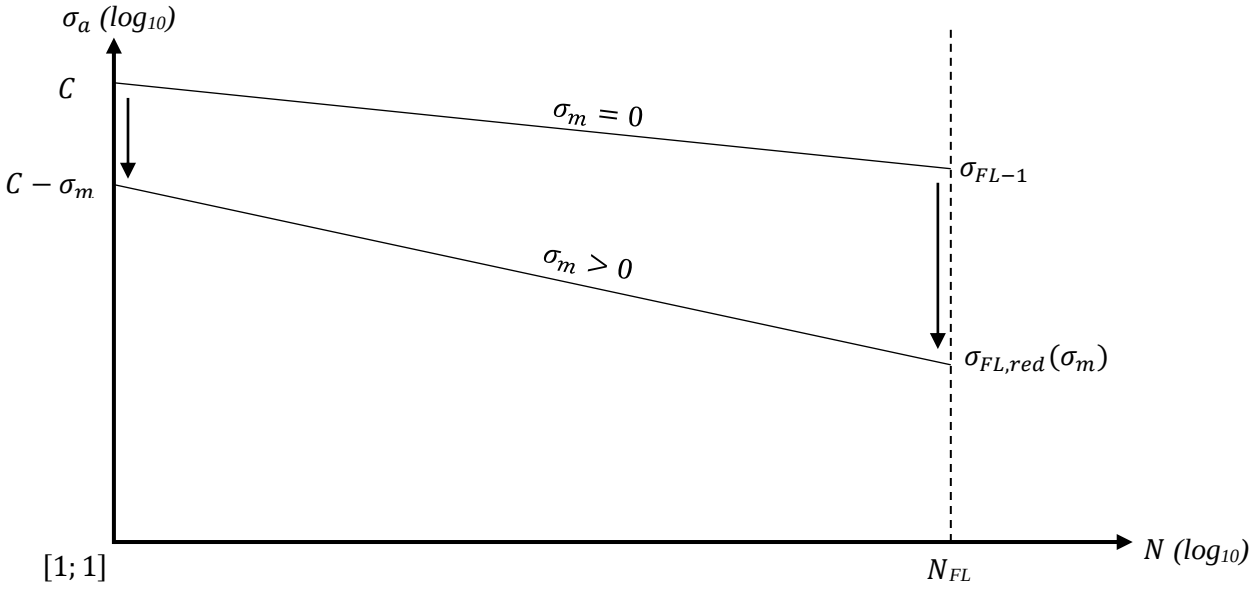

Figure 15 – Reduced fatigue limit – optimized, modified method
***C* corresponds to the regression coefficient *M*, or in case of the Haibach model, $\frac{\sigma_{FL-1}}{M}$**

FEMFAT shift

The FEMFAT shift represents a further decrease in predicted fatigue life based on the influence of several factors described in [21]. Only one of these factors is considered in this thesis, the mean stress effect. For any reduced fatigue limit approaches in this chapter, the FEMFAT shift was applied, but both results, the original and the shifted ones, are kept separated in the practical part of the thesis.

As can be seen in (51), the original fatigue life prediction of the reduced fatigue limit approach $N_{orignal\ prediction}$ is further decreased (as $\frac{N_{FL,red}}{N_{FL}}$ is always less than 1) based on the ratio of the original fatigue limit of the (R = -1) curve and the reduced fatigue limit $\sigma_{FL,red}$, which is calculated using models listed in 1.7. The reduced fatigue limit $\sigma_{FL,red}$, at least for all of the models discussed in this thesis, does not increase with an increase in mean stress.

$$N = N_{original\ prediction} \cdot \frac{N_{FL,red}}{N_{FL}}$$

$$where$$

$$N_{FL,red} = N_{FL}^{\left(\frac{\log_{10}(\sigma_{FL,red})}{\log_{10}(\sigma_{FL-1})}\right)^{\frac{1}{16}}}$$

(51)

Note that the nomenclature used in (51) has been adjusted to fit the rest of this thesis. The original equations have also been heavily simplified compared to the source material, as they originally incorporated many different factors which are not taken into account in this thesis, for example, the influence of a thermomechanical load.

1.9 Parameters determining the quality of achieved results

In order to judge the accuracy, usability, etc. of achieved fatigue life predictions from various methods, several different parameters are observed.

Fatigue life error Δ_{FL}

Given by relationship (52), Δ_{FL} characterizes the relative error of the decadic logarithms of the measured ($N_{experiment}$) and calculated ($N_{predicted}$) fatigue lives. The sign of the value ofΔ_{FL} determines whether the predicted results are on the conservative (+) or non-conservative (-) side.

$$\Delta_{FL} = \frac{\log_{10}(N_{experiment}) - \log_{10}(N_{predicted})}{\log_{10}(N_{experiment})}$$

(52)

Once Δ_{FL} has been calculated across all values from a certain group of data, for example, one data set of experimental values from fatigue experiments performed on specimens that originate from the same batch, the mean value, standard deviation, and range of Δ_{FL} can be calculated.

The mean value of a set of Δ_{FL} is, in an ideal case, 0, though being close to 0 does not necessarily imply that the achieved results are of high quality, as such results can still be subjected to a high amount of scatter, see 1.4.

The standard deviation of a set of Δ_{FL}, given by (53), quantifies the scatter of the achieved results. The minimum value of standard deviation is 0, which would symbolize a perfect fit of the model onto experimental data. Such fit, again, due to the nature of experimental fatigue data, is impossible (assuming that the data set has a sufficient number of points).

$$std(\Delta_{FL}) = \sqrt{\frac{1}{N-1}\sum_{i=1}^{N}\left(\Delta_{FL,i} - \overline{\Delta_{FL}}\right)^2},$$

(53)

Both the mean value and standard deviation of Δ_{FL} are comparable across datasets, as they are relative values, and do not necessarily grow with larger datasets, unlike, for example, the sum of squares of errors.

The range of Δ_{FL} is simply defined as the difference between the largest and smallest value of Δ_{FL}. Again, this gives information about the scatter, though it is less comparable across datasets in contrast to the standard deviation, as the range will tend to grow with larger data sets. This means that poor datasets, which will tend to have less scatter as they contain fewer measurements, do seem to provide better results (smaller ranges of Δ_{FL}) than rich data sets whilst looking at the values of range.

Mean square errors of fatigue lives

The sum of squares of error of fatigue lives is defined in (50). Due to the fact the sum of these errors always grows the richer the data set gets, the mean value of square errors gives a more comparable result across different data sets.

Coefficient of determination of fatigue lives

The coefficient of determination, or R^2, is maximized as the sum of squares of errors is minimized. It is given by (54).The maximum achievable value of R^2 is 1, which would symbolize a perfect fit. Values lower than 0 symbolize a fit that is worse than simply using a mean value of the logarithms of fatigue lives $\overline{\log_{10}(N_{experiment})}$ as a logarithm of predicted fatigue life instead of a more sophisticated model. R^2 is quite a useful parameter when judging the quality of a fatigue life prediction method, since it takes the amount of experimental data scatter into account. The $\sum variance$ value increases with an increase in scatter of the experimental data. This in turn causes the significance of $\sum square\ errors$ to lessen. R^2 is also comparable across different data sets.

$$R^2 = 1 - \frac{\sum square\ errors}{\sum variance}$$

$$where$$

$$\sum square\ errors = \sum_i \left(\log_{10}(N_{i,experiment}) - \log_{10}(N_{i,predicted})\right)^2$$

$$and$$

$$\sum variance = \sum_i \left(\log_{10}(N_{i,experiment}) - \overline{\log_{10}(N_{experiment})}\right)^2$$

(54)

2. ABOUT EXPERIMENTAL DATA

2.1 Data acceptance criteria

No experimental campaign that would be tailored for the needs of this thesis has been realized, all data presented here has been adopted from prior works by various authors. The experiments of these authors have been done for different studies, the areas to which they paid attention in their works often differ from areas important for obtaining results that would be valuable for this thesis. For this reason, many data sets that have been carefully extracted from various papers, books and technical reports have been

at last discarded for not fulfilling the criteria set for thesis, which are described in this chapter. As the total amount of experimental data gathered is quite large, these criteria can be fairly strict, while still retaining enough data for a valuable analysis.

Firstly, the experiment should be accurately described in the paper evaluated for adopting published data. A poor description of the specimens and experimental procedures can be the root of many uncertainties down the line, and the entire corresponding data set can be ultimately discarded. In the works by Pomp and Hempel [30], for example, it is noted that some of the specimens have been subjected to loads of different magnitudes for a good number of cycles before finally settling at nominal values. This can have a very large impact on the fatigue life, when compared to specimens that have not been subjected to noticeable over/underloading during some part of the experiment. For this reason alone, this data set, which is probably larger than any data set actually used in this thesis, was discarded. Note that sometimes, authors will further expand information about particular data points with some remarks. These can often reveal that an experiment on a specific specimen has not been successful, in the sense that the failure condition (which determines the end of the experiment) did not occur strictly due to fatigue. Typical examples of this include that the specimen has buckled or cracked somewhere else than in the critical section, for example, in the grips. Such experimental points are not used for calculations in this thesis.

Most authors present data in the forms of S-N curves. This does not mean the data is necessarily presented in graphs, but that the data is presented in groups of points, and in these groups, there is only one independent (for example, stress amplitude σ_a) and one dependent variable (fatigue life N). This means that for all experimental points in a curve, either the stress ratio R, the mean stress σ_m or some other stress metric (but this is not very common) must be kept constant. Note that the loading frequency should also be, in an ideal case, kept constant. It is, however, often difficult to keep the mentioned values constant for all experimental points. All the data used in this thesis is pre-processed using the Visual Basic macro based FinLiv software. This software only allows the input of data of constant σ_m or R into a single curve. For data that does not exactly follow this trend (and frankly, it often does not, it is up to the courtesy of the authors to present data as accurately as possible, which would show that some of these "constant" values can fluctuate), a simple but quite strict criterion based on the equivalent stress amplitude model SWT (15) has been devised.

The fluctuating value of R or σ_m is idealized in order to be kept constant for all points across the curve. This usually means using the mean or most common value for all points. Then, a relative error in terms of equivalent stress amplitude according to the SWT method is calculated, as shown in (55). If this error is less than 0.5 %, the data points with the idealized values are used. If not, they are discarded, and if this happens, the idealized values of the remainder of the data points can be often further adjusted in order to come closer to the real values of these data points.

$$Relative\ Error = \frac{\sigma_{a,eq,idealized} - \sigma_{a,eq,real}}{\sigma_{a,eq,real}} \quad (55)$$

Quantifying whether fluctuations of the loading frequency across points in a single curve / data set is not a straightforward task. It is, however, noted when a data set suffers from this uncertainty in 2.3.

Another requirement on the individual S-N curves is a sufficient amount of data points spread out across a satisfyingly large spectrum of stress magnitude values. This is due to the fact that this thesis is concerned with the low to high cycle fatigue regions of fatigue life, see Figure 4. In order to classify which fatigue life region specific points belong to, an assumption is made that they must follow the linear trend, described by the Basquin line or the power law model, see 1.2. Whether this is true or not is decided based on the visualized points forming an S-N curve. Considering the scattered nature of fatigue data, for this procedure to be as objective as possible, a sufficient number of data points (5 being the minimum accepted here, though this number is far from ideal) has to be available. Ideally, the transition area into the "infinite" life region is determinable from this S-N curve as well, hence the need

for a sufficiently wide spectrum of load stresses. An ideal data set has a well-defined transition area into both, the giga-cycle fatigue region and the quasi-static region (see Figure 4), as this makes determining which data points belong to the regions of our interest quite simple and arguably objective. Extra care is being taken when approving the (R = -1) and (R = 0) curves of any data sets, as these hold particular importance for reasons obvious from chapters 1.3, 1.6 and 1.7. Luckily, the authors of experiments are aware of this (also, these curves form the basis for fatigue life prediction when other factors are taken into account, not just the mean stress effect), and the two curves, when available, do tend to be quite data-rich in most works.

Finally, it is worth considering whether the data set given by an author is presented in a fashion that makes its acquisition with enough accuracy possible. This is often debatable when the author presents data only in graphs. It can be considered important to note whether a graph is computer generated or drawn by hand, the latter being quite common in older works. A problem that has caused some data sets to be discarded was that the S-N curves presented were simply too flat, meaning the horizontal axis of the graph of the S-N curve simply has not had its scale set in an appropriate way. This problem mainly occurs with the more modern works, where the graphs are computer generated. Data originally presented in graphs that has been used in this thesis has been extracted using the tool WebPlotDigitizer [32]. Of course, data presented in raw numbers in tables is ideal for the purposes of further analysis.

2.2 Synthesis of the (R = 0) curve

Often, there is no (R = 0) curve available from the author. This is inconvenient, as this curve is mandatory for the application of several fatigue life prediction models, both from the equivalent stress amplitude and reduced fatigue limit approach, as is apparent in 1.6 and 1.7. For this reason, a method has been devised in order to synthesize properties of this curves, even if it is not available in a particular data set.

A basis of this is the Kohout-Věchet [31] model of the S-N curve, a 4-parameter model (56) which, unlike the Basquin or power law model described in 1.2, was designed to describe the entirety of the Wöhler curve, not just the linear region. The resulting S-N curve has a 2 nearly horizontal parts, much like the general form of the Wöhler curve shown in Figure 5.

$$\sigma_a = A \cdot \left(\frac{N+B}{N+C}\right)^{\beta} \quad (56)$$

When an (R = 0) is not available, the Kohout -Věchet can be used to obtain the Haigh diagram, based on the other available curves. First, the 4 coefficients of the Kohout Věchet model for all the available curves have to be obtained via a non-linear regression. Afterwards, two fatigue strengths $\sigma_{FS,1}$ and $\sigma_{FS,2}$ for two corresponding fatigue lives N_1 and N_2 are calculated for each of the available curves (ideally, these fatigue lives lie somewhere in the fatigue life domains covered in all of the available curves). Using these values, two curves of constant fatigue lives (N_1 and N_2) can be constructed in the Haigh diagram, each of them being defined by the same number of points as the number of used curves for this procedure. A polynomial of the second degree is used fit the $\sigma_a = \sigma_a(\sigma_m)$ relation defining these two curves in the Haigh diagram, which usually results with the coefficient of determination R^2 greater than 0.95, even if five or more curves are used for this approximation. Once this is done, the fatigue strengths $\sigma_{FS,1,R=0}$ $\sigma_{FS,2,R=0}$ corresponding to the two fatigue lives N_1 and N_2 are found using these polynomials for the unknown R = 0 curves available. The slope defining constant of the power law model (4) W_0 of the synthesized (R = 0) curve is given by (57). Note that $N_2 > N_1$.

$$W_0 = \frac{\log_{10} N_2 - \log_{10} N_1}{\log_{10}\left(\sigma_{FS,2,R=0}\right) - \log_{10}\left(\sigma_{FS,1,R=0}\right)} \quad (57)$$

The second constant of the power law model C_0 can be calculated, for example, via (58).

$$C_0 = {\sigma_{FS,2,R=0}}^{W_0} \cdot N_2 \quad \textbf{(58)}$$

Finally, the fatigue limit σ_{FL0} of the synthesized (R = 0) curve can be calculated through (59).

$$\sigma_{FL0} = \left(\frac{C_0}{N_{FL}}\right)^{\frac{1}{W_0}} \quad \textbf{(59)}$$

In cases where the shared fatigue life domain of the curves of the data set is not wide enough, or when no curve of stress ratios R greater than 0 (this would result in extrapolation) is available, this approximation becomes unreliable, and thus, is not performed in this thesis, and the fatigue life prediction methods that rely on the availability of the (R = 0) are skipped for such data sets.

2.3 Description of used data sets

The description of each set is accompanied by a graph with S-N curves. When points of an S-N curve have been directly used in calculations which serve as a basis for the practical part of this thesis, all the valid points of the S-N curve, even the unused ones, are shown in the graph. The used points are highlighted, the unused ones stay hollow. The striped lines are the best-fit power law curves. In the legend of each graph, the constant parameters of the S-N curves are noted. The constant parameters are either the stress ratio R, or the mean stress σ_m ('Sm' [MPa] in the legend).

To avoid extrapolation, the fatigue lives of used points, N must not drastically exceed the bounds of the life domain set by the (R = -1) curve. These bounds correspond to the lowest and highest fatigue lives N of the experimental points used for to gain the C_{-1} and W_{-1} coefficients of the power law model – see 1.2.

BaB, Bai [3]

Two data sets have been extracted from graphs presented in this thesis, each of them containing a combination of constant stress ratio R (namely -1 and 0) and constant mean stress σ_m S-N curves. The BaB and Bai sets contain fatigue data obtained from tensile load type experiments on the Ck35 and 34CrMo4 steels, respectively.

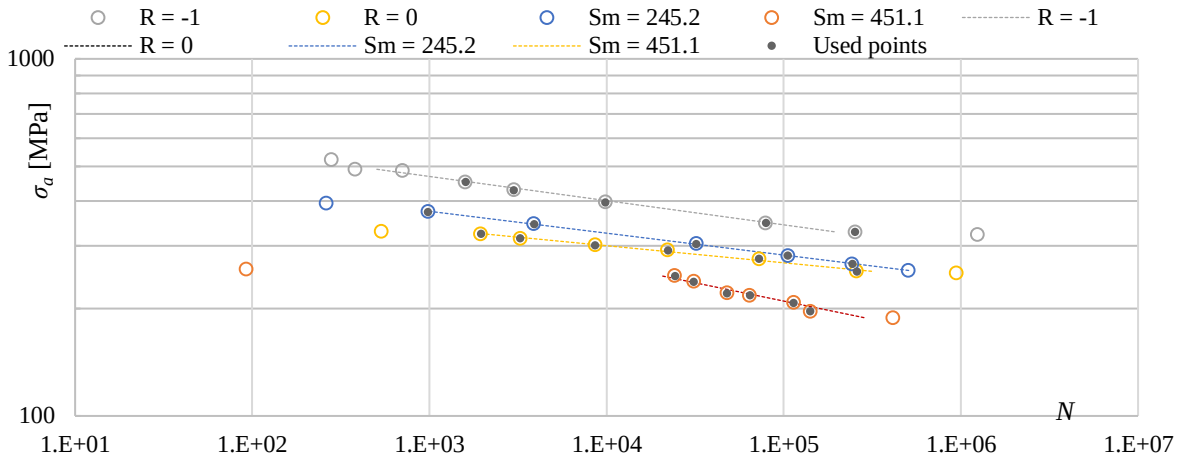

Figure 16 – BaB data set

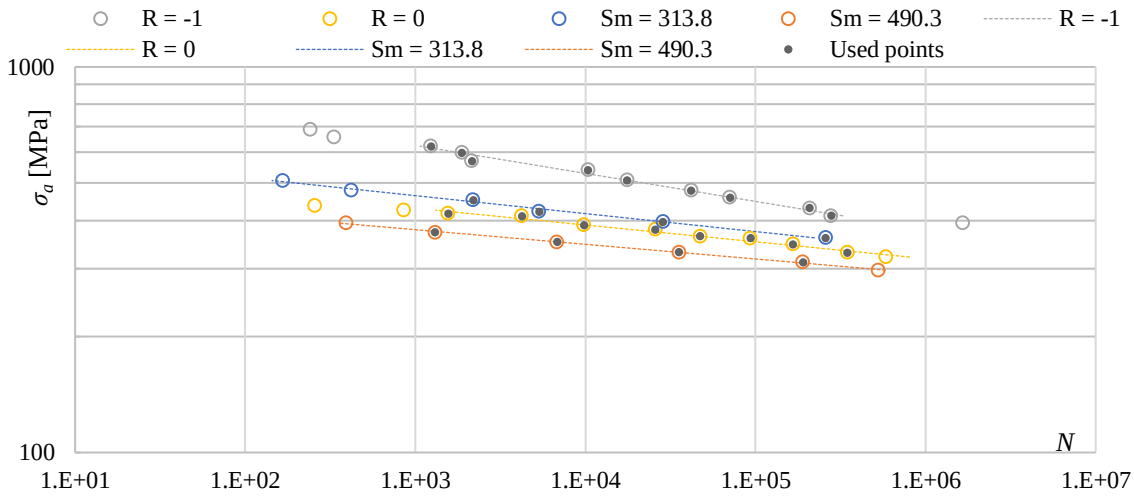

Figure 17 – Bai data set

FAD3, FAD4 [4]

The two data sets both contain data from tensile fatigue experiments performed on 2124-T851 aluminum alloy probes, with the surface of the specimens used in FAD4 being further grinded following the turning. The S-N curves of constant stress ratios *R*, going as high as 0.7 in FAD3, include the (R = 0) curve in both data sets.

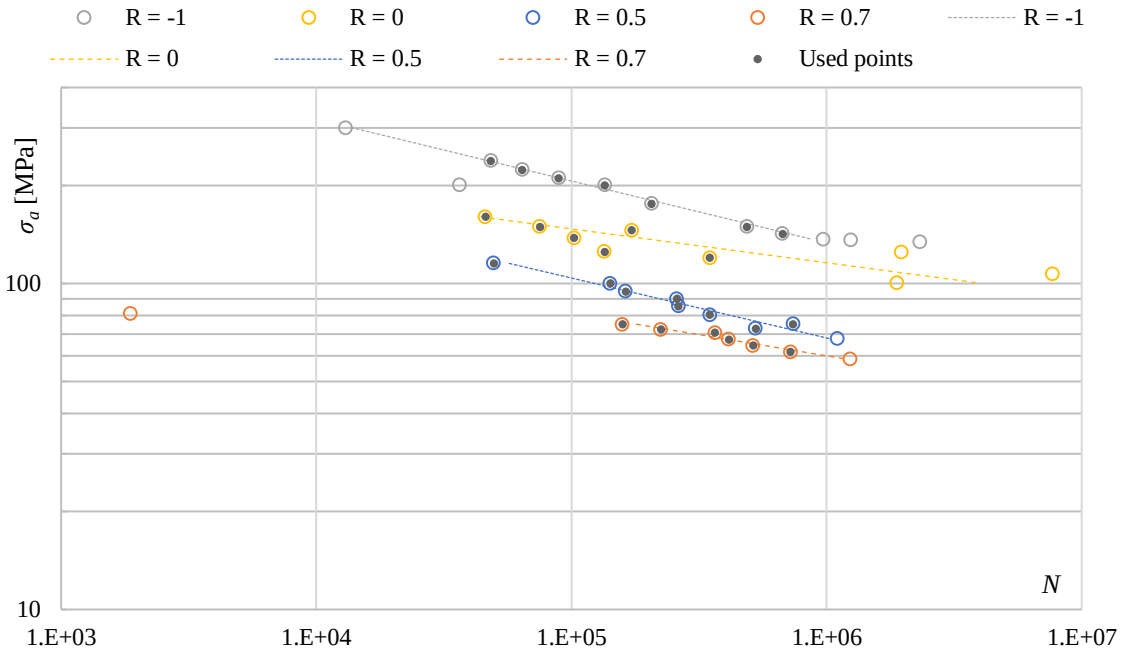

Figure 18 – FAD3 data set

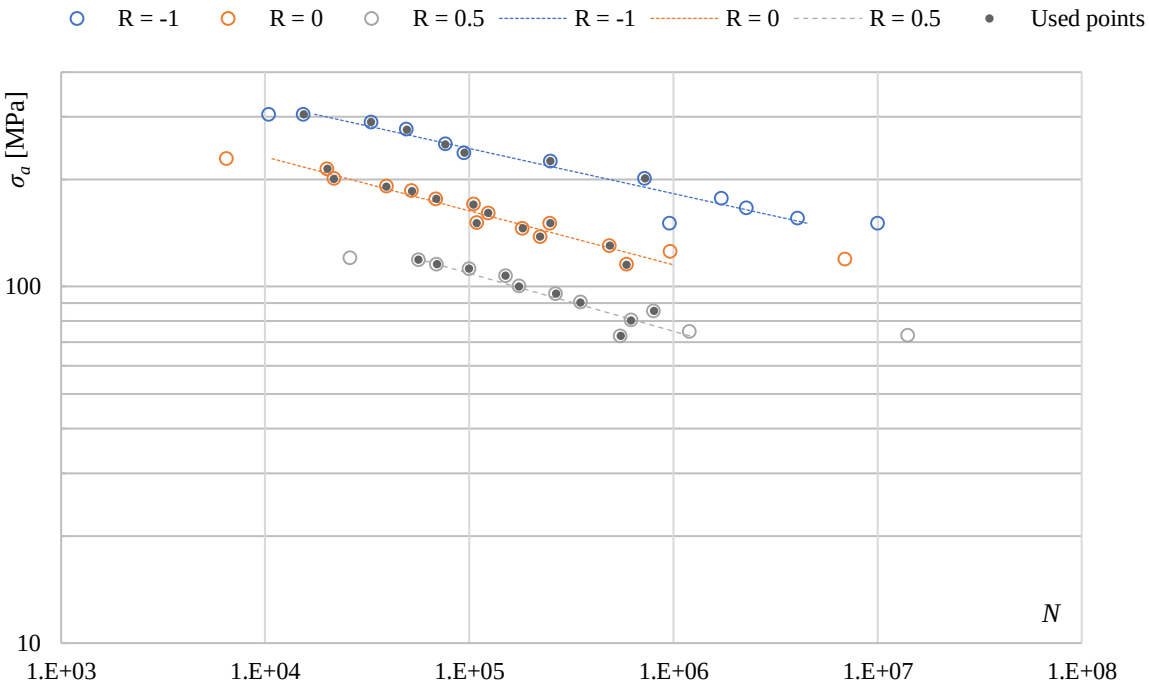

Figure 19 – FAD4 data set

Fin [5]

The technical report contains plain bending and torsion (not used here) load fatigue experimental data. The material used for these tests is the 75S-T61 aluminum alloy. A total of 5 S-N curves of constant mean stress (ranging from 0 to 448 MPa) have been extracted from graphs presented in the report. This means that no (R = 0) curve is available, though using the curve synthesis method described in this chapter, the needed values have been approximated.

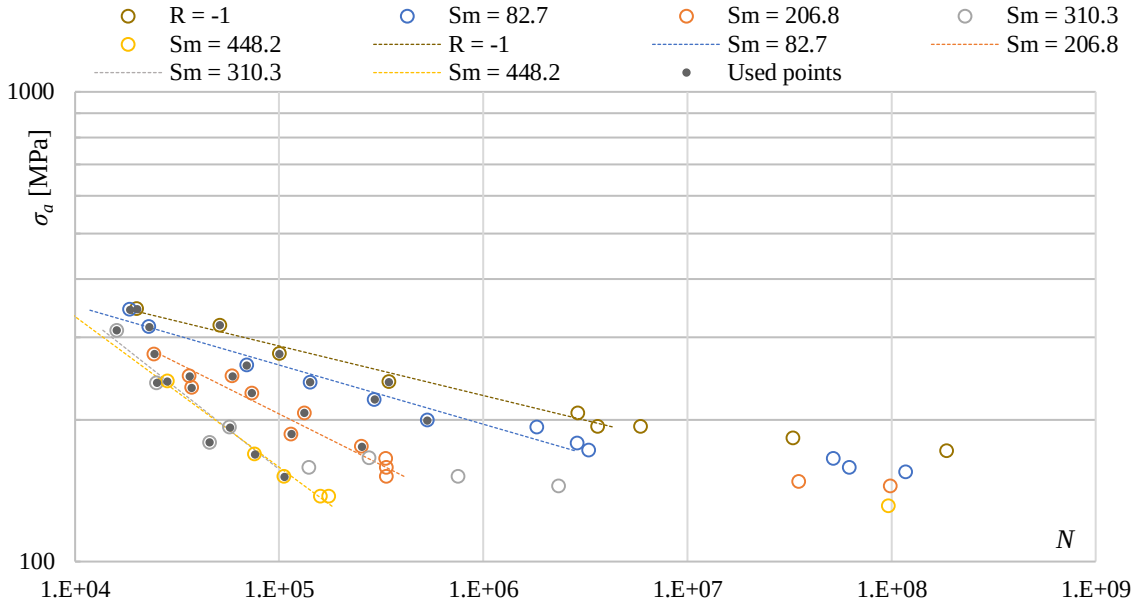

Figure 20 – Fin data set

GBA, GBB [6]

This report contains a large amount of data (conveniently presented in tables) from fatigue experiments where sheet type specimens have been subjected to tensile loading. Both used data sets are comprised of S-N curves of constant stress ratios R, though the parameters of the (R = 0) curve have been approximated for both sets, as such curve is not readily available for either. The stress ratios R range from -1 up to 0.6, and each of the data sets contains an (R = 0.02) curve, making the approximation of the (R = 0) curve parameters quite credible. The data sets GBA, GBB are differentiated through the use of different materials for the experiments, the 24S-T3 and 75S-T6 aluminum alloys, respectively.

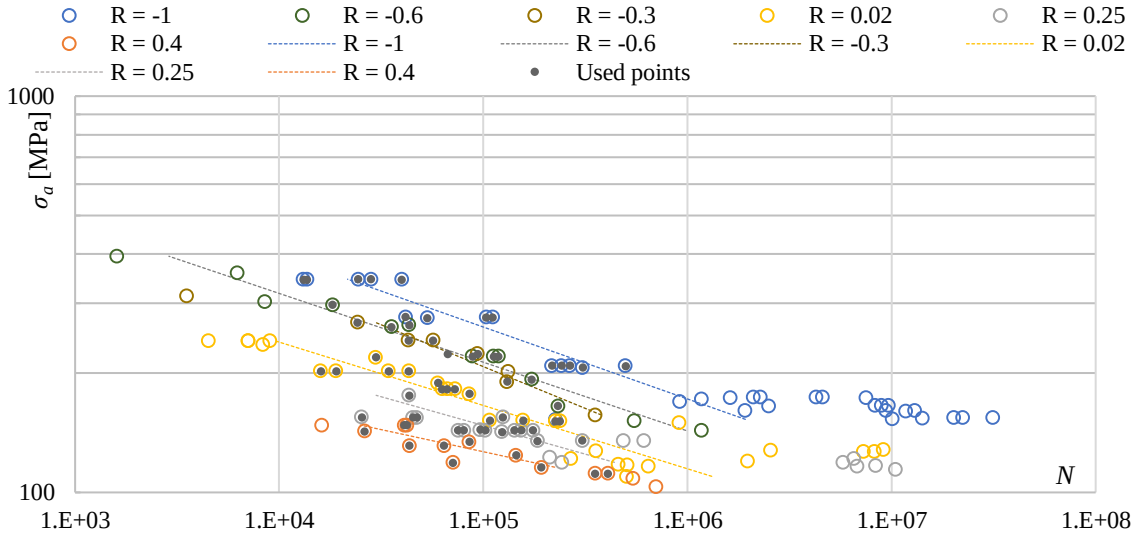

Figure 21 – GBA data set

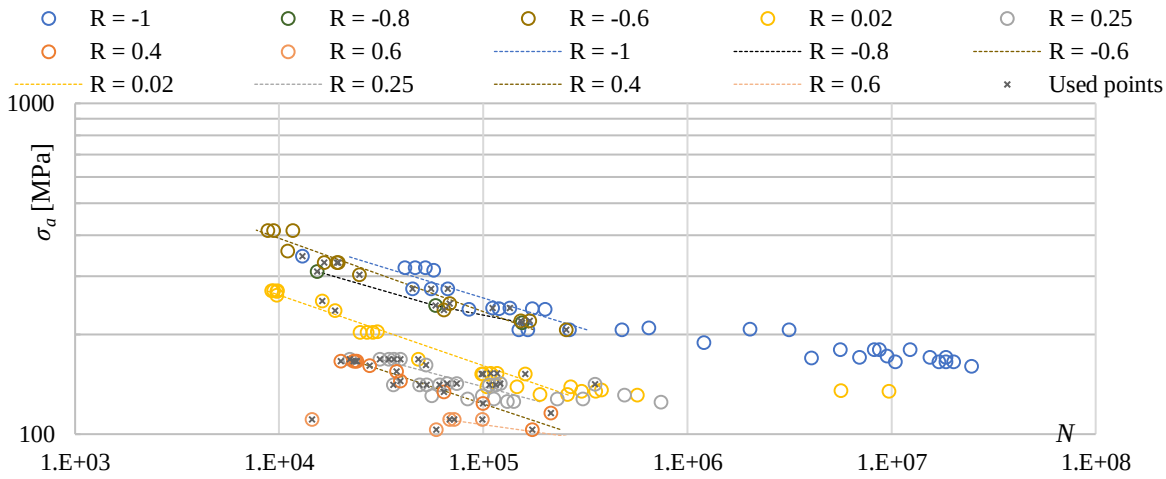

Figure 22 – GBB data set

GrN [7]

In the paper, results of tensile and torsion (not used in this thesis) load fatigue experiments are presented in graphs. The final data set is made up of two S-N curves of constant stress ratios R, the (R = -1) and (R = 0). The material used is the GGG-60 cast iron.

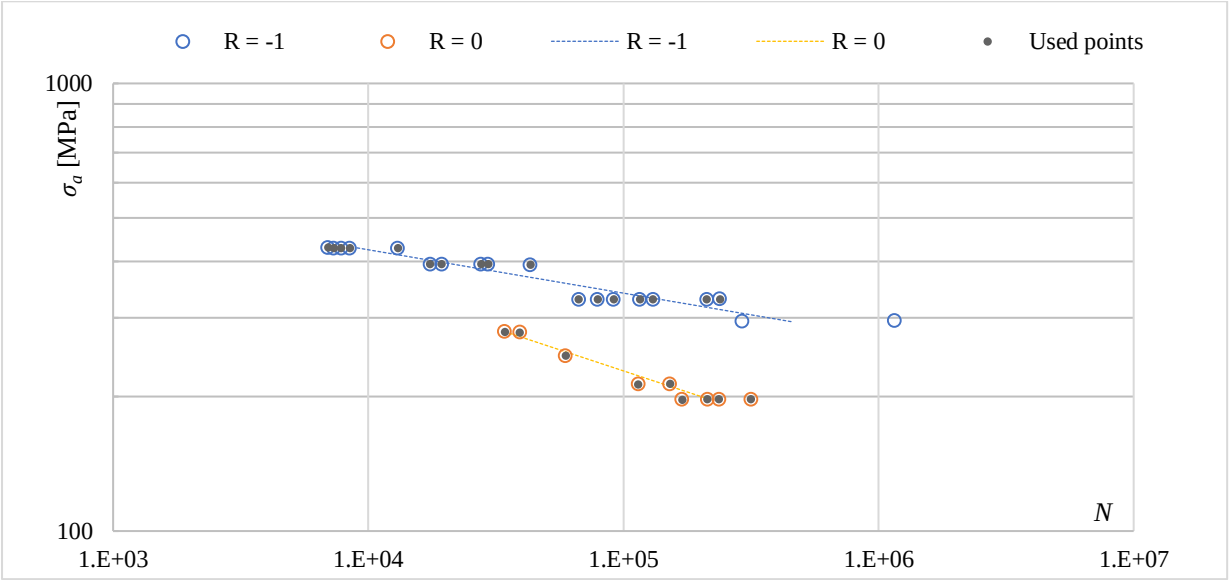

Figure 23 – GrN data set

Han [8]

The original work contains a large amount of experimental data with bending and torsion (not used in this thesis) types loads. The data used in this thesis, originating from experiments on plate specimens, consist of 5 S-N curves of constants mean stress σ_m levels. The mean stress defining one of these curves surpasses the ultimate tensile strength R_m of the used material, the SAE 4340 steel. This can cause problems for some of the used fatigue life prediction methods, namely for the unoptimized reduced fatigue limit approach described in 1.3 and 1.8, where the vertical position of "leftmost" point is given by R_m - σ_m, which in this case is a negative number. Generally, data sets where the specimens have been loaded through bending do cause problems when using any model that is partially based on the idea that a load of size R_m causes immediate failure, as this is not the true for bending. Though no (R = 0) curve is available in Hanley's work, its parameters have been approximated.

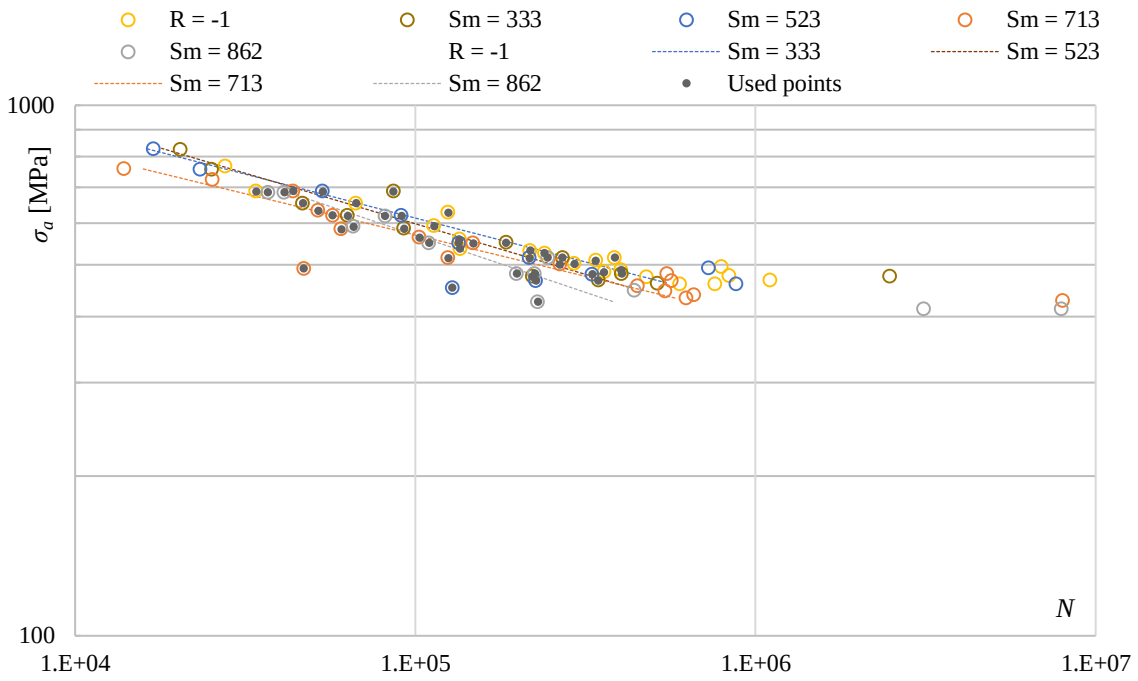

Figure 24 – Han data set

KLN [9]

The paper contains more data based on torsion (not used in this thesis) and bending type load experiments. The raw data forming a total of 4 S-N curves of constant mean stress σ_m has been received from the authors directly. However, the available data does not allow for an accurate approximation of the parameters of the (R = 0) curve, as this would require extrapolation (due to the fact that all the available stress ratios R are less than zero). The material used is the 2017A-T4 aluminum alloy.

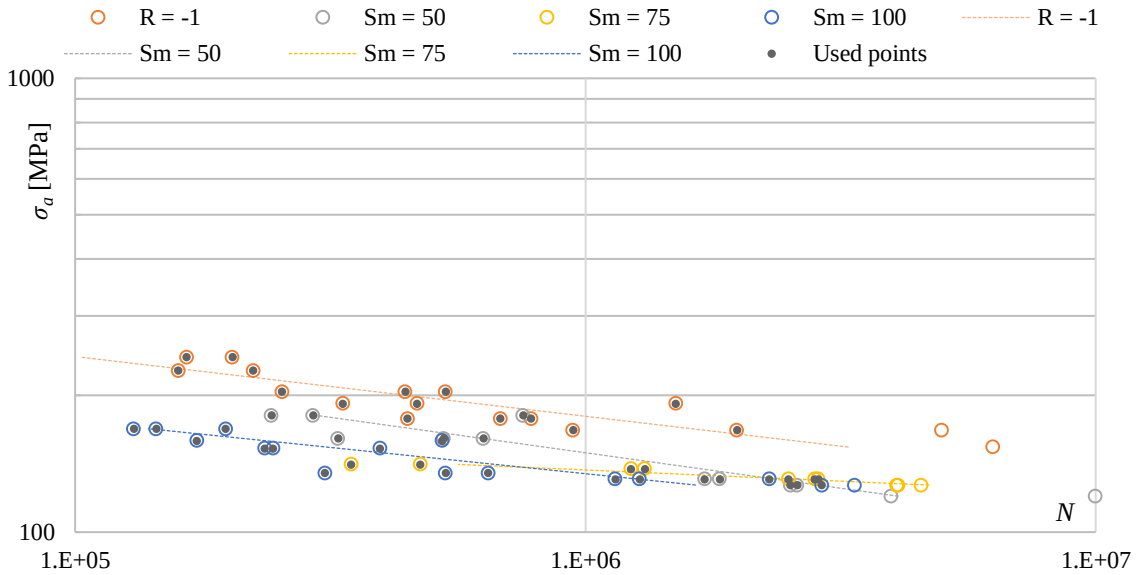

Figure 25 – KLN data set

No40 [11]

The sheet contains fatigue data presented in tables. The No40 set contains fatigue data obtained from tensile type load experiments on steel JIS SPV 50 specimens. The set contains an (R = -1) and (R = 0) curve, while two points of stress ratio R = 0.5 have been also used.

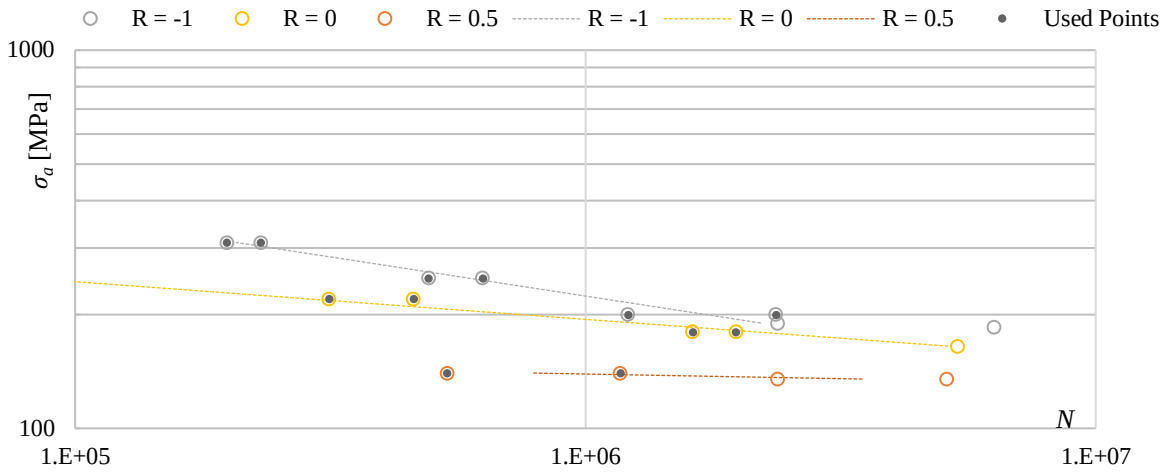

Figure 26 – No40 data set

Ra1 [12]

The thesis presents data from fatigue experiments on specimens subjected to tensile loading in tables. There are 3 S-N curves of constant stress ratios *R* available (-1, 0, 0.5). The material of the probe type specimens was the EN-GJV-450 cast iron.

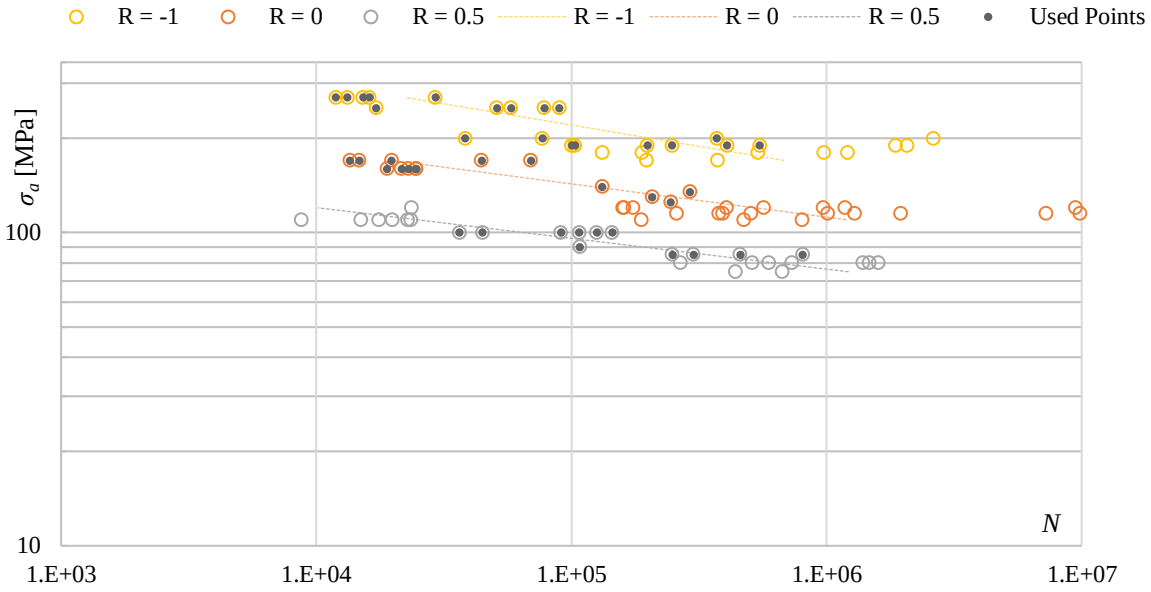

Figure 27 – Ra1 data set

SaL [14]

Bending and torsion (not used in this thesis) type load fatigue experiment results are presented in tables in this paper. Using the 5 available constants mean stress σ_m curves, the parameters of the ($R = 0$) curve have been approximated using the technique described earlier in this chapter. 14S-T aluminum alloy probes have been used.

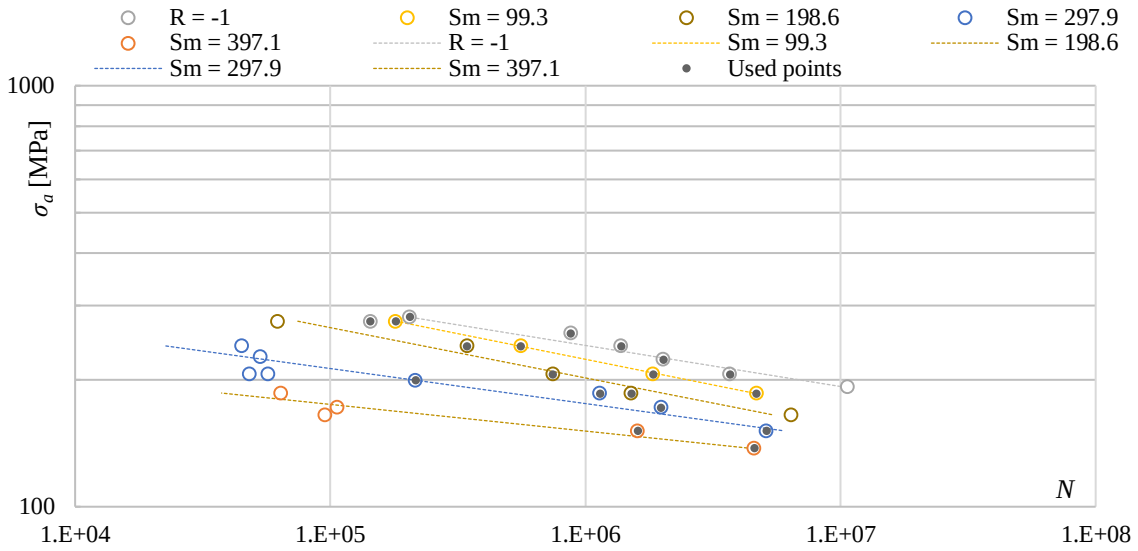

Figure 28 – SaL data set

PRb [16]

The tables of experimental plain bending and torsion (not use in this thesis) type load fatigue data hav been obtained from the authors (they are not directly presented in the referenced work). The used material is the 18G2A steel. The three available S-N curves are of constant stress ratios *R*.

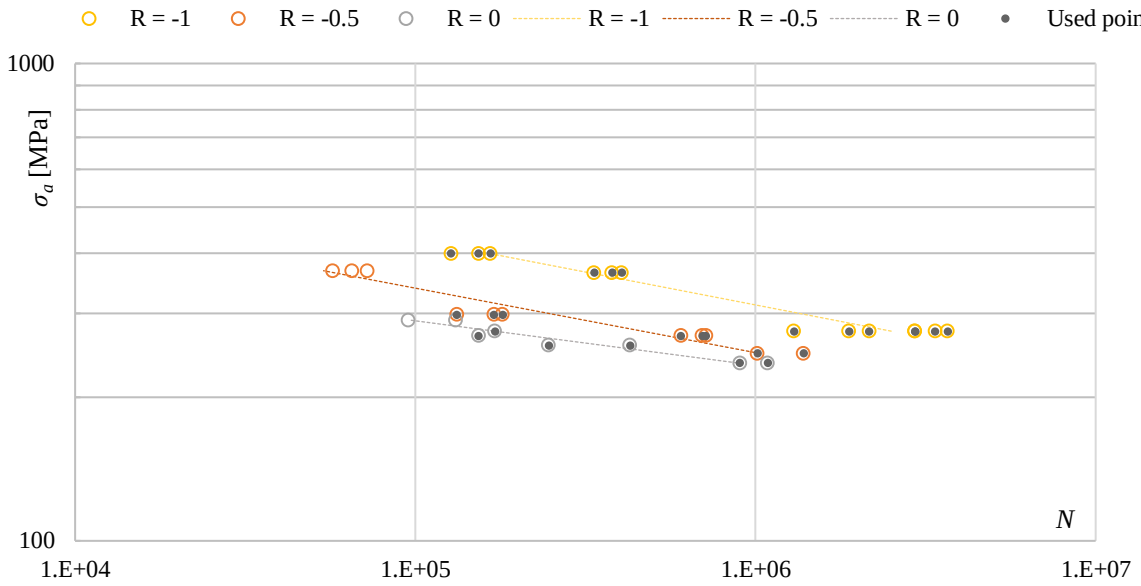

Figure 29 – PRb data set

SCa [13]

Fatigue test results of experiments on notched and unnotched specimens are presented in this report. The material used was the 7075-T6 aluminum alloy. The SCa set consists of 3 dense curves, the stress ratios *R* available being -1, -0.5 and 0. The results are presented in the form of tables. According to the author, two different testing machines have been used for the experiments, one operating at 5 Hz, the other at 29.2 Hz. Which machine was used to perform each individual experiment is not said, though the author claims fatigue tests for lives in excess of 10 000 cycles have been usually performed on the faster machine.

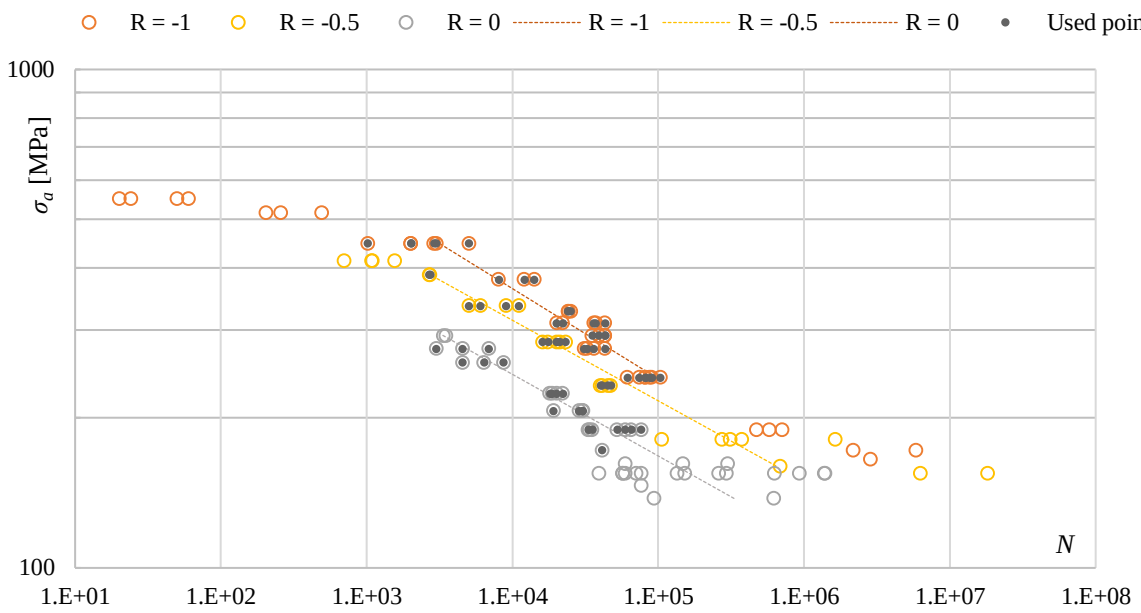

Figure 30 – SCa data set

AIS [1]

In the article, 8 curves of different constant mean stress levels are presented in a single graph. Three of these curves are not used in this thesis, as the present mean stress is compressive. The yield strength of the specimens is not given, it has been estimated through linear interpolation using the given ultimate tensile strength and known mechanical properties of the same material from a different source – the D16T aluminum alloy. As the curves are of constant mean stress rather than stress ratio, the $R = 0$ curve is not present, though several points of R close to 0 are available. Using the Kohout-Věchet S-N curve model, the (R = 0) curve has been approximated using the approach described earlier in this chapter.

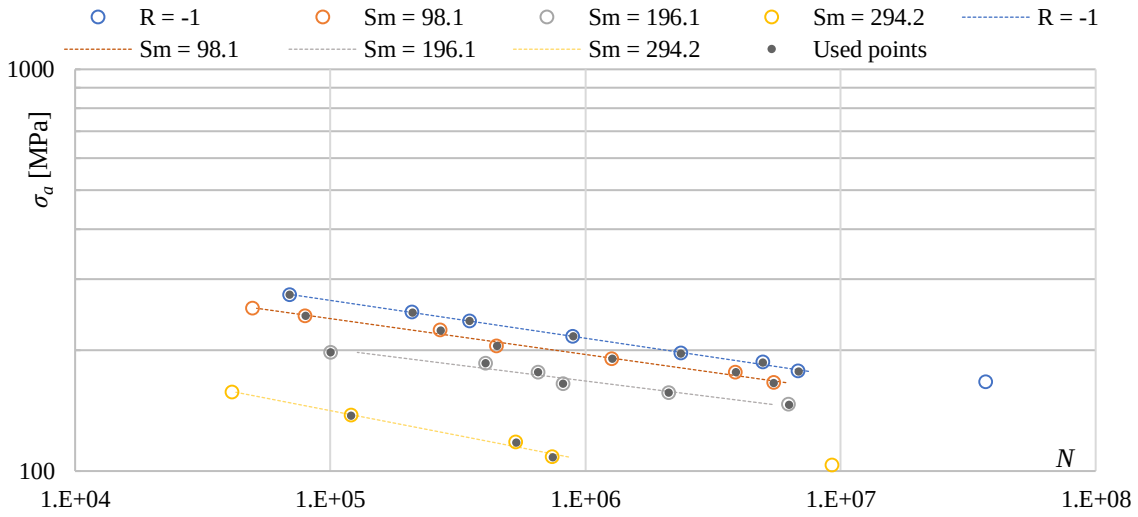

Figure 31 - AIS data set

Tra [15]

The report focuses on the fatigue properties of S.A.E. 4340 steel at various elevated temperatures. Two of the curves presented in the article (via graphs) are used in this thesis, as the experiments from which these curves are composed have been performed at room temperature and on unnotched specimens. Only two points of the ($R = 0$) curve have been used in this thesis, as lifetimes the other data points from this curve lie outside the interpolation area of the $R = -1$ curve. Although not rich, the data set remains valuable, as the mean stresses of the two aforementioned data points are quite high.

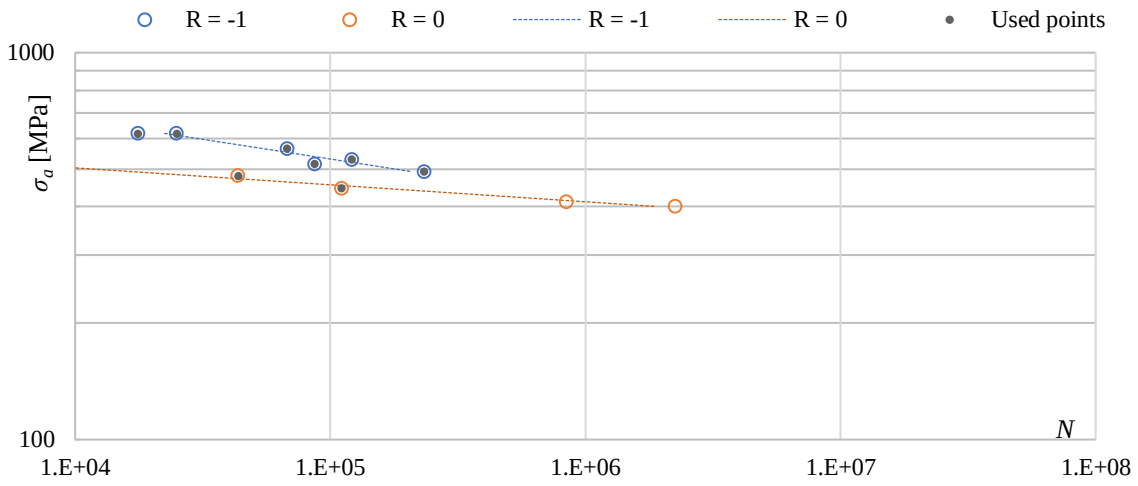

Figure 32 – Tra data set

LaB0x [10]

The data sets LaB01, LaB02 and LaB03 contain fatigue data based on experiments on extruded aluminum alloys 14-T6, 24-T4 and 75S-T6, respectively. All the data has been taken directly from result tables. LaB01 and LaB03 both contain 4 curves of constant stress ration *R* ranging from -1 to approximately 0.46, and although they do not have the (*R* = 0) curves available, their parameters have been approximated using the Kohout Věchet S-N curve model. LaB02 consists of two sole curves of stress ratios *R* = -1 and *R* = -0.37.

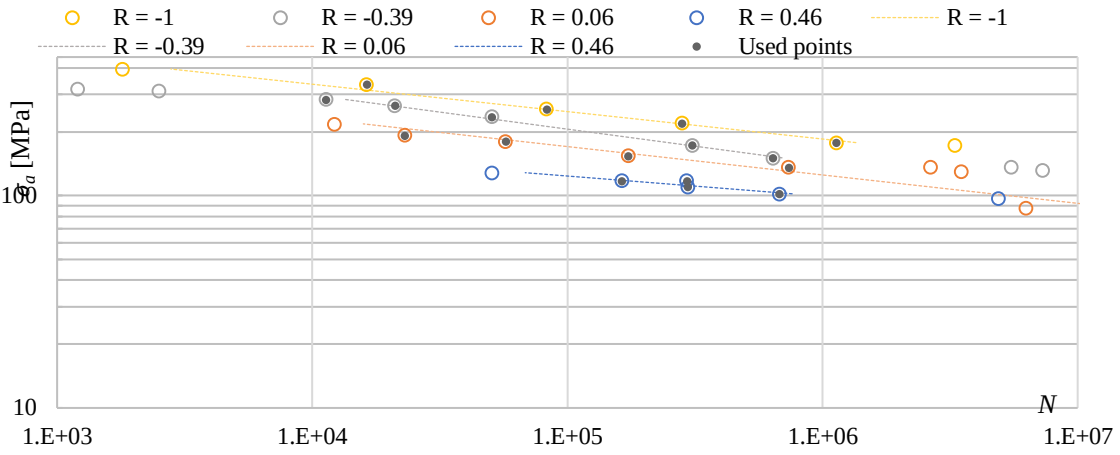

Figure 33 – LaB01 data set

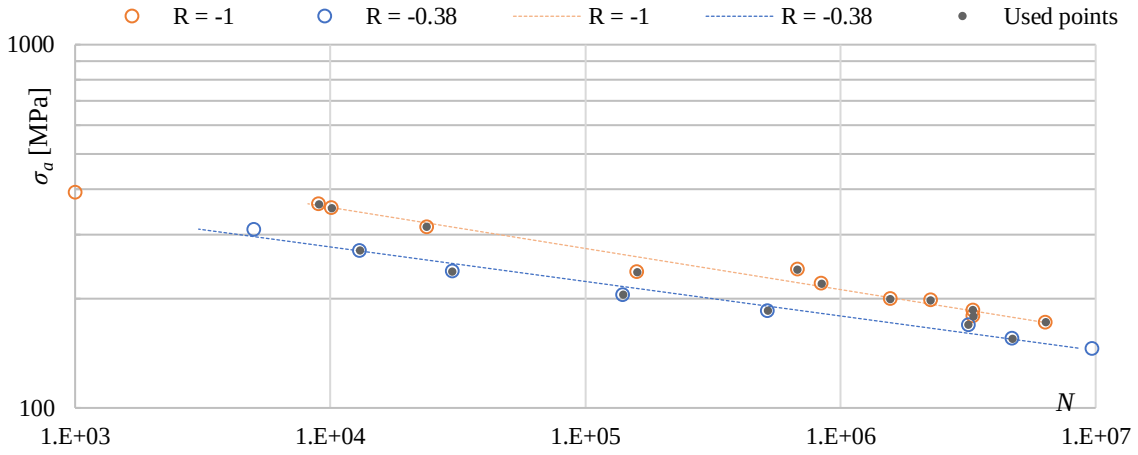

Figure 34 – LaB02 data set

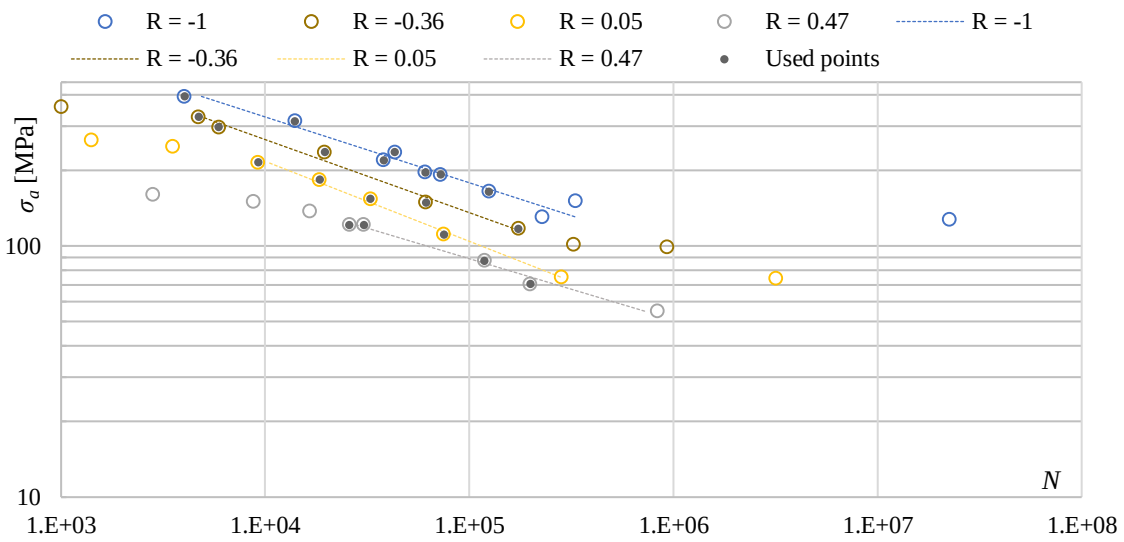

Figure 35 – LaB03 data set

BEL [2]

The thesis contains a large amount of fatigue data for the DTD 166B stainless steel in sheet form. The experiments on the unnotched specimens, presented in tables, are split into three groups in the original thesis, as they cover a different region of the S-N curve or use a different experimental procedure. The experiments have been performed on two different machines, which operate on different frequencies. As two of these groups contain mostly low cycle fatigue data, they have been omitted in this thesis. The set still contains a large amount of useable data (35 points used in this thesis), with the stress ratio R ranging from -1 to 0.5. Although the R = 0 curve is not present, it has been approximated using the Kohout-Věchet S-N curve model.

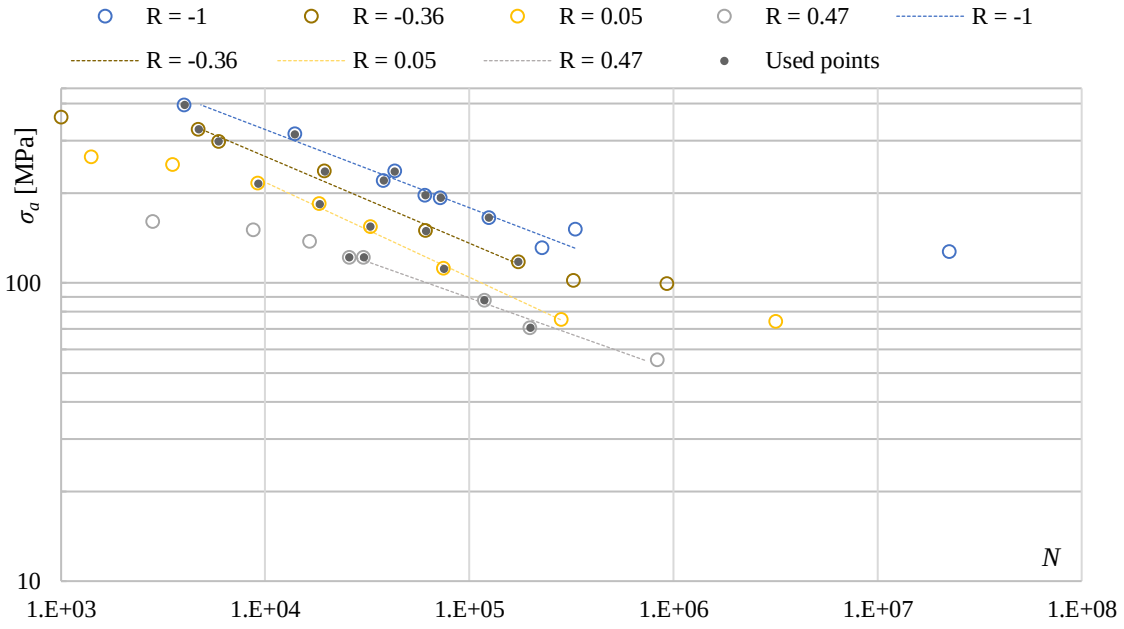

Figure 36 – BEL data set

3. PRACTICAL PART

In the practical part of this thesis, results achieved through the various approaches described in the theoretical parts will be presented and analyzed. In order to make the presented result tables more transparent, colors are applied to the cells, generally speaking, green for better results (in terms of fatigue life prediction accuracy), red for worse. Note that the color scales differ between presented tables, as different approaches often have result values of different orders of magnitude. Because of this, the color scale is chosen ad-hoc for each table in order to provide a suitable color contrast.

Some limitations are in place due to the nature of some of the approaches explored in this thesis – not all available data can be used for every model. These cases are described when the corresponding results are presented.

To be able to find some trends in the available results, they have been split into several categories based on properties of the experimental data that forms the foundation these results:

- R – the stress ratio, which can be used to, for example, filter out the points of the (R = -1) curve
- $N_{experiment}$ – the experimental fatigue life can help distinguish between results obtained in different domains of fatigue life
- R_e/R_m – both material parameters have effect on crack propagation, their ratio can be expected to have some sort of tie to fatigue life
- *Material type* – fatigue properties are known to differ across material types
- *Load type* – bending and tensile (push-pull) type loading has a large impact on the S-N curves

The 'Consistent' category shown in, for example, Table 4, denotes that the data sets from which results in this category have been obtained could have been used for every single analysis. This means that, for example, the Han set is not included, as it could not be used for unoptimized equivalent stress amplitude (and other) approaches based on the ultimate tensile strength R_m, as is noted in 2.1.

Note that whenever a table listing results of each available data set is presented (such as Table 3), the values in the bottom four rows (Mean, Max, Min, Standard Deviation) are calculated from the values in the table above them, not from the individual values of Δ_{FL} of each point. Also, when the loading type is given in the table, 'T' stands for tensile, 'B' for bending.

In tables where results of various different categories of data are presented (like in Table 4), the values are calculated from all the individual values of Δ_{FL} corresponding to data points contained in the groups defined in the leftmost columns in the table.

3.1 Analysis of achieved results

An overview of the available data

A summary of the available data is presented in Table 1. The 21 datasets sum up to a total of 667 useable experimental points. Most of the available data sets originate from tensile load type experiments. The features of the (R = 0) curve are unavailable to only 2 data sets, as for the rest, the said curve was either readily available, or could have been approximated ('Appr.' in Table 1) via the procedure described in 2.2. The materials are categorized by three broad groups – aluminum alloys, steels and cast irons, though the last group is only comprised of two data sets, while the aluminum alloy group is the most voluminous. Considering the ultimate tensile strength R_m and yield strength R_e, it can be seen that a large spectrum of materials of different strengths is available – see Figure 37.

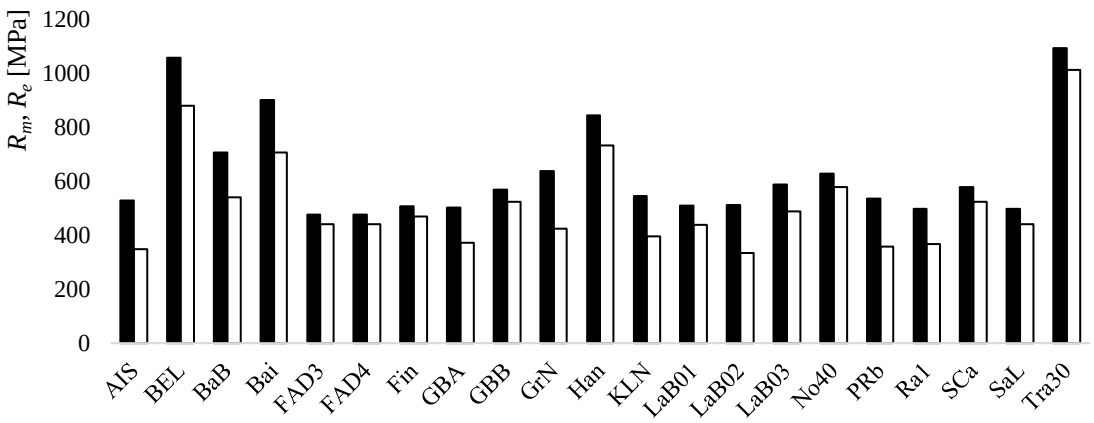

Figure 37 – the ultimate tensile strength R_m (black bars) and yield strength R_e (white bars) values of individual data sets

Set	Points	Load	(R = 0)	Material	Mat. type	R_m [MPa]	R_e [MPa]	σ_{FL-1} [MPa]	σ_{FL0} [MPa]	C_{-1} [MPa^W_{-1}]	W_{-1}	C_0 [MPa^W_0]	W_0	N_{FL}
AIS	22	T	Appr.	D16T	Al alloy	530	349	178	155	5.4E+30	10.6	2.2E+46	18.0	7.0E+06
BEL	35	T	Appr.	DTD 166B	Steel	1058	880	386	296	6.5E+20	5.9	2.4E+21	6.4	3.0E+05
BaB	22	T	Avail.	Ck35	Steel	706	539	318	255	2.6E+42	14.8	5.9E+55	20.9	3.0E+05
Bai	25	T	Avail.	34CrMo4	Steel	902	706	409	333	3.2E+41	13.8	2.8E+63	23.0	3.5E+05
FAD3	27	T	Avail.	2124-T851	Al alloy	477	440	139	119	1.6E+17	5.3	7.4E+25	9.6	8.0E+05
FAD4	30	T	Avail.	2424-T851	Al alloy	477	440	183	115	7.1E+23	7.9	4.1E+19	6.6	1.0E+06
Fin	25	B	Appr.	75S-T61	Al alloy	508	470	238	162	2.1E+28	9.5	2.6E+21	7.1	6.0E+05
GBA	68	T	Appr.	24S-T3	Al alloy	503	372	195	131	2.4E+20	6.4	1.1E+19	6.3	5.0E+05
GBB	58	T	Appr.	75S-T6	Al alloy	569	524	194	136	1.1E+18	5.5	2.9E+17	5.6	3.6E+05
GrN	26	T	Avail.	GGG-60	Cast iron	637	425	304	183	1.4E+31	10.3	3.3E+17	5.3	3.2E+05
Han	47	B	Appr.	SAE 4340	Steel	844	732	498	479	1.5E+24	6.9	5.4E+25	7.5	4.1E+05
KLN	49	B	No	2017A-T4	Al alloy	545	395	156	N/A	1.4E+23	7.6	N/A	N/A	3.0E+06
LaB01	17	T	Appr.	14S-T6	Al alloy	510	438	186	128	3.9E+24	8.2	5.7E+22	7.9	1.2E+06
LaB02	17	T	No	24S-T4	Al alloy	512	335	170	N/A	3.6E+26	8.8	N/A	N/A	7.0E+06
LaB03	20	T	Appr.	75S-T6	Al alloy	587	489	149	90	3.9E+13	3.8	3.4E+11	3.2	2.0E+05
No40	12	T	Avail.	JIS SPV 50	Steel	628	579	187	178	2.2E+17	4.8	9.4E+28	10.0	2.4E+06
PRb	27	B	Avail.	18G2A	Steel	535	357	258	205	1.3E+24	7.3	2.5E+31	10.7	4.0E+06
Ra1	44	T	Avail.	EN-GJV-450	Cast iron	498	368	177	121	1.8E+22	7.4	1.9E+25	9.4	5.0E+05
SCa	69	T	Avail.	7075-T6	Al alloy	579	524	228	157	7.9E+18	5.8	3.8E+18	6.1	1.5E+05
SaL	19	B	Appr.	14S-T	Al alloy	498	441	207	174	2.7E+30	10.2	3.5E+30	10.6	5.0E+06
Tra30	8	T	Avail.	SAE 4340	Steel	1093	1013	495	442	5.3E+31	9.8	4.9E+65	22.8	2.0E+05

Table 1 – Overview of the data available, with regard to the reduced fatigue limit approach N_{FL} limitation, 'T' stands for tensile loading, 'B' for bending

Equivalent stress amplitude – unoptimized

An (approximate but with a low enough error) solution to the implicitly given equation for the unoptimized Linear method (28) could have not been found for a total of 10 points. All of these points share a common trait – a high stress ratio R (resulting in extrapolation), see Table 2. Interestingly, the AIS data set contains a third point on the (σ_m = 294 MPa) curve with stress amplitude σ_a = 138 MPa, for which a solution was found, albeit with the lowest value Δ_{FL} = -0.28 of the whole data set, the following values being better by a whole order magnitude. A similar phenomenon can be seen in the FAD3 set, where 3 more points from the (R = 0.5) curve and 5 more points from the (R = 0.7) curve are available, for all of which, a solution has been found, while their stress amplitudes σ_a are higher than of their siblings in Table 2.

Set	σ_a [MPa]	σ_m [MPa]	R
AIS	118	294	0.43
AIS	108	294	0.46
FAD3	90	271	0.50
FAD3	86	257	0.50
FAD3	81	242	0.50
FAD3	73	219	0.50
FAD3	75	226	0.50
FAD3	62	351	0.70
No40	140	420	0.50
No40	140	420	0.50

Table 2 – List of points unsolved with the equivalent stress amplitude unoptimized Linear model

Comparability of the results of the unoptimized equivalent stress amplitude models could be considered to be questionable if these 10 points would not have been removed from the rest of the results. However, with such a small amount of missing points (1.5 % out of the total 667 points), the 10 points have been kept in the results of the other models in this group.

Furthermore, the unoptimized Walker and Linear methods could have not been applied to sets where the (R = 0) curve is unavailable and could have not been approximated either – the KLN and LaB02 sets. Also, the three unoptimized models which feature the ultimate tensile strength R_m could not have been applied to the Han data set, as the mean stresses present are often higher than said material parameter, which causes the equivalent stress amplitude $\sigma_{a,eq}$ to become negative.

In Table 3, two important numbers for the judgement of the qualities of the achieved results for each data set are shown – the mean and standard deviation value of Δ_{FL}. The mean value tells us around which values the achieved results are spread, with the amount of scatter being defined by the standard deviation – see 1.4. As has been noted in 1.9, a negative value of Δ_{FL} represents a non-conservative prediction, meaning that the predicted fatigue life $N_{predicted}$ is higher than the measured fatigue life $N_{experiment}$.

By looking at Table 3, it can be seen that of the models not utilizing the parameters of the ($R = 0$) curve (SWT, Goodman, Gerber, Dietmann), the SWT model does exhibit a trend of having the lowest standard deviation of Δ_{FL}, while its mean value of Δ_{FL} remains generally close to zero, veering slightly to the conservative side.

Data information				Mean value of Δ_{FL}						Standard deviation of Δ_{FL}					
Set	Points	Load	R_m [MPa]	Walk.	Lin.	SWT	Good.	Gerb.	Diet.	Walk.	Lin.	SWT	Good.	Gerb.	Diet.
AIS	22	T	530	-0.09	-0.01	0.04	0.09	-0.07	-0.03	0.27	0.07	0.06	0.07	0.08	0.08
BEL	35	T	1058	0.00	0.02	0.03	0.12	-0.02	-0.01	0.03	0.04	0.04	0.13	0.06	0.04
BaB	22	T	706	-0.04	0.00	0.08	0.39	-0.05	0.01	0.10	0.05	0.06	0.28	0.10	0.04
Bai	25	T	902	-0.01	0.00	0.04	0.25	-0.08	-0.02	0.06	0.04	0.08	0.21	0.10	0.06
FAD3	27	T	477	-0.11	-0.04	0.01	0.10	-0.03	-0.05	0.51	0.14	0.02	0.17	0.12	0.06
FAD4	30	T	477	0.00	0.02	-0.04	0.05	-0.14	-0.12	0.02	0.03	0.05	0.14	0.12	0.11
Fin	25	B	508	0.01	0.01	0.04	0.34	0.08	0.07	0.04	0.04	0.07	0.46	0.33	0.20
GBA	68	T	503	0.01	0.02	-0.01	0.06	-0.09	-0.07	0.04	0.04	0.05	0.07	0.08	0.07
GBB	58	T	569	-0.02	0.00	-0.02	0.06	-0.09	-0.08	0.05	0.04	0.05	0.12	0.09	0.08
GrN	26	T	637	0.00	0.00	-0.02	0.01	-0.09	-0.06	0.03	0.03	0.05	0.09	0.13	0.10
Han	47	B	844	-0.01	-0.01	0.12	N/A	N/A	N/A	0.04	0.04	0.10	N/A	N/A	N/A
KLN	49	B	545	N/A	N/A	-0.02	-0.04	-0.09	-0.07	N/A	N/A	0.04	0.05	0.08	0.06
LaB01	17	T	510	0.00	0.01	-0.01	0.05	-0.11	-0.08	0.03	0.04	0.03	0.08	0.08	0.07
LaB02	17	T	512	N/A	N/A	-0.01	0.00	-0.05	-0.03	N/A	N/A	0.04	0.03	0.08	0.05
LaB03	20	T	587	0.00	0.01	-0.01	-0.01	-0.07	-0.06	0.02	0.03	0.02	0.05	0.07	0.06
No40	12	T	628	0.29	0.00	0.03	0.06	0.00	0.01	0.67	0.02	0.04	0.08	0.03	0.02
PRb	27	B	535	-0.02	-0.02	-0.02	0.03	-0.05	-0.03	0.04	0.04	0.04	0.08	0.06	0.04
Ra1	44	T	498	0.00	0.02	-0.05	-0.02	-0.15	-0.13	0.06	0.09	0.07	0.07	0.13	0.11
SCa	69	T	579	0.00	0.00	-0.01	0.02	-0.06	-0.04	0.04	0.04	0.04	0.06	0.07	0.05
SaL	19	B	498	-0.01	0.00	0.09	0.25	0.06	0.07	0.04	0.03	0.07	0.27	0.14	0.09
Tra30	8	T	1093	0.00	0.00	0.04	0.08	0.01	0.02	0.03	0.03	0.07	0.16	0.02	0.05
Mean				0.00	0.00	0.01	0.09	-0.06	-0.03	0.11	0.05	0.05	0.13	0.10	0.07
Max				0.29	0.02	0.12	0.39	0.08	0.07	0.67	0.14	0.10	0.46	0.33	0.20
Min				-0.11	-0.04	-0.05	-0.04	-0.15	-0.13	0.02	0.02	0.02	0.03	0.02	0.02
Standard deviation				0.08	0.02	0.04	0.12	0.06	0.05	0.18	0.03	0.02	0.10	0.06	0.04

Table 3 - mean and standard deviation values of Δ_{FL} of the unoptimized equivalent stress amplitude approach methods for each available data set

Some conclusions can be made based on Table 4. The quality of the results of the SWT model is generally the best of the models in the table. The results improve moderately when only tensile load type data sets are considered (the bottom half of Table 4).

In Table 4, the Goodman and Gerber models show no strong trends when it comes to accuracy of predicted results. The Dietmann method does seem to fair quite well compared to the rest when it comes to steels, especially when looking at results of the tensile load type data sets only.

Data information			Mean value of Δ_{FL}				Standard dev. value of Δ_{FL}			
		Total points	SWT	Good.	Gerb.	Diet.	SWT	Good.	Gerb.	Diet.
	All	667	0.01	0.08	-0.07	-0.05	0.07	0.18	0.12	0.09
	Consistent	418	0.00	0.08	-0.07	-0.05	0.06	0.16	0.10	0.09
R	<-1;0>	460	0.00	0.03	-0.06	-0.03	0.06	0.11	0.09	0.07
	(-1;0>	242	0.01	0.07	-0.11	-0.06	0.07	0.15	0.09	0.08
	(0;1)	207	0.01	0.18	-0.09	-0.08	0.09	0.26	0.18	0.13
	(0;0.3>	108	0.03	0.13	-0.11	-0.08	0.10	0.25	0.16	0.12
	(0.3;1)	99	-0.01	0.22	-0.07	-0.09	0.07	0.26	0.19	0.14
N	<50 000	223	0.00	0.10	-0.07	-0.04	0.07	0.21	0.13	0.10
	<50 000;200 000>	233	0.01	0.08	-0.07	-0.06	0.07	0.19	0.12	0.09
	>200 000	211	0.02	0.05	-0.06	-0.05	0.07	0.14	0.11	0.09
R_e/R_m	<0.7	92	0.00	0.03	-0.06	-0.04	0.05	0.08	0.09	0.07
	<0.7;0.8>	208	-0.01	0.08	-0.10	-0.07	0.07	0.19	0.10	0.09
	<0.8;0.9>	138	0.06	0.11	-0.03	-0.02	0.08	0.17	0.10	0.08
	>0.9	229	-0.01	0.08	-0.06	-0.05	0.05	0.21	0.15	0.11
Material type	Al alloy	421	0.00	0.06	-0.07	-0.05	0.05	0.18	0.13	0.09
	Cast iron	70	-0.04	-0.01	-0.13	-0.11	0.06	0.08	0.13	0.11
	Steel	176	0.06	0.16	-0.04	-0.01	0.08	0.21	0.08	0.05
Load type	Tensile	500	0.00	0.07	-0.08	-0.06	0.06	0.15	0.10	0.08
	Bending	167	0.04	0.10	-0.02	-0.01	0.09	0.28	0.18	0.12
Tensile type loads only										
	All	500	0.00	0.07	-0.08	-0.06	0.06	0.15	0.10	0.08
	Consistent	372	0.00	0.08	-0.08	-0.06	0.06	0.16	0.10	0.08
R	<-1;0>	330	0.00	0.04	-0.06	-0.03	0.06	0.11	0.09	0.07
	(-1;0>	165	0.01	0.08	-0.12	-0.06	0.07	0.14	0.09	0.08
	(0;1)	170	-0.02	0.14	-0.12	-0.10	0.06	0.19	0.11	0.09
	(0;0.3>	77	-0.01	0.08	-0.14	-0.10	0.06	0.16	0.07	0.07
	(0.3;1)	93	-0.02	0.18	-0.10	-0.11	0.06	0.19	0.14	0.11
N	<50 000	207	-0.01	0.09	-0.08	-0.05	0.06	0.17	0.10	0.08
	<50 000;200 000>	181	0.00	0.07	-0.08	-0.06	0.05	0.15	0.10	0.08
	>200 000	112	0.01	0.05	-0.08	-0.06	0.06	0.11	0.11	0.10
R_e/R_m	<0.7	65	0.00	0.03	-0.07	-0.04	0.06	0.08	0.10	0.08
	<0.7;0.8>	159	0.00	0.11	-0.10	-0.07	0.08	0.20	0.11	0.09
	<0.8;0.9>	72	0.01	0.07	-0.06	-0.04	0.04	0.11	0.08	0.06
	>0.9	204	-0.01	0.05	-0.07	-0.06	0.05	0.12	0.10	0.08
Material type	Al alloy	328	-0.01	0.05	-0.08	-0.06	0.05	0.10	0.09	0.08
	Cast iron	70	-0.04	-0.01	-0.13	-0.11	0.06	0.08	0.13	0.11
	Steel	102	0.05	0.20	-0.04	0.00	0.06	0.22	0.08	0.05

Table 4 - mean and standard deviation values of Δ_{FL} of the unoptimized equivalent stress amplitude approach models for different categories of underlying experimental data

Consider Table 5, where the minimum values of Δ_{FL} are shown. This essentially gives information about the worst result achieved in terms of safety in regard to $\Delta_{FL.}$ Note that the color codification (Green – Good, Red – Bad) does not really apply here. These results are here mostly to emphasize the importance of applying some sort of a safety factor when making fatigue life predictions in practice. The aim in this thesis was to mainly judge the accuracy of achieved results. Due to the scattered nature of fatigue data, a high precision (in terms of minimizing the error in $\log_{10}(N)$) will, ideally, result in about 50 % of results on the conservative, and 50% of the results on the unconservative side.

Logically, of the four models not utilizing the (R = 0) curve (SWT, Goodman, Gerber, Dietmann), Goodman's model tends to give the most conservative results – see Figure 10. As the Dietmann model tends to be more conservative than the Gerber model for lower mean stress σ_m values, it does show overall slightly higher values.

Data information				Minimum values of Δ_{FL}					
Set	Points	Load	R_m [MPa]	Walk.	Lin.	SWT	Good.	Gerb.	Diet.
AIS	22	T	530	-1.00	-0.28	-0.06	-0.01	-0.27	-0.24
BEL	35	T	1058	-0.10	-0.10	-0.10	-0.10	-0.14	-0.10
BaB	22	T	706	-0.32	-0.15	-0.03	-0.03	-0.21	-0.04
Bai	25	T	902	-0.20	-0.15	-0.15	-0.07	-0.29	-0.21
FAD3	27	T	477	-1.42	-0.57	-0.04	-0.06	-0.20	-0.17
FAD4	30	T	477	-0.05	-0.04	-0.18	-0.23	-0.45	-0.41
Fin	25	B	508	-0.08	-0.05	-0.05	-0.03	-0.19	-0.13
GBA	68	T	503	-0.09	-0.09	-0.13	-0.10	-0.25	-0.23
GBB	58	T	569	-0.18	-0.10	-0.19	-0.10	-0.29	-0.24
GrN	26	T	637	-0.07	-0.07	-0.13	-0.11	-0.34	-0.27
Han	47	B	844	-0.17	-0.16	-0.05	N/A	N/A	N/A
KLN	49	B	545	N/A	N/A	-0.10	-0.14	-0.25	-0.21
LaB01	17	T	510	-0.05	-0.06	-0.06	-0.09	-0.20	-0.18
LaB02	17	T	512	N/A	N/A	-0.08	-0.07	-0.20	-0.14
LaB03	20	T	587	-0.02	-0.03	-0.06	-0.11	-0.20	-0.17
No40	12	T	628	-0.03	-0.03	-0.03	-0.03	-0.05	-0.03
PRb	27	B	535	-0.12	-0.13	-0.11	-0.07	-0.18	-0.14
Ra1	44	T	498	-0.16	-0.16	-0.17	-0.16	-0.34	-0.33
SCa	69	T	579	-0.15	-0.15	-0.15	-0.15	-0.22	-0.18
SaL	19	B	498	-0.09	-0.07	-0.05	-0.05	-0.05	-0.05
Tra30	8	T	1093	-0.04	-0.04	-0.04	-0.04	-0.04	-0.04
Mean				-0.23	-0.13	-0.09	-0.09	-0.22	-0.17
Max				-0.02	-0.03	-0.03	-0.01	-0.04	-0.03
Min				-1.42	-0.57	-0.19	-0.23	-0.45	-0.41
Standard deviation				0.36	0.13	0.05	0.05	0.10	0.10

Table 5 – minimum values of Δ_{FL} of the unoptimized equivalent stress amplitude approach methods for each available data set

Referring back to Table 3, the Walker and Linear models that utilize the parameters of the (R = 0) curve overall seem to provide a high level of prediction accuracy, with some noticeable spikes however (AIS, BaB, FAD3, No40, Ra1). Note that although the Linear model seems to fair substantially better than Walker's model when it comes to the AIS, FAD3 and No40 data sets, it was said that some points from these sets have not been solved through the unoptimized Linear method, meaning that the problematic points have only been taken into account when judging the accuracy of the Walker method. An

additional problem comes from the fact that these two models are also used here to make fatigue life predictions on points belonging to the (R = 0) curve. These prediction are quite meaningless, as a description of the (R = 0) has to be known in order to utilize these two models, and when a life prediction is made for such points, these two quite complex models reduce back to the power law model of the known curve, see 1.6 - Unoptimized models.

In order to judge qualities of the unoptimized Walker and Linear equivalent stress amplitude models in a fair way, the summarizing result tables have to be constructed from data with the problematic points exempted. In Table 6, points for which a solution using the unoptimized Linear model was not found have also been removed from the results of the Walker model. The number of missing points due to this problem, and also the amount of remaining points after removing any (R = -1) and (R = 0) points is shown in the rightmost two columns. Here you can also see that for the No40 set, no results are presented when all points from these two curves are removed, as the remaining 2 points have not been solved using the linear model.

From Table 6, we can see that interestingly, the quality of the fatigue life prediction does not get drastically affected for the Walker and Linear models when removing the points of the (R = -1) and (R = 0) curves. Also, the data sets where the parameters of the (R = 0) curve, which are essential for the unoptimized Walker and Linear models, have been approximated, do not show signs of producing worse results. For most of the available data sets, the results of both models are quite similar, for the AIS, BaB and FAD3 data sets however, the Linear model does produce noticeably better results. This seems to be due to the fact that the Walker model produces generally worse results when extrapolating outside the two defining curves compared to the Linear model – see Figure 38. Values of R greater than 0 are extrapolated.

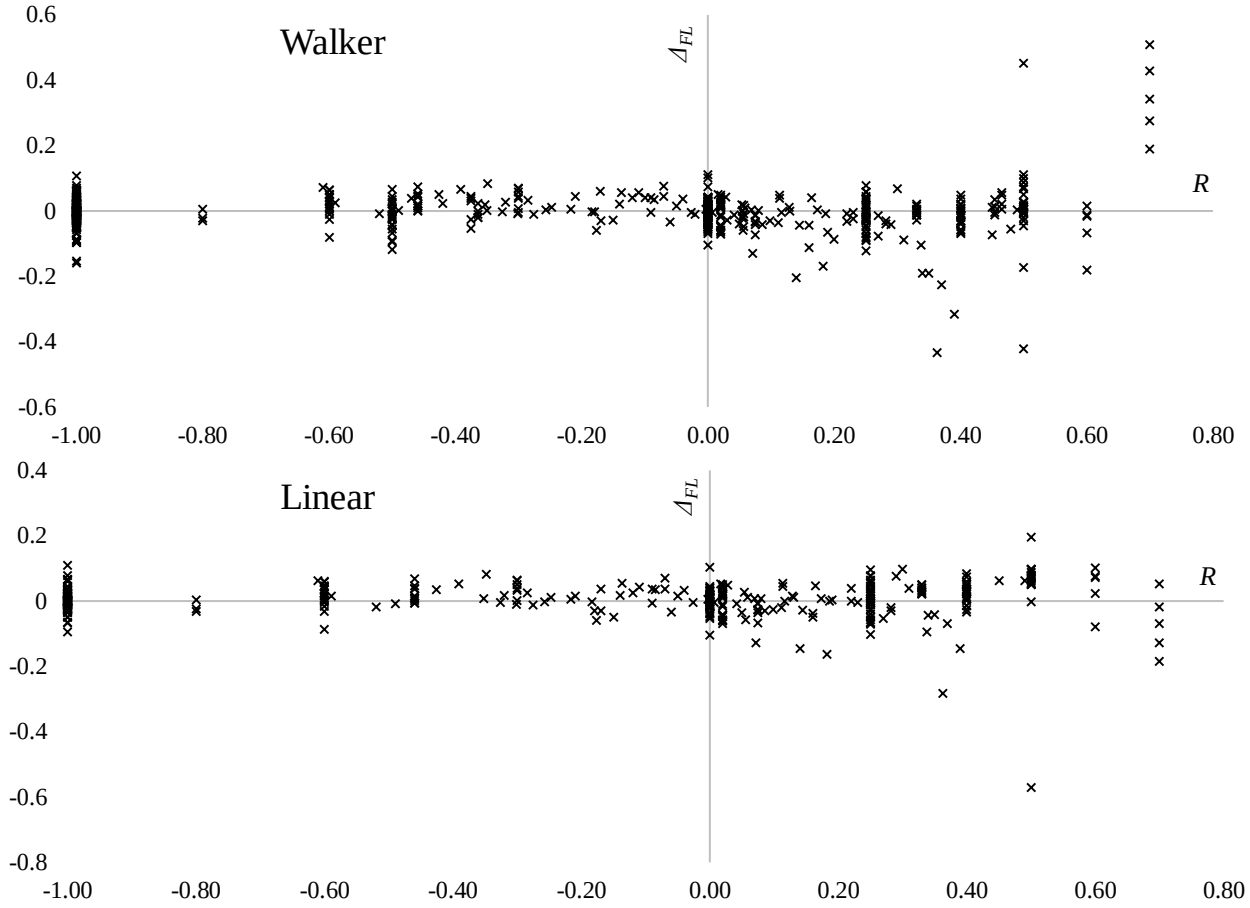

Figure 38 - Δ_{FL} of individual points plotted against the stress ratio R

Data information						Mean value of Δ_{FL}				Standard dev. of Δ_{FL}				Points		
Set	Load	C_{-1}	W_{-1}	C_0	W_0	Walk.	Lin.	Walk.*	Lin.*	Walk.	Lin.	Walk.*	Lin.*	Orig.	Excl. R = -1/0	Unsolv.
AIS	T	5.4E+30	10.6	2.2E+46	18.0	-0.01	-0.01	-0.02	-0.01	0.10	0.07	0.13	0.09	22	15	2
BEL	T	6.5E+20	5.9	2.4E+21	6.4	0.00	0.02	0.01	0.02	0.03	0.04	0.03	0.04	35	27	0
BaB	T	2.6E+42	14.8	5.9E+55	20.9	-0.04	0.00	-0.07	0.00	0.10	0.05	0.14	0.07	22	11	0
Bai	T	3.2E+41	13.8	2.8E+63	23.0	-0.01	0.00	-0.04	-0.02	0.06	0.04	0.09	0.07	25	8	0
FAD3	T	1.6E+17	5.3	7.4E+25	9.6	0.07	-0.04	0.20	-0.08	0.22	0.14	0.33	0.23	27	14	6
FAD4	T	7.1E+23	7.9	4.1E+19	6.6	0.00	0.02	0.01	0.06	0.02	0.03	0.02	0.03	30	10	0
Fin	B	2.1E+28	9.5	2.6E+21	7.1	0.01	0.01	0.01	0.01	0.04	0.04	0.03	0.04	25	19	0
GBA	T	2.4E+20	6.4	1.1E+19	6.3	0.01	0.02	0.01	0.02	0.04	0.04	0.04	0.04	68	54	0
GBB	T	1.1E+18	5.5	2.9E+17	5.6	-0.02	0.00	-0.02	0.00	0.05	0.04	0.05	0.05	58	52	0
GrN	T	1.4E+31	10.3	3.3E+17	5.3	0.00	0.00	N/A	N/A	0.03	0.03	N/A	N/A	26	0	0
Han	B	1.5E+24	6.9	5.4E+25	7.5	-0.01	-0.01	-0.01	-0.01	0.04	0.04	0.05	0.05	47	34	0
KLN	B	1.4E+23	7.6	N/A	N/A	N/A	N/A	N/A	N/A	N/A	N/A	N/A	N/A	N/A	N/A	N/A
LaB01	T	3.9E+24	8.2	5.7E+22	7.9	0.00	0.01	0.00	0.02	0.03	0.04	0.03	0.05	17	13	0
LaB02	T	3.6E+26	8.8	N/A	N/A	N/A	N/A	N/A	N/A	N/A	N/A	N/A	N/A	N/A	N/A	N/A
LaB03	T	3.9E+13	3.8	3.4E+11	3.2	0.00	0.01	0.01	0.01	0.02	0.03	0.03	0.03	20	13	0
No40	T	2.2E+17	4.8	9.4E+28	10.0	0.00	0.00	N/A	N/A	0.02	0.02	N/A	N/A	12	2	2
PRb	B	1.3E+24	7.3	2.5E+31	10.7	-0.02	-0.02	-0.07	-0.08	0.04	0.04	0.03	0.03	27	8	0
Ra1	T	1.8E+22	7.4	1.9E+25	9.4	0.00	0.02	0.04	0.14	0.06	0.09	0.05	0.05	44	11	0
SCa	T	7.9E+18	5.8	3.8E+18	6.1	0.00	0.00	0.01	0.00	0.04	0.04	0.03	0.03	69	15	0
SaL	B	2.7E+30	10.2	3.5E+30	10.6	-0.01	0.00	-0.01	0.00	0.04	0.03	0.04	0.03	19	13	0
Tra30	T	5.3E+31	9.8	4.9E+65	22.8	0.00	0.00	N/A	N/A	0.03	0.03	N/A	N/A	8	0	0
Mean						0.00	0.00	0.00	0.00	0.05	0.05	0.07	0.06			
Max						0.07	0.02	0.20	0.14	0.22	0.14	0.33	0.23			
Min						-0.04	-0.04	-0.07	-0.08	0.02	0.02	0.02	0.03			
Standard deviation						0.02	0.02	0.06	0.05	0.05	0.03	0.08	0.05			

Table 6 - mean and standard deviation values of Δ_{FL} of the unoptimized equivalent stress amplitude approach Walker and Linear models for each available data set, the three rightmost columns give information on missing points, the '*' mark means that the results in the respective column have the points with R = -1 and R = 0 removed, set names in bold letters indicate that the parameters of the (R = 0) curve have been approximated

The fact that the extrapolated values, at least in the $R \in (0; 0.3)$, region do not however generally show behavior of being less accurate compared to the interpolated values can be considered to be unexpected. What seems to have a bigger impact on the quality of produced results is the scale of change in the values of the defining parameters of the S-N curve, namely *C* and *W*. This change has been quantified as $\log_{10} C_0 \,/\, \log_{10} C_{-1}$ and W_0/W_{-1}. For both the Walker and Linear model, it can be seen from Figure 39 that there is a tendency of producing more scattered result with the increase in the ratio of these two parameters (no matter which one).

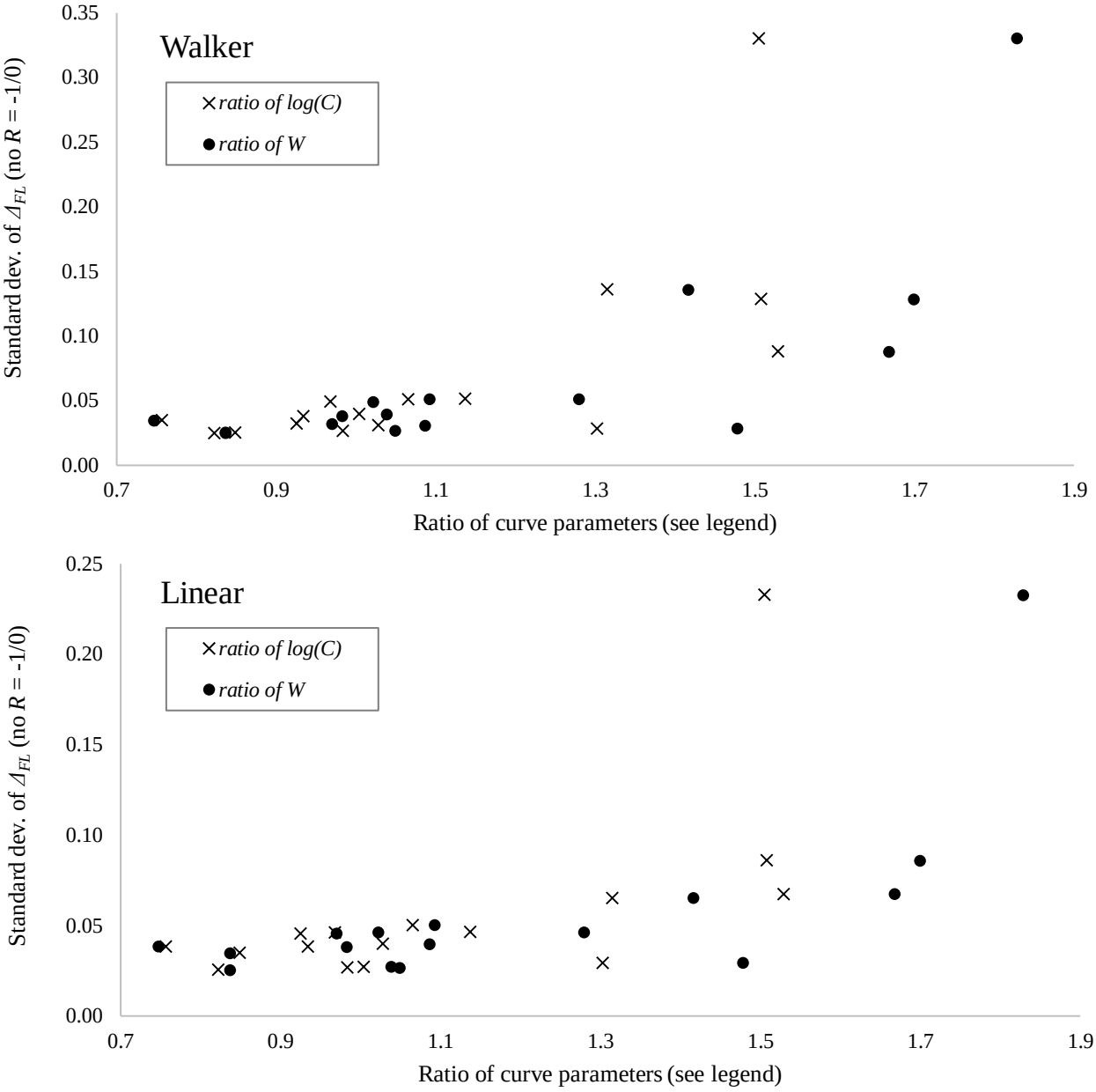

Figure 39 – the values of standard deviations of Δ_{FL} of individual data sets plotted against ratios of values the power law model constants defining the (R = -1) and (R = 0) curves

Reduced fatigue limit – unoptimized

The Han data set results are not available for any of the unoptimized reduced fatigue limit models. The problem is, in essence, the same as with the unoptimized equivalent stress amplitude approach, where the models based on the ultimate tensile strength R_m could not be used, as in the Han data set, the mean stress σ_m often exceeds the ultimate tensile strength R_m. In the unoptimized reduced fatigue limit approach however, this causes a problem before any particular model is even considered, as the leftmost point of the ($\sigma_m > 0$) curve is vertically shifted into a negative value – see Figure 7.

The results of the FEMFAT, Linear and Haibach models are unavailable for the KLN and LaB02 datasets, as these are missing the parameters of the ($R = 0$) curve, which are necessary for said models.

Furthermore, 4 points are excluded from the results of the FEMFAT and Linear model results for the FAD4 and LaB03 data sets, as both of these sets contain 4 points of mean stress σ_m greater than the intercepting point of the two models with the horizontal axis in the Haigh diagram – see Figure 11 and Figure 12. This leaves the reduced fatigue limit $\sigma_{FL,red}$ undefined for these specific 8 points.

It is also worth noting that in some cases, the results obtained from the Linear and FEMFAT models are exactly the same. This happens for one of two reasons.

As has been noted in 1.7 - Unoptimized models, the lower mean stress line of the FEMFAT model is, in the Haigh diagram, identical to the Linear model. The value of the mean stress σ_m at the point where the Linear model intercepts the horizontal axis can be lower than the breaking point σ_m^* - see Figure 12. When this occurs, the breaking point of the line in the Haigh diagram of the FEMFAT model is not present at all, making the single straight line identical to that of the line in the Haigh diagram of the Linear model.

Another scenario exists, where the maximum mean stress σ_m value in a data set is lower than the breaking point σ_m^* of the FEMFAT model. This causes all the reduced fatigue limit $\sigma_{FL,red}$ values to be calculated from the lower mean stress σ_m segment of the FEMFAT model, which, as has been noted, is identical to the Linear model.

For a summarization where either of these two cases are present, see Table 7.

Set	No breaking point in the FEMFAT model	No mean stress greater than σ_m^*
AIS		
BEL		
BaB		
Bai		
FAD3		
FAD4	x	
Fin		
GBA		
GBB	x	
GrN		x
Han		
KLN	N/A	
LaB01	x	
LaB02	N/A	
LaB03	x	
No40		
PRb		
Ra1		x
SCa	x	
SaL		
Tra30		x

Table 7 – A summary of the cases where the results from the Linear and FEMFAT models are identical

Similar behavior could also be expected from the Haibach model, namely if the maximum stress σ_m of a data set would be lower than the fatigue limit σ_{FL0} of the (R = 0) curve, see Figure 13. This would cause the results to, again, be the same as for the Linear model, since the lowest mean stress σ_m segment of the Haibach model is identical to the line created by the Linear model. This is, however, not the case for any of the data sets used in this thesis.

In Table 8 and Table 9, there were originally two columns in the mean value and standard deviation sections for each of the models. One corresponding to the original values which are calculated via the method described in 1.3 - Reduced fatigue limit approach, and one corresponding to the values obtained through shifting the predicted fatigue lives via the procedure in 1.8 - FEMFAT shift. However, there was very little difference in the mean and standard deviation values of Δ_{FL} (only 0.02 in the extremes for both).

Many trends observable in Table 9 seem to be applicable to generally all the available unoptimized reduced fatigue models, except for Haibach. This can be attributed the unusual Haigh diagram (compared to the other used models in this thesis) of the said model.

Looking at the upper part of Table 9 where the tensile and bending load type experimental fatigue data are mixed, a large drop in the accuracy of the prediction (based on the standard deviation of Δ_{FL}) is visible with an increase in the stress ratio R. For Smith's model however, this drop is less pronounced. The mean value of Δ_{FL} however remains largely on the conservative side, except for the Haibach model, as the results produced by it start becoming quite unconservative in the high stress ratio R region.

The accuracy of all the models seems to generally decrease with the increase in the material parameter ratio of R_e/R_m, again, except for Haibach model, which shows mixed results in this regard.

All results may seem to generally improve when the models are applied to cast irons, however, this may be attributed to the fact that the two only available cast iron data sets in this thesis are also of the tensile type loading. Glancing at the results split into the bending and tensile loading type categories, it is quite obvious that accuracy generally improves for the latter type. The reason for this may be the fact that the assumption that break will occur when stress reaches the ultimate tensile strength R_m, which is rooted in the basis of the unoptimized reduced fatigue limit models (except for Linear and Haibach), while also leaving a footprint in the core of the reduced fatigue limit approach (see Figure 7), is not correct when considering bending and not tensile type loading. Following the trend of breaking trends, Haibach's model does seem to give improved results for bending compared to tensile type loads.

Moving on to the lower half of Table 9 (where only tensile load type data sets are present), it seems that the trend of decreased accuracy with higher values of the stress ratio R is less pronounced. Noticeably however, the results of the Gerber model have shifted to the non-conservative side. Also, even though overall results of the Haibach model are worse for purely tensile load type data sets, a noticeable improvement in the $R \in (0; 0.3 >$ region is visible.

Results of all models have improved considerably for the data sets with high ratios of R_e/R_m, except for the Haibach model, which shows mixed results.

Overall, the Gerber model tends to give unconservative results. The Goodman model provides more accurate, and also, more conservative results in comparison. Smith's model shows a slight increase in the standard deviation of Δ_{FL}, while moving the results largely to the conservative side.

While the FEMFAT and Linear models require the parameters of the (R = 0) curve which makes them generally more demanding input-data wise, they show similar standard deviations of Δ_{FL} like Goodman. Compared to the Linear model however, the other two tend to provide more conservative results.

A good generalization of the Haibach model, is that it breaks the rules set by the rest. The fact that the means of Δ_{FL} tend to be generally close to zero loses value as the standard deviation of Δ_{FL} is generally

quite high. Along with the model of Smith, Haibach's model does seem to show some merit when the results of the bending type load sets are observed compared to the rest of the models.

Data information					Mean value of Δ_{FL}						Standard dev. of Δ_{FL}					
Set	Points	Load	σ_{FL-1}	σ_{FL0}	Good.	Gerb.	Smith	FEM.	Lin.	Haib.	Good.	Gerb.	Smith	FEM.	Lin.	Haib.
AIS	22	T	178	155	0.09	-0.05	0.17	-0.01	-0.06	-0.10	0.07	0.09	0.13	0.04	0.15	0.23
BEL	35	T	386	296	0.15	0.05	0.19	0.12	0.12	0.03	0.16	0.14	0.17	0.14	0.14	0.07
BaB	22	T	318	255	0.39	0.12	0.49	0.25	0.13	-0.30	0.28	0.25	0.31	0.28	0.22	0.88
Bai	25	T	409	333	0.25	0.04	0.34	0.11	0.07	0.03	0.22	0.12	0.27	0.15	0.09	0.08
FAD3	27	T	139	119	0.15	0.05	0.20	0.05	-0.16	-0.44	0.24	0.31	0.22	0.34	0.41	2.25
FAD4	30	T	183	115	0.07	-0.13	0.16	0.14	0.14	0.07	0.18	0.27	0.16	0.14	0.14	0.14
Fin	25	B	238	162	0.42	1.15	0.38	0.41	0.41	0.13	0.62	2.85	0.41	0.60	0.59	0.46
GBA	68	T	195	131	0.08	-0.06	0.15	0.12	0.12	0.06	0.10	0.13	0.11	0.11	0.11	0.08
GBB	58	T	194	136	0.09	-0.03	0.15	0.13	0.13	0.02	0.16	0.20	0.14	0.16	0.16	0.12
GrN	26	T	304	183	0.01	-0.12	0.06	0.05	0.05	0.04	0.10	0.20	0.12	0.12	0.12	0.10
Han	47	B	498	479	N/A	N/A	N/A	N/A	N/A	N/A	N/A	N/A	N/A	N/A	N/A	N/A
KLN	49	B	156	N/A	-0.04	-0.09	0.00	N/A	N/A	N/A	0.05	0.08	0.04	N/A	N/A	N/A
LaB01	17	T	186	128	0.06	-0.10	0.14	0.12	0.12	0.03	0.09	0.12	0.12	0.13	0.13	0.07
LaB02	17	T	170	N/A	0.00	-0.03	0.02	N/A	N/A	N/A	0.03	0.05	0.05	N/A	N/A	N/A
LaB03	20	T	149	90	0.00	-0.06	0.04	0.06	0.06	0.04	0.06	0.09	0.06	0.08	0.08	0.05
No40	12	T	187	178	0.08	0.03	0.11	-0.07	-0.09	-0.13	0.11	0.06	0.13	0.14	0.19	0.29
PRb	27	B	258	205	0.05	0.01	0.07	0.03	0.03	0.02	0.11	0.12	0.11	0.12	0.11	0.11
Ra1	44	T	177	121	-0.02	-0.19	0.06	0.05	0.05	-0.05	0.07	0.17	0.11	0.12	0.12	0.07
SCa	69	T	228	157	0.03	-0.03	0.07	0.04	0.04	0.03	0.07	0.09	0.09	0.08	0.08	0.07
SaL	19	B	207	174	0.28	0.27	0.30	0.26	0.07	0.07	0.32	0.50	0.29	0.47	0.21	0.18
Tra30	8	T	495	442	0.09	0.03	0.11	0.01	0.01	0.00	0.17	0.07	0.21	0.04	0.04	0.03
Mean					0.11	0.04	0.16	0.10	0.07	-0.02	0.16	0.30	0.16	0.18	0.17	0.29
Max					0.42	1.15	0.49	0.41	0.41	0.13	0.62	2.85	0.41	0.60	0.59	2.25
Min					-0.04	-0.19	0.00	-0.07	-0.16	-0.44	0.03	0.05	0.04	0.04	0.04	0.03
Standard deviation					0.13	0.28	0.13	0.11	0.12	0.14	0.13	0.61	0.10	0.15	0.13	0.53

Table 8 – mean and standard deviation values of Δ_{FL} of the unoptimized reduced fatigue limit models for each available data set

Data information			Mean value of Δ_{FL}						Standard deviation of Δ_{FL}					
		Total points	Good.	Gerb.	Smith	FEM.	Lin.	Haib.	Good.	Gerb.	Smith	FEM.	Lin.	Haib.
	All	667	0.09	0.02	0.15	0.11	0.08	-0.01	0.22	0.64	0.20	0.23	0.22	0.55
	Consistent	418	0.10	-0.02	0.15	0.10	0.09	0.01	0.18	0.21	0.19	0.18	0.13	0.23
R	<-1;0>	460	0.04	-0.03	0.08	0.04	0.04	0.03	0.12	0.14	0.14	0.10	0.10	0.11
	(-1;0>	242	0.08	-0.06	0.15	0.08	0.08	0.07	0.16	0.19	0.16	0.12	0.12	0.14
	(0;1)	207	0.22	0.12	0.30	0.24	0.16	-0.10	0.32	1.15	0.23	0.34	0.35	0.94
	(0;0.3>	108	0.16	0.07	0.23	0.17	0.16	0.05	0.30	1.20	0.22	0.27	0.27	0.19
	(0.3;1)	99	0.28	0.17	0.36	0.30	0.16	-0.23	0.32	1.10	0.23	0.38	0.42	1.27
N	<50 000	223	0.12	0.07	0.16	0.13	0.12	0.06	0.24	0.77	0.22	0.22	0.21	0.21
	<50 000;200 000>	233	0.10	0.02	0.15	0.12	0.09	-0.02	0.23	0.73	0.21	0.23	0.21	0.31
	>200 000	211	0.06	-0.05	0.11	0.06	0.00	-0.09	0.17	0.25	0.17	0.23	0.23	0.99
R_e/R_m	<0.7	92	0.04	-0.05	0.08	0.03	0.01	-0.01	0.09	0.14	0.12	0.10	0.13	0.16
	<0.7;0.8>	208	0.09	-0.06	0.15	0.12	0.10	-0.03	0.19	0.17	0.22	0.16	0.13	0.35
	<0.8;0.9>	138	0.13	0.04	0.17	0.14	0.10	0.04	0.20	0.28	0.20	0.25	0.15	0.10
	>0.9	229	0.11	0.10	0.15	0.11	0.09	-0.02	0.27	1.01	0.21	0.28	0.30	0.80
Material type	Al alloy	421	0.09	0.03	0.13	0.12	0.09	0.00	0.22	0.76	0.19	0.26	0.26	0.65
	Cast iron	70	-0.01	-0.16	0.06	0.05	0.05	-0.02	0.08	0.19	0.11	0.12	0.12	0.09
	Steel	176	0.18	0.05	0.23	0.10	0.07	-0.04	0.22	0.15	0.25	0.19	0.16	0.40
Load type	Tensile	500	0.09	-0.04	0.15	0.09	0.07	-0.02	0.17	0.18	0.18	0.16	0.18	0.58
	Bending	167	0.13	0.25	0.14	0.23	0.17	0.08	0.36	1.39	0.27	0.46	0.41	0.29
Tensile type loads only														
	All	500	0.09	-0.04	0.15	0.09	0.07	-0.02	0.17	0.18	0.18	0.16	0.18	0.58
	Consistent	372	0.09	-0.04	0.15	0.10	0.09	0.01	0.17	0.17	0.19	0.15	0.13	0.24
R	<-1;0>	330	0.04	-0.04	0.08	0.04	0.04	0.03	0.11	0.11	0.14	0.08	0.08	0.07
	(-1;0>	165	0.09	-0.07	0.17	0.07	0.07	0.05	0.14	0.14	0.16	0.09	0.09	0.08
	(0;1)	170	0.17	-0.05	0.27	0.19	0.13	-0.11	0.21	0.28	0.18	0.22	0.27	0.97
	(0;0.3>	77	0.10	-0.09	0.19	0.13	0.11	0.03	0.16	0.16	0.16	0.13	0.11	0.09
	(0.3;1)	93	0.23	-0.01	0.33	0.24	0.14	-0.23	0.22	0.34	0.18	0.26	0.35	1.30
N	<50 000	207	0.10	0.01	0.15	0.11	0.10	0.05	0.18	0.16	0.20	0.15	0.14	0.15
	<50 000;200 000>	181	0.09	-0.06	0.15	0.10	0.08	-0.03	0.17	0.18	0.18	0.17	0.14	0.31
	>200 000	112	0.06	-0.10	0.13	0.04	-0.01	-0.15	0.13	0.21	0.15	0.16	0.26	1.17
R_e/R_m	<0.7	65	0.04	-0.07	0.09	0.02	0.00	-0.02	0.09	0.15	0.12	0.09	0.14	0.18
	<0.7;0.8>	159	0.12	-0.05	0.20	0.12	0.10	-0.03	0.21	0.19	0.23	0.16	0.13	0.35
	<0.8;0.9>	72	0.09	-0.02	0.14	0.10	0.10	0.03	0.14	0.14	0.15	0.13	0.13	0.06
	>0.9	204	0.07	-0.03	0.13	0.07	0.05	-0.04	0.15	0.20	0.15	0.18	0.21	0.83
Material type	Al alloy	328	0.07	-0.05	0.12	0.09	0.07	-0.01	0.13	0.17	0.14	0.16	0.19	0.68
	Cast iron	70	-0.01	-0.16	0.06	0.05	0.05	-0.02	0.08	0.19	0.11	0.12	0.12	0.09
	Steel	102	0.21	0.06	0.28	0.11	0.08	-0.06	0.23	0.16	0.26	0.20	0.17	0.44

Table 9 – mean and standard deviation values of Δ_{FL} of the unoptimized reduced fatigue limit approach models for different categories of underlying experimental data

Finally, consider Table 10, where the minimum values of Δ_{FL} for each data set and unoptimized reduced fatigue model are shown. These values can be interpreted as the most "unsafe" fatigue life predictions made. Noticeably, not a single conservative value is present in the table, which means that at least one predicted fatigue life per model per data set has been unconservative. The shift of the fatigue based on [21] (see 1.8 - FEMFAT shift) has the potential to change this, as it always decreases the predicted fatigue life. This shift, however, is too small, as the largest change of the minimum Δ_{FL} values in Table 10 is 0.01. As expected, the Gerber model is nearly in all cases the most unconservative. On the other end of the spectrum, Smith's model provides, in general, the most conservative results, while also having the lowest standard deviation of the minimum Δ_{FL} values, meaning it is quite consistent in providing the most values around the mean value of unconservative Δ_{FL} = -0.05.

As has been noted before, the color coding here merely provides contrast to the table, and the (Red – Bad, Green – Good) scheme does not apply here, as minimum Δ_{FL} is not an indicator of fatigue life prediction accuracy.

Set	Minimum Δ_{FL}											
	Goodman		Gerber		Smith		FEMFAT		Linear		Haibach	
	Orig.	FEM.	Orig.	FEM.	Orig.	FEM.	Orig.	FEM.	Orig.	FEM.	Orig.	FEM.
AIS	-0.01	-0.01	-0.34	-0.34	-0.01	-0.01	-0.14	-0.14	-0.52	-0.51	-0.78	-0.77
BEL	-0.10	-0.10	-0.15	-0.15	-0.10	-0.10	-0.10	-0.10	-0.10	-0.10	-0.10	-0.10
BaB	-0.02	-0.02	-0.18	-0.18	-0.02	-0.02	-0.02	-0.02	-0.28	-0.28	-2.96	-2.95
Bai	-0.07	-0.07	-0.13	-0.13	-0.07	-0.07	-0.07	-0.07	-0.07	-0.07	-0.16	-0.16
FAD3	-0.06	-0.05	-0.29	-0.29	-0.01	-0.01	-0.30	-0.29	-2.05	-2.04	-11.28	-11.27
FAD4	-0.24	-0.24	-0.77	-0.77	-0.02	-0.02	-0.04	-0.03	-0.04	-0.03	-0.21	-0.20
Fin	-0.03	-0.03	-0.25	-0.25	-0.03	-0.03	-0.03	-0.03	-0.03	-0.03	-1.06	-1.05
GBA	-0.10	-0.10	-0.33	-0.33	-0.06	-0.06	-0.09	-0.09	-0.09	-0.09	-0.09	-0.09
GBB	-0.10	-0.09	-0.38	-0.38	-0.02	-0.02	-0.04	-0.03	-0.04	-0.03	-0.26	-0.25
GrN	-0.11	-0.11	-0.52	-0.52	-0.07	-0.07	-0.07	-0.07	-0.07	-0.07	-0.07	-0.07
Han	N/A	N/A	N/A	N/A	N/A	N/A	N/A	N/A	N/A	N/A	N/A	N/A
KLN	-0.14	-0.14	-0.26	-0.26	-0.07	-0.07	N/A	N/A	N/A	N/A	N/A	N/A
LaB01	-0.09	-0.09	-0.35	-0.34	-0.03	-0.03	-0.06	-0.06	-0.06	-0.06	-0.08	-0.07
LaB02	-0.07	-0.07	-0.13	-0.13	-0.07	-0.07	N/A	N/A	N/A	N/A	N/A	N/A
LaB03	-0.12	-0.11	-0.27	-0.27	-0.04	-0.04	-0.02	-0.02	-0.02	-0.02	-0.02	-0.02
No40	-0.03	-0.03	-0.03	-0.03	-0.03	-0.03	-0.41	-0.41	-0.54	-0.54	-0.80	-0.80
PRb	-0.06	-0.06	-0.14	-0.14	-0.05	-0.05	-0.10	-0.10	-0.10	-0.10	-0.10	-0.10
Ra1	-0.16	-0.16	-0.53	-0.52	-0.16	-0.16	-0.16	-0.16	-0.16	-0.16	-0.20	-0.19
SCa	-0.15	-0.15	-0.27	-0.27	-0.15	-0.15	-0.15	-0.15	-0.15	-0.15	-0.15	-0.15
SaL	-0.05	-0.05	-0.06	-0.06	-0.05	-0.05	-0.05	-0.05	-0.45	-0.45	-0.32	-0.32
Tra30	-0.04	-0.04	-0.04	-0.04	-0.04	-0.04	-0.04	-0.04	-0.04	-0.04	-0.04	-0.04
Mean	-0.09	-0.09	-0.27	-0.27	-0.05	-0.05	-0.11	-0.10	-0.27	-0.26	-1.04	-1.03
Max	-0.01	-0.01	-0.03	-0.03	-0.01	-0.01	-0.02	-0.02	-0.02	-0.02	-0.02	-0.02
Min	-0.24	-0.24	-0.77	-0.77	-0.16	-0.16	-0.41	-0.41	-2.05	-2.04	-11.28	-11.27
St. dev.	0.06	0.06	0.18	0.18	0.04	0.04	0.10	0.10	0.48	0.47	2.65	2.65

Table 10 - minimum values of Δ_{FL} of the unoptimized reduced fatigue limit models for each available data set, 'Orig.' means that the FEMFAT shift has not been applied to the results in the column, 'FEM.' means it has

Some of the values for the Linear and Haibach models are quite extreme. For the Linear model calculations on the data set FAD3, and for the Haibach model calculations on FAD3, BaB, Fin data sets, the $\sigma_{FL,red}$ and R_m-σ_m values were very close (difference of around 1 MPa in some cases) for some data points of high stress ratio R. This caused the corresponding curves of non-zero mean stress (see Figure 7) to become extremely flat, meaning that a change in σ_a of size 1 MPa meant a change in fatigue life of several orders of magnitude. In the cases of FAD3 and Fin, $\sigma_{FL,red}$ can actually be lower than R_m-σ_m. This leads to the creation of bizarre S-N curves, where the predicted fatigue life increases with the increase in stress amplitude σ_a.

Unoptimized reduced fatigue limit and equivalent stress approach results compared

As these two approaches have similar input data requirements, it makes sense to compare the achieved results. Strikingly, although the unoptimized equivalent stress amplitude approach is less robust, and though it requires lower number of input values from the user (there is no need to determine the fatigue limits σ_{FL} or the corresponding fatigue life N_{FL}), looking in the bottom rows of Table 11, it produces generally much less scatter in terms of precision of achieved results in comparison to its competitor. It is also objectively simpler to apply, as the calculation process is quite straightforward.

For information about what data could not be used for the results presented in this chapter, refer to the beginning of the earlier chapters where the results of the singled-out categories have been analyzed. Also, note that all the reduced fatigue limit approach results presented here are not subjected to the FEMFAT shift, as the difference in the results has been shown to be insignificant.

Consider the Goodman and Gerber models of both approaches. The reduced fatigue limit versions have been derived from their equivalent stress amplitude counterparts – see 1.5. Looking at the standard deviation values in Table 11, it can be seen that the equivalent stress amplitude versions of these two models provide generally more accurate results. Only in one case for the Goodman (KLN) and in one case for the Gerber model (LaB02), the reduced fatigue limit approach variants fair better. The difference, however, is quite insignificant.

If we compare the results between the two approaches row by row, the reduced fatigue limit approach fairs better than the equivalent stress approach only in two cases – for the AIS and KLN sets, again, only very negligibly. Overall, the standard deviation values are generally noticeably lower for the equivalent stress amplitude approach – see the mean values in the bottom rows of Table 11.

It is also worth noting that with the SWT model, which is arguably the simplest model to apply of the ones showcased in this chapter, it does provide some of the best results in terms of standard deviation of Δ_{FL}. In fact, only in the case of five data sets (AIS, Bai, KLN, LaB02, Tra30), some model from the reduced fatigue limit approach family achieved a better value. The difference between these results are all of order 10^{-2} or lower.

On the other hand, several instances where SWT fairs better in the order of 10^{-1} compared to the best results of the reduced fatigue limit approach for the same data set are present (BaB, FAD3, Fin, SaL).

Also, SWT is the single model that could be used for any of the data without restrictions.

Set	Standard deviation of Δ_{FL}											
	Eq. stress amplitude – unoptimized						Reduced fatigue limit – unoptimized					
	Walk.	Lin.	SWT	Good.	Gerb.	Diet.	Good.	Gerb.	Smith	FEM.	Lin.	Haib.
AIS	0.27	0.07	0.06	0.07	0.08	0.08	0.07	0.09	0.13	0.04	0.15	0.23
BEL	0.03	0.04	0.04	0.13	0.06	0.04	0.16	0.14	0.17	0.14	0.14	0.07
BaB	0.10	0.05	0.06	0.28	0.10	0.04	0.28	0.25	0.31	0.28	0.22	0.88
Bai	0.06	0.04	0.08	0.21	0.10	0.06	0.22	0.12	0.27	0.15	0.09	0.08
FAD3	0.51	0.14	0.02	0.17	0.12	0.06	0.24	0.31	0.22	0.34	0.41	2.25
FAD4	0.02	0.03	0.05	0.14	0.12	0.11	0.18	0.27	0.16	0.14	0.14	0.14
Fin	0.04	0.04	0.07	0.46	0.33	0.20	0.62	2.85	0.41	0.60	0.59	0.46
GBA	0.04	0.04	0.05	0.07	0.08	0.07	0.10	0.13	0.11	0.11	0.11	0.08
GBB	0.05	0.04	0.05	0.12	0.09	0.08	0.16	0.20	0.14	0.16	0.16	0.12
GrN	0.03	0.03	0.05	0.09	0.13	0.10	0.10	0.20	0.12	0.12	0.12	0.10
Han	0.04	0.04	0.10	N/A	N/A	N/A	N/A	N/A	N/A	N/A	N/A	N/A
KLN	N/A	N/A	0.04	0.05	0.08	0.06	0.05	0.08	0.04	N/A	N/A	N/A
LaB01	0.03	0.04	0.03	0.08	0.08	0.07	0.09	0.12	0.12	0.13	0.13	0.07
LaB02	N/A	N/A	0.04	0.03	0.08	0.05	0.03	0.05	0.05	N/A	N/A	N/A
LaB03	0.02	0.03	0.02	0.05	0.07	0.06	0.06	0.09	0.06	0.08	0.08	0.05
No40	0.67	0.02	0.04	0.08	0.03	0.02	0.11	0.06	0.13	0.14	0.19	0.29
PRb	0.04	0.04	0.04	0.08	0.06	0.04	0.11	0.12	0.11	0.12	0.11	0.11
Ra1	0.06	0.09	0.07	0.07	0.13	0.11	0.07	0.17	0.11	0.12	0.12	0.07
SCa	0.04	0.04	0.04	0.06	0.07	0.05	0.07	0.09	0.09	0.08	0.08	0.07
SaL	0.04	0.03	0.07	0.27	0.14	0.09	0.32	0.50	0.29	0.47	0.21	0.18
Tra30	0.03	0.03	0.07	0.16	0.02	0.05	0.17	0.07	0.21	0.04	0.04	0.03
Mean	0.11	0.05	0.05	0.13	0.10	0.07	0.16	0.30	0.16	0.18	0.17	0.29
Max	0.67	0.14	0.10	0.46	0.33	0.20	0.62	2.85	0.41	0.60	0.59	2.25
Min	0.02	0.02	0.02	0.03	0.02	0.02	0.03	0.05	0.04	0.04	0.04	0.03
St. dev.	0.18	0.03	0.02	0.10	0.06	0.04	0.13	0.61	0.10	0.15	0.13	0.53

Table 11 – standard deviation values of Δ_{FL} of the unoptimized reduced fatigue limit and equivalent stress amplitude models for each available data set

Now, consider the summary of the mean values of Δ_{FL}, presented in Table 12. The reduced fatigue limit approach models do tend to show more conservative values, while the values of the equivalent stress amplitude approach tend to generally be closer to zero. This, in conjunction with the standard deviation values of Δ_{FL} in Table 11, implies that the equivalent stress amplitude approach provides generally more accurate results than the reduced fatigue limit approach.

The unoptimized reduced fatigue limit approach obviously lacks in terms of accuracy compared to equivalent stress amplitude approach in this chapter. It is however worth to also look at the results from a safety standpoint. From Table 12, it is notable that the reduced fatigue limit approach models are generally on the conservative side, especially, the Goodman, Smith, FEMFAT and Linear models. All the underlying results are, however, still quite scattered, as has been shown through the standard deviation values of Δ_{FL}.

If we look at the standard deviation of the mean values of Δ_{FL}, it can be seen that for all the equivalent stress amplitude models, other than the Goodman model, the values are lower compared to any of the reduced fatigue limit approach models. This makes the results of the equivalent stress amplitude approach models more consistent, which could lead to a better establishment of some kind of a safety factor.

Set	Mean values of Δ_{FL}											
	Eq. stress amp. – unoptimized						Reduced fatigue limit – unoptimized					
	Walk.	Lin.	SWT	Good.	Gerb.	Diet.	Good.	Gerb.	Smith	FEM.	Lin.	Haib.
AIS	-0.09	-0.01	0.04	0.09	-0.07	-0.03	0.09	-0.05	0.17	-0.01	-0.06	-0.10
BEL	0.00	0.02	0.03	0.12	-0.02	-0.01	0.15	0.05	0.19	0.12	0.12	0.03
BaB	-0.04	0.00	0.08	0.39	-0.05	0.01	0.39	0.12	0.49	0.25	0.13	-0.30
Bai	-0.01	0.00	0.04	0.25	-0.08	-0.02	0.25	0.04	0.34	0.11	0.07	0.03
FAD3	-0.11	-0.04	0.01	0.10	-0.03	-0.05	0.15	0.05	0.20	0.05	-0.16	-0.44
FAD4	0.00	0.02	-0.04	0.05	-0.14	-0.12	0.07	-0.13	0.16	0.14	0.14	0.07
Fin	0.01	0.01	0.04	0.34	0.08	0.07	0.42	1.15	0.38	0.41	0.41	0.13
GBA	0.01	0.02	-0.01	0.06	-0.09	-0.07	0.08	-0.06	0.15	0.12	0.12	0.06
GBB	-0.02	0.00	-0.02	0.06	-0.09	-0.08	0.09	-0.03	0.15	0.13	0.13	0.02
GrN	0.00	0.00	-0.02	0.01	-0.09	-0.06	0.01	-0.12	0.06	0.05	0.05	0.04
Han	-0.01	-0.01	0.12	N/A	N/A	N/A	N/A	N/A	N/A	N/A	N/A	N/A
KLN	N/A	N/A	-0.02	-0.04	-0.09	-0.07	-0.04	-0.09	0.00	N/A	N/A	N/A
LaB01	0.00	0.01	-0.01	0.05	-0.11	-0.08	0.06	-0.10	0.14	0.12	0.12	0.03
LaB02	N/A	N/A	-0.01	0.00	-0.05	-0.03	0.00	-0.03	0.02	N/A	N/A	N/A
LaB03	0.00	0.01	-0.01	-0.01	-0.07	-0.06	0.00	-0.06	0.04	0.06	0.06	0.04
No40	0.29	0.00	0.03	0.06	0.00	0.01	0.08	0.03	0.11	-0.07	-0.09	-0.13
PRb	-0.02	-0.02	-0.02	0.03	-0.05	-0.03	0.05	0.01	0.07	0.03	0.03	0.02
Ra1	0.00	0.02	-0.05	-0.02	-0.15	-0.13	-0.02	-0.19	0.06	0.05	0.05	-0.05
SCa	0.00	0.00	-0.01	0.02	-0.06	-0.04	0.03	-0.03	0.07	0.04	0.04	0.03
SaL	-0.01	0.00	0.09	0.25	0.06	0.07	0.28	0.27	0.30	0.26	0.07	0.07
Tra30	0.00	0.00	0.04	0.08	0.01	0.02	0.09	0.03	0.11	0.01	0.01	0.00
Mean	0.00	0.00	0.01	0.09	-0.06	-0.03	0.11	0.04	0.16	0.10	0.07	-0.02
Max	0.29	0.02	0.12	0.39	0.08	0.07	0.42	1.15	0.49	0.41	0.41	0.13
Min	-0.11	-0.04	-0.05	-0.04	-0.15	-0.13	-0.04	-0.19	0.00	-0.07	-0.16	-0.44
St. dev.	0.08	0.02	0.04	0.12	0.06	0.05	0.13	0.28	0.13	0.11	0.12	0.14

Table 12 - mean values of Δ_{FL} of the unoptimized reduced fatigue limit and equivalent stress amplitude models for each available data set

Finally, the minimum values of Δ_{FL} are presented in Table 13. These can be interpreted as the worst case, and depending on the application, most dangerous fatigue life predictions made. There is not a single positive value in the main part of the table, which means that in order for the predictions to be safely useable in a practical design, some safety factor would still have to be applied in some part of the life prediction process.

Of the equivalent stress amplitude approach models, the SWT and Goodman models provide some of the highest results, meaning that their least conservative results are generally quite close to zero. The results of these two models are very similar. The Smith model of the reduced fatigue limit approach family, with the Goodman model coming in second, do provide some of the closest-to-zero minimum values of Δ_{FL}, even closer than the results coming from the mentioned equivalent stress amplitude models.

Again, however, if we look at the amount of scatter of the underlying results quantified by the standard deviation of Δ_{FL}, it does scale down the potential qualities of all the reduced fatigue limit approach models, including that of Smith.

Set	Minimum values of Δ_{FL}											
	Eq. stress amp. – unoptimized						Reduced fatigue limit - unoptimized					
	Walk.	Lin.	SWT	Good.	Gerb.	Diet.	Good.	Gerb.	Smith	FEM.	Lin.	Haib.
AIS	-1.00	-0.28	-0.06	-0.01	-0.27	-0.24	-0.01	-0.34	-0.01	-0.14	-0.52	-0.78
BEL	-0.10	-0.10	-0.10	-0.10	-0.14	-0.10	-0.10	-0.15	-0.10	-0.10	-0.10	-0.10
BaB	-0.32	-0.15	-0.03	-0.03	-0.21	-0.04	-0.02	-0.18	-0.02	-0.02	-0.28	-2.96
Bai	-0.20	-0.15	-0.15	-0.07	-0.29	-0.21	-0.07	-0.13	-0.07	-0.07	-0.07	-0.16
FAD3	-1.42	-0.57	-0.04	-0.06	-0.20	-0.17	-0.06	-0.29	-0.01	-0.30	-2.05	-11.28
FAD4	-0.05	-0.04	-0.18	-0.23	-0.45	-0.41	-0.24	-0.77	-0.02	-0.04	-0.04	-0.21
Fin	-0.08	-0.05	-0.05	-0.03	-0.19	-0.13	-0.03	-0.25	-0.03	-0.03	-0.03	-1.06
GBA	-0.09	-0.09	-0.13	-0.10	-0.25	-0.23	-0.10	-0.33	-0.06	-0.09	-0.09	-0.09
GBB	-0.18	-0.10	-0.19	-0.10	-0.29	-0.24	-0.10	-0.38	-0.02	-0.04	-0.04	-0.26
GrN	-0.07	-0.07	-0.13	-0.11	-0.34	-0.27	-0.11	-0.52	-0.07	-0.07	-0.07	-0.07
Han	-0.17	-0.16	-0.05	N/A	N/A	N/A	N/A	N/A	N/A	N/A	N/A	N/A
KLN	N/A	N/A	-0.10	-0.14	-0.25	-0.21	-0.14	-0.26	-0.07	N/A	N/A	N/A
LaB01	-0.05	-0.06	-0.06	-0.09	-0.20	-0.18	-0.09	-0.35	-0.03	-0.06	-0.06	-0.08
LaB02	N/A	N/A	-0.08	-0.07	-0.20	-0.14	-0.07	-0.13	-0.07	N/A	N/A	N/A
LaB03	-0.02	-0.03	-0.06	-0.11	-0.20	-0.17	-0.12	-0.27	-0.04	-0.02	-0.02	-0.02
No40	-0.03	-0.03	-0.03	-0.03	-0.05	-0.03	-0.03	-0.03	-0.03	-0.41	-0.54	-0.80
PRb	-0.12	-0.13	-0.11	-0.07	-0.18	-0.14	-0.06	-0.14	-0.05	-0.10	-0.10	-0.10
Ra1	-0.16	-0.16	-0.17	-0.16	-0.34	-0.33	-0.16	-0.53	-0.16	-0.16	-0.16	-0.20
SCa	-0.15	-0.15	-0.15	-0.15	-0.22	-0.18	-0.15	-0.27	-0.15	-0.15	-0.15	-0.15
SaL	-0.09	-0.07	-0.05	-0.05	-0.05	-0.05	-0.05	-0.06	-0.05	-0.05	-0.45	-0.32
Tra30	-0.04	-0.04	-0.04	-0.04	-0.04	-0.04	-0.04	-0.04	-0.04	-0.04	-0.04	-0.04
Mean	-0.23	-0.13	-0.09	-0.09	-0.22	-0.17	-0.09	-0.27	-0.05	-0.11	-0.27	-1.04
Max	-0.02	-0.03	-0.03	-0.01	-0.04	-0.03	-0.01	-0.03	-0.01	-0.02	-0.02	-0.02
Min	-1.42	-0.57	-0.19	-0.23	-0.45	-0.41	-0.24	-0.77	-0.16	-0.41	-2.05	-11.28
St. dev.	0.36	0.13	0.05	0.05	0.10	0.10	0.06	0.18	0.04	0.10	0.48	2.65

Table 13 - minimum values of Δ_{FL} of the unoptimized reduced fatigue limit and equivalent stress amplitude models for each available data set

Equivalent stress amplitude – 1(2) degrees of freedom

In the case of the Han data set, the results of the Klubberg model are not available, as the present mean stress values of σ_m are often higher than the ultimate tensile strength R_m. No other optimized equivalent stress amplitude model utilizes R_m, thus, this problem is isolated. No data points outside this case had to be exempted from the results in this chapter.

From Table 14, it can be seen that the optimized models have, in many cases, comparable results in terms of prediction accuracy. In general, the Gerber and Klubberg models do tend to have more scattered overall results. Although the exponential model is the only model that features not one but two optimization coefficients in this table, its results do not stand out, and are quite comparable to models like Walker, Kwofie, Bergmann, Linear, Dietmann or Haibach.

Data information				Standard deviation of Δ_{FL}								
Set	Points	Load	Mat. type	Walk.	Kwof.	Berg.	Lin.	Diett.	Gerb.	Exp.	Klubb.	Haib.
AIS	22	T	Al alloy	0.07	0.07	0.06	0.06	0.04	0.02	0.02	0.04	0.08
BEL	35	T	Steel	0.03	0.03	0.03	0.04	0.04	0.06	0.03	0.06	0.03
BaB	22	T	Steel	0.05	0.04	0.05	0.03	0.04	0.10	0.03	0.10	0.07
Bai	25	T	Steel	0.09	0.07	0.09	0.06	0.06	0.08	0.06	0.06	0.09
FAD3	27	T	Al alloy	0.02	0.03	0.02	0.05	0.07	0.09	0.03	0.12	0.04
FAD4	30	T	Al alloy	0.04	0.09	0.04	0.10	0.12	0.15	0.09	0.12	0.05
Fin	25	B	Al alloy	0.06	0.09	0.06	0.10	0.10	0.12	0.09	0.29	0.07
GBA	68	T	Al alloy	0.04	0.05	0.04	0.05	0.06	0.08	0.05	0.06	0.05
GBB	58	T	Al alloy	0.04	0.06	0.04	0.07	0.08	0.10	0.06	0.09	0.05
GrN	26	T	Cast iron	0.05	0.08	0.05	0.08	0.09	0.11	0.05	0.09	0.05
Han	47	B	Steel	0.04	0.04	0.04	0.04	0.04	0.04	0.04	N/A	0.04
KLN	49	B	Al alloy	0.04	0.04	0.04	0.04	0.04	0.05	0.04	0.04	0.04
LaB01	17	T	Al alloy	0.03	0.06	0.03	0.05	0.06	0.08	0.05	0.06	0.04
LaB02	17	T	Al alloy	0.04	0.03	0.04	0.03	0.03	0.04	0.03	0.03	0.04
LaB03	20	T	Al alloy	0.02	0.04	0.02	0.05	0.05	0.06	0.04	0.05	0.02
No40	12	T	Steel	0.03	0.02	0.03	0.02	0.02	0.02	0.02	0.03	0.03
PRb	27	B	Steel	0.04	0.04	0.04	0.04	0.05	0.06	0.02	0.05	0.04
Ra1	44	T	Cast iron	0.06	0.06	0.06	0.07	0.09	0.12	0.06	0.07	0.06
SCa	69	T	Al alloy	0.04	0.04	0.04	0.04	0.05	0.06	0.04	0.05	0.04
SaL	19	B	Al alloy	0.03	0.03	0.03	0.03	0.03	0.04	0.03	0.11	0.03
Tra30	8	T	Steel	0.02	0.02	0.02	0.02	0.02	0.02	0.02	0.02	0.02
Mean				0.04	0.05	0.04	0.05	0.06	0.07	0.04	0.08	0.05
Max				0.09	0.09	0.09	0.10	0.12	0.15	0.09	0.29	0.09
Min				0.02	0.02	0.02	0.02	0.02	0.02	0.02	0.02	0.02
Standard deviation				0.02	0.02	0.02	0.02	0.03	0.04	0.02	0.06	0.02

Table 14 – standard deviation values of Δ_{FL} of the optimized equivalent stress amplitude models for each available data set

More pronounced differences are visible in Table 15, where the mean values of Δ_{FL} are shown. The values tend to veer slightly to the unconservative side but are generally quite close to zero. The Gerber, Dietmann and Klubberg models do feature results that are less conservative compared to the other models listed in the table (with the Gerber model being the worst in this regard).

Data information				Mean values of Δ_{FL}								
Set	Points	Load	Mat. type	Walk.	Kwof.	Berg.	Lin.	Diett.	Gerb.	Exp.	Klubb.	Haib.
AIS	22	T	Al alloy	0.01	0.02	0.01	0.02	0.02	-0.01	0.00	0.01	0.01
BEL	35	T	Steel	0.00	0.00	0.00	0.00	-0.01	-0.03	0.00	-0.01	0.00
BaB	22	T	Steel	0.00	0.01	0.00	0.00	-0.01	-0.05	0.00	-0.02	0.01
Bai	25	T	Steel	-0.01	0.00	-0.01	0.00	-0.01	-0.02	-0.01	-0.01	-0.01
FAD3	27	T	Al alloy	0.00	-0.01	0.00	-0.02	-0.05	-0.06	0.00	-0.02	0.00
FAD4	30	T	Al alloy	0.00	0.00	0.01	-0.02	-0.06	-0.09	0.01	-0.01	0.01
Fin	25	B	Al alloy	0.01	0.00	0.00	-0.01	-0.03	-0.07	0.00	-0.05	0.01
GBA	68	T	Al alloy	0.01	0.01	0.01	0.00	-0.02	-0.04	0.01	0.00	0.01
GBB	58	T	Al alloy	0.00	0.00	0.00	-0.02	-0.04	-0.07	0.00	-0.01	0.01
GrN	26	T	Cast iron	0.00	-0.01	0.00	-0.01	-0.01	-0.02	0.00	-0.01	0.00
Han	47	B	Steel	0.00	0.00	0.00	0.00	0.00	-0.01	0.00	N/A	0.00
KLN	49	B	Al alloy	-0.01	-0.01	-0.01	-0.01	-0.01	-0.02	0.00	-0.01	-0.01
LaB01	17	T	Al alloy	0.00	0.01	0.00	0.00	-0.02	-0.05	0.00	-0.01	0.01
LaB02	17	T	Al alloy	0.00	0.00	0.00	0.00	0.00	0.00	0.00	0.00	0.00
LaB03	20	T	Al alloy	0.00	0.00	0.00	-0.01	-0.02	-0.04	0.00	-0.01	0.00
No40	12	T	Steel	0.00	0.00	0.00	0.00	0.00	-0.01	0.00	0.00	0.00
PRb	27	B	Steel	-0.01	-0.01	-0.01	-0.01	-0.02	-0.03	0.00	-0.01	-0.01
Ra1	44	T	Cast iron	-0.02	-0.01	-0.01	-0.03	-0.05	-0.07	-0.01	-0.02	-0.01
SCa	69	T	Al alloy	0.00	0.00	0.00	0.00	-0.01	-0.02	0.00	0.00	0.00
SaL	19	B	Al alloy	0.00	0.00	0.00	0.00	0.00	-0.02	0.00	-0.02	0.01
Tra30	8	T	Steel	0.00	0.00	0.00	0.00	0.00	0.00	0.00	0.00	0.00
Mean				0.00	0.00	0.00	-0.01	-0.02	-0.04	0.00	-0.01	0.00
Max				0.01	0.02	0.01	0.02	0.02	0.00	0.01	0.01	0.01
Min				-0.02	-0.01	-0.01	-0.03	-0.06	-0.09	-0.01	-0.05	-0.01
Standard deviation				0.01	0.01	0.01	0.01	0.02	0.03	0.00	0.01	0.01

Table 15 – mean values of Δ_{FL} of the optimized equivalent stress amplitude models for each available data set

In Table 16, the visible trends are not substantial enough to determine unique qualities of the available models, in other words, models with good results tend to generally stay true to these good results no matter what kind of filtering we apply to the underlying data. Let us examine the results of the upper half of the table.

Incrementation of the stress ratio R does seem to moderately reduce the quality of the results of the Dietmann, Gerber and Klubberg models. No pronounced trends are visible in the $N_{experimental}$ category, although the Klubberg model has gotten slightly better results in the highest life domain.

In terms of the material parameter ration R_e/R_m, it can be seen that the results of the models that have been based on the ultimate tensile strength R_m in their unoptimized variant (Linear, Dietmann, Gerber) and Klubberg (which is a hybrid model, weighing between the Goodman and Gerber model, both based on R_m) do seem to worsen when this ratio increases. Except for the Exponential and Kwofie model, the rest of the models do seem to achieve slightly better results with the increase of said ratio.

Some models (Linear, Dietmann, Gerber, Exponential) seem to give the larger values of standard deviation of Δ_{FL} for cast iron compared to the other two available material categories. Unfortunately, the data forming the cast iron group is comprised of only two data sets, which makes any assumptions about cast irons unsubstantiated. The Kwofie, Linear, Gerber, Dietmann and Klubberg models produce worse results for aluminum alloys compared to steels.

Interestingly, the load type does not seem to have a major impact on the results of the optimized equivalent stress amplitude models, with a few exceptions. The most prominent one is the Klubberg model, which is the only optimized model that directly uses the ultimate tensile strength R_m. As has been noted before, such approaches often struggle with the bending type load cases. This is neatly confirmed here, as the standard deviation of Δ_{FL} for bending is double that of tensile loading. It is worth reminding that the Han data set has not been used for the Klubberg model, as has been explained in the beginning of this chapter. However, 5 other data sets (with 120 points out of the original 167) still remain as a basis of this particular result, making the conclusion that this model is not a good choice for bending type loads justifiable. Other than this extreme case, the Linear, Dietmann, Gerber and Haibach models do seem to achieve slightly better results for bending than for tensile loads, however, this improvement is quite small, and all the other models presented here (except for Klubberg) fair either practically the same, or better, for both of the load cases.

The conclusion that the load type does not seem to have an overall major impact on most of the results leads to the fact that the trends described here, which have been based on the upper half of the table, where both the tensile and bending type load data are mixed, do translate to the bottom part.

Data information			Standard deviation of Δ_{FL}								
		Total points	Walk.	Kwof.	Berg.	Lin.	Diett.	Gerb.	Exp.	Klubb.	Haib.
	All	667	0.04	0.05	0.04	0.06	0.07	0.08	0.05	0.09	0.05
	Consistent	418	0.05	0.05	0.05	0.06	0.06	0.09	0.05	0.07	0.05
R	<-1;0>	460	0.04	0.05	0.04	0.05	0.05	0.07	0.05	0.06	0.04
	(-1;0>	242	0.05	0.06	0.05	0.06	0.06	0.08	0.05	0.07	0.05
	(0;1)	207	0.05	0.06	0.05	0.07	0.09	0.11	0.06	0.14	0.06
	(0;0.3>	108	0.05	0.07	0.05	0.07	0.08	0.09	0.06	0.13	0.06
	(0.3;1)	99	0.04	0.06	0.04	0.07	0.09	0.12	0.05	0.13	0.05
N	<50 000	223	0.05	0.06	0.05	0.06	0.07	0.09	0.06	0.10	0.06
	<50 000;200 000>	233	0.04	0.05	0.04	0.05	0.06	0.08	0.04	0.10	0.04
	>200 000	211	0.04	0.05	0.04	0.05	0.06	0.07	0.04	0.07	0.04
R_e/R_m	<0.7	92	0.05	0.06	0.05	0.06	0.06	0.07	0.03	0.06	0.05
	<0.7;0.8>	208	0.05	0.05	0.05	0.05	0.06	0.09	0.05	0.06	0.06
	<0.8;0.9>	138	0.03	0.04	0.03	0.04	0.04	0.06	0.04	0.07	0.03
	>0.9	229	0.04	0.06	0.04	0.07	0.08	0.10	0.06	0.12	0.05
Material type	Al alloy	421	0.04	0.06	0.04	0.06	0.07	0.09	0.05	0.10	0.05
	Cast iron	70	0.06	0.06	0.05	0.07	0.09	0.12	0.06	0.08	0.05
	Steel	176	0.05	0.04	0.05	0.04	0.04	0.06	0.04	0.06	0.05
Load type	Tensile	500	0.04	0.05	0.04	0.06	0.07	0.09	0.05	0.07	0.05
	Bending	167	0.04	0.05	0.04	0.05	0.05	0.07	0.05	0.14	0.04
Tensile type loads only											
	All	500	0.04	0.05	0.04	0.06	0.07	0.09	0.05	0.07	0.05
	Consistent	372	0.05	0.05	0.05	0.06	0.07	0.09	0.05	0.07	0.05
R	<-1;0>	330	0.04	0.05	0.04	0.05	0.06	0.08	0.05	0.05	0.05
	(-1;0>	165	0.05	0.06	0.05	0.06	0.07	0.09	0.05	0.07	0.05
	(0;1)	170	0.05	0.06	0.05	0.07	0.09	0.11	0.05	0.10	0.06
	(0;0.3>	77	0.05	0.06	0.05	0.06	0.07	0.08	0.05	0.07	0.06
	(0.3;1)	93	0.04	0.06	0.04	0.08	0.09	0.12	0.05	0.11	0.05
N	<50 000	207	0.05	0.06	0.05	0.06	0.07	0.09	0.06	0.07	0.05
	<50 000;200 000>	181	0.04	0.05	0.04	0.06	0.07	0.09	0.04	0.08	0.04
	>200 000	112	0.04	0.06	0.04	0.06	0.08	0.09	0.04	0.07	0.05
R_e/R_m	<0.7	65	0.05	0.06	0.05	0.06	0.06	0.07	0.04	0.06	0.06
	<0.7;0.8>	159	0.06	0.05	0.06	0.06	0.07	0.09	0.05	0.07	0.06
	<0.8;0.9>	72	0.03	0.04	0.03	0.04	0.05	0.07	0.04	0.06	0.03
	>0.9	204	0.04	0.05	0.04	0.06	0.08	0.10	0.05	0.08	0.04
Material type	Al alloy	328	0.04	0.05	0.04	0.06	0.07	0.09	0.05	0.07	0.05
	Cast iron	70	0.06	0.06	0.05	0.07	0.09	0.12	0.06	0.08	0.05
	Steel	102	0.05	0.04	0.05	0.04	0.04	0.07	0.04	0.07	0.06

Table 16 – standard deviation values of Δ_{FL} of the optimized equivalent stress amplitude approach models for different categories of underlying experimental data

In terms of the mean values of Δ_{FL}, from Table 17, it can be seen that some of the more problematic models in terms of standard deviation of Δ_{FL} are also fairing worse here. There does not seem to be a need to dissect the results of the Gerber model in detail here, as they can be summarized as generally the most scattered and unconservative of all the presented models in this chapter.

Looking at the stress ratio R, there seems to be a trend (Walker, Kwofie, Bergmann, Linear and Exponential models) of results shifting from the conservative to the unconservative side with its increase. Interestingly, there seems to be common for the models to achieve the worst results in the (0;0.3>, with somewhat of an improvement if the higher stress ratios are also included (this category is dominated by the GBA, GBB, Han, LaB01, LaB03 and BEL data sets). The results of the Klubberg and Haibach model, however, seem to have seemingly random values corresponding to the individual categories of stress ratio.

The Kwofie, Linear, Dietmann, Exponential and Klubberg models seem to become unconservative in higher fatigue life domains. Other than that, the experimental fatigue life $N_{experiment}$ does not seem to have a large effect on the mean values of Δ_{FL}, which is quite desirable, as this means that the qualities of the equivalent stress amplitude are kept across a large spectrum of life domains..

The increase of R_e/R_m ratio seems to also shift some of the results to the unconservative side, namely for the Linear, Dietmann and Klubberg models.

Other than the Dietmann model becoming more unconservative for Al alloys compared to steel, these two materials do not seem to have a pronounced differences in the mean value of Δ_{FL}. Cast irons seem to be the most problematic of the three, but again, there is only little data to support this (in Table 15, it can even be seen that the mean Δ_{FL} values of these two data sets are largely different).

The bending type load seems to cause a general small shift into the unconservative side (except for Dietmann), with the most pronounced effect being present for the Klubberg model. This can be, again, attributed the dependence of the model on the ultimate tensile strength R_m.

Data information			Mean value of Δ_{FL}								
		Total points	Walk.	Kwof.	Berg.	Lin.	Diett.	Gerb.	Exp.	Klubb.	Haib.
	All	667	0.00	0.00	0.00	-0.01	-0.02	-0.04	0.00	-0.01	0.00
	Consistent	418	0.00	0.00	0.00	-0.01	-0.02	-0.04	0.00	-0.01	0.00
R	<-1;0>	460	0.00	0.00	0.00	0.00	-0.01	-0.03	0.00	-0.02	0.01
	(-1;0>	242	0.01	0.01	0.01	0.00	-0.02	-0.06	0.01	-0.03	0.02
	(0;1)	207	-0.01	-0.01	-0.01	-0.01	-0.03	-0.05	-0.01	0.00	-0.01
	(0;0.3>	108	-0.01	-0.01	-0.01	-0.02	-0.05	-0.08	-0.01	-0.04	0.00
	(0.3;1)	99	-0.01	-0.01	-0.01	-0.01	-0.02	-0.01	-0.01	0.04	-0.03
N	<50 000	223	-0.01	0.01	-0.01	0.00	-0.01	-0.03	0.01	0.00	0.00
	<50 000;200 000>	233	0.00	-0.01	0.00	-0.01	-0.02	-0.04	0.00	-0.01	0.00
	>200 000	211	0.01	-0.01	0.01	-0.01	-0.02	-0.04	-0.01	-0.02	0.01
R_e/R_m	<0.7	92	0.00	0.00	0.00	0.00	-0.01	-0.02	0.00	0.00	0.00
	<0.7;0.8>	208	0.00	0.00	0.00	-0.01	-0.02	-0.04	0.00	-0.01	0.00
	<0.8;0.9>	138	0.00	0.00	0.00	0.00	-0.01	-0.02	0.00	-0.01	0.00
	>0.9	229	0.00	0.00	0.00	-0.01	-0.03	-0.05	0.00	-0.01	0.00
Material type	Al alloy	421	0.00	0.00	0.00	-0.01	-0.02	-0.04	0.00	-0.01	0.00
	Cast iron	70	-0.01	-0.01	-0.01	-0.02	-0.04	-0.05	-0.01	-0.01	-0.01
	Steel	176	0.00	0.00	0.00	0.00	-0.01	-0.02	0.00	-0.01	0.00
Load type	Tensile	500	0.00	0.00	0.00	-0.01	-0.02	-0.04	0.00	-0.01	0.00
	Bending	167	0.00	0.00	0.00	-0.01	-0.01	-0.03	0.00	-0.02	0.00
Tensile type loads only											
	All	500	0.00	0.00	0.00	-0.01	-0.02	-0.04	0.00	-0.01	0.00
	Consistent	372	0.00	0.00	0.00	-0.01	-0.02	-0.04	0.00	-0.01	0.00
R	<-1;0>	330	0.00	0.01	0.00	0.00	-0.01	-0.04	0.01	-0.01	0.01
	(-1;0>	165	0.01	0.01	0.01	0.00	-0.03	-0.07	0.01	-0.02	0.02
	(0;1)	170	-0.01	-0.01	-0.01	-0.02	-0.04	-0.05	-0.01	0.00	-0.01
	(0;0.3>	77	-0.01	-0.01	-0.01	-0.03	-0.06	-0.10	-0.01	-0.04	0.01
	(0.3;1)	93	0.00	-0.01	-0.01	0.00	-0.02	-0.02	-0.01	0.03	-0.03
N	<50 000	207	-0.01	0.01	-0.01	0.00	-0.01	-0.03	0.01	0.00	0.00
	<50 000;200 000>	181	0.00	0.00	0.00	-0.01	-0.03	-0.05	0.00	-0.01	0.00
	>200 000	112	0.01	-0.01	0.01	-0.01	-0.03	-0.05	-0.01	-0.02	0.01
R_e/R_m	<0.7	65	0.00	0.00	0.00	0.00	0.00	-0.01	0.00	0.00	0.00
	<0.7;0.8>	159	0.00	0.00	0.00	-0.01	-0.02	-0.05	0.00	-0.01	0.00
	<0.8;0.9>	72	0.00	0.00	0.00	-0.01	-0.02	-0.04	0.00	-0.01	0.00
	>0.9	204	0.00	0.00	0.00	-0.01	-0.03	-0.05	0.00	-0.01	0.00
Material type	Al alloy	328	0.00	0.00	0.00	-0.01	-0.02	-0.04	0.00	-0.01	0.01
	Cast iron	70	-0.01	-0.01	-0.01	-0.02	-0.04	-0.05	-0.01	-0.01	-0.01
	Steel	102	0.00	0.00	0.00	0.00	-0.01	-0.03	0.00	-0.01	0.00

Table 17 - mean values of Δ_{FL} of the optimized equivalent stress amplitude approach models for different categories of underlying experimental data

Of the 9 tested models in this chapter, 5 seem to provide quite universally, highly similar good results. These are the Walker, Kwofie, Bergmann, Exponential and Haibach models. In order to provide some more distinguishment between them, the predictability of the values of the best-fit optimized coefficients can be examined.

Since this is the case, the Exponential model will be left out, as it is the only one that features two instead of a single optimization parameter, making predictability relatively more difficult.

Consider Table 18. It makes sense to split tensile and bending type load data sets, as this can be considered to have a major impact on the shape of the S-N curves, and thus, also on the optimization coefficients.

Data information					R^2				Coefficient of the $\sigma_{a,eq}$ model				
Set	Load	Material	R_m [MPa]	R_e [MPa]	Walk.	Kwof.	Berg.	Haib.	Walk.	Kwof.	Kwof.*	Berg.	Haib.
AIS	T	Al alloy	530	349	0.61	0.57	0.66	0.44	0.58	1.7E-03	0.91	0.75	0.38
BEL	T	Steel	1058	880	0.68	0.68	0.67	0.73	0.60	7.3E-04	0.77	0.71	0.39
BaB	T	Steel	706	539	0.92	0.92	0.93	0.81	0.59	1.0E-03	0.71	0.75	0.37
Bai	T	Steel	902	706	0.83	0.90	0.83	0.80	0.58	7.7E-04	0.70	0.78	0.35
FAD3	T	Al alloy	477	440	0.91	0.76	0.90	0.68	0.53	2.3E-03	1.11	0.91	0.58
FAD4	T	Al alloy	477	440	0.85	0.08	0.83	0.67	0.41	2.6E-03	1.25	1.34	0.61
GBA	T	Al alloy	503	372	0.73	0.60	0.73	0.66	0.45	2.2E-03	1.08	1.17	0.55
GBB	T	Al alloy	569	524	0.69	0.33	0.68	0.57	0.43	2.1E-03	1.18	1.25	0.61
GrN	T	Cast iron	637	425	0.80	0.51	0.80	0.80	0.40	1.8E-03	1.12	1.28	0.51
LaB01	T	Al alloy	510	438	0.94	0.83	0.94	0.92	0.48	2.2E-03	1.11	1.08	0.52
LaB02	T	Al alloy	512	335	0.96	0.97	0.96	0.96	0.46	2.2E-03	1.12	1.09	0.49
LaB03	T	Al alloy	587	489	0.97	0.83	0.97	0.97	0.44	2.3E-03	1.38	1.23	0.58
No40	T	Steel	628	579	0.79	0.83	0.82	0.69	0.68	1.1E-03	0.69	0.51	0.28
Ra1	T	Cast iron	498	368	0.67	0.69	0.70	0.70	0.40	2.9E-03	1.44	1.41	0.63
SCa	T	Al alloy	579	524	0.91	0.87	0.91	0.91	0.44	1.7E-03	1.00	1.17	0.48
Tra30	T	Steel	1093	1013	0.93	0.93	0.93	0.93	0.75	3.7E-04	0.41	0.41	0.19
Fin	B	Al alloy	508	470	0.56	-0.05	0.56	0.46	0.57	1.2E-03	0.62	0.80	0.39
Han	B	Steel	844	732	0.62	0.57	0.64	0.62	0.89	1.2E-04	0.10	0.16	0.09
KLN	B	Al alloy	545	395	0.73	0.73	0.73	0.72	0.40	3.2E-03	1.76	1.26	0.54
PRb	B	Steel	535	357	0.81	0.78	0.82	0.78	0.44	1.5E-03	0.82	1.19	0.48
SaL	B	Al alloy	498	441	0.88	0.88	0.90	0.84	0.71	9.8E-04	0.49	0.46	0.26

Table 18 – coefficients of determination R^2 and optimization parameter values of several of the optimized equivalent stress amplitude models, 'Kwof.' shows values of the optimization parameter divided by the ultimate tensile strength R_m, in Kwof.*, this value is multiplied by R_m

Several different vectors of dependent values have been tested for linear and second-degree polynomial fits. These included the material parameters R_m and R_e and their ratios, as well as the power law model constants C and W of the (R = -1) and (R = 0) curves and their ratios. The ones that stood out by being able to provide a good fit for some of the coefficients of the equivalent stress amplitude models are presented in the leftmost column of Table 19.

In the section with the results from tensile load type experimental data, a high-quality fit is available for the Kwofie model when the ultimate tensile strength R_m is chosen as the independent variable. The dependence on R_m is desirable, as this material parameter is commonly available. This fit is shown in Figure 40, with the corresponding equation (60).

Independent variable	R^2									
	Linear function					Second degree polynomial				
	Walk.	Kwof.	Kwof.*	Berg.	Haib.	Walk.	Kwof.	Kwof.*	Berg.	Haib.
	Tensile load									
R_m	0.50	0.77	0.59	0.44	0.54	0.50	0.84	0.60	0.45	0.56
R_e	0.52	0.68	0.56	0.45	0.48	0.54	0.69	0.56	0.45	0.49
W_0	0.51	0.41	0.54	0.48	0.52	0.51	0.47	0.54	0.49	0.52
$\log_{10}C_{-1}/\log_{10}C_0$	0.58	0.20	0.35	0.55	0.35	0.75	0.39	0.56	0.71	0.61
	Bending load									
R_m	0.51	0.29	0.24	0.40	0.54	0.98	0.81	0.81	0.98	0.98
R_e	0.79	0.50	0.45	0.71	0.79	0.82	0.51	0.47	0.79	0.80
W_0	0.17	0.25	0.25	0.17	0.15	0.84	0.96	0.92	0.73	0.88
$\log_{10}C_{-1}/\log_{10}C_0$	0.00	0.00	0.00	0.02	0.00	0.76	0.55	0.62	0.85	0.74
	Bending load (no Han)									
R_m	0.94	0.71	0.73	0.95	0.92	0.98	0.89	0.89	0.99	0.95
R_e	0.49	0.19	0.20	0.55	0.41	0.49	0.46	0.47	0.56	0.41
W_0	0.00	0.01	0.02	0.00	0.01	N/A	N/A	N/A	N/A	N/A
$\log_{10}C_{-1}/\log_{10}C_0$	0.15	0.24	0.27	0.20	0.09	N/A	N/A	N/A	N/A	N/A

Table 19 – quality of fit of optimization parameters of several equivalent stress amplitude models for different variants of independent variables

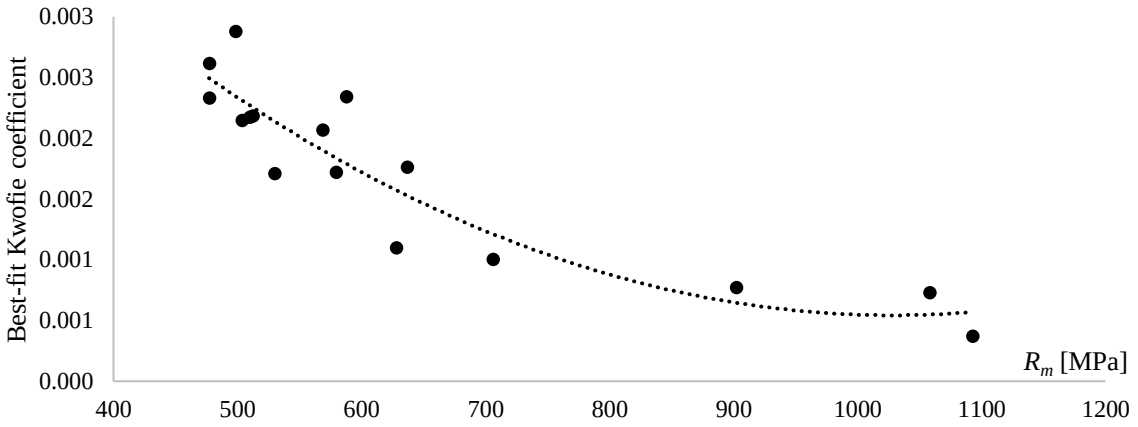

Figure 40 – fit of the Kwofie coefficient $\tilde{\alpha}(R_m)$ relation

$$\tilde{\alpha}(R_m) = 6.42 \cdot 10^{-9} \cdot {R_m}^2 - 1.32 \cdot 10^{-5} \cdot R_m + 7.33 \cdot 10^{-3} \quad (60)$$

Finding similar fits for the bending type loads is more problematic here, as there are only 5 datasets available for this, see Table 18. Looking into Table 19, there seems to be a decent fit of the Walker, Bergmann and Haibach model coefficients when the ultimate tensile strength R_m is chosen as the independent variable. However, the coefficient of determination R^2 may be quite misleading in this case. Due to the small available amount of underlying data sets, a visual inspection of the fit is in place, which reveals how problematic it is. Figure 41 shows that the good value of R^2 of the fit is a result of using the second degree polynomial, since four of the available points lie on an almost straight line, while the point corresponding to Han, which lies very far away from the rest of the data points, dictates how the polynomial "bends". Also, it can be expected that the function should be at least monotonous in the inspected interval. Figure 41 corresponds to the Walker coefficient γ, however, the exact same behavior applies to the fit of the other two mentioned models, with just one difference – for the Bergmann and Haibach, the graphs show a concave function.

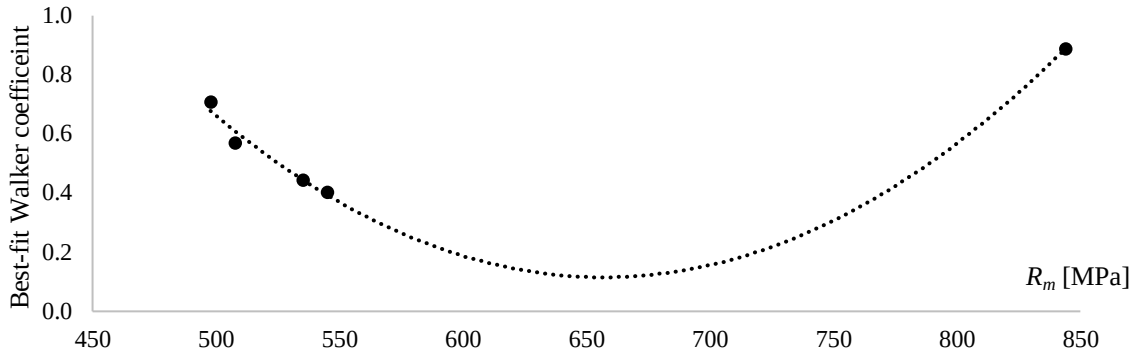

Figure 41 – a fit of the Walker coefficient for different sets of bending type load experimental data sets, where R_m is chosen as the independent variable

Removing Han from the bending data sets reduces the amount of data points available to four. Looking at fits to independent variables derived from the ($R = 0$) curve removes another data set, with only three remaining. This causes the second-degree polynomial fit to always have the perfect R^2 of 1.

When looking back at the fits to different material parameters, the linear fits of the coefficients of the Walker and Haibach to the yield strength R_e seem to stand out for the bending type load data sets, even while not excluding Han. This is a good clue that the data points follow a monotonous trend. Looking at the corresponding second degree polynomial fits (61) in Figure 42, they do seem to be far more reasonable than what has been shown in Figure 41. However, more data sets would definitely be desirable in order to judge whether these fits can be trusted or not, especially to cover the region between Han and the four neighboring points.

$$\gamma_{Walker} = -2.57 \cdot 10^{-6} \cdot {R_e}^2 + 4.06 \cdot 10^{-3} \cdot R_e - 7.08 \cdot 10^{-1}$$

$$M_{Haibach} = 1.64 \cdot 10^{-6} \cdot {R_e}^2 - 2.91 \cdot 10^{-3} \cdot R_e + 1.34$$

(61)

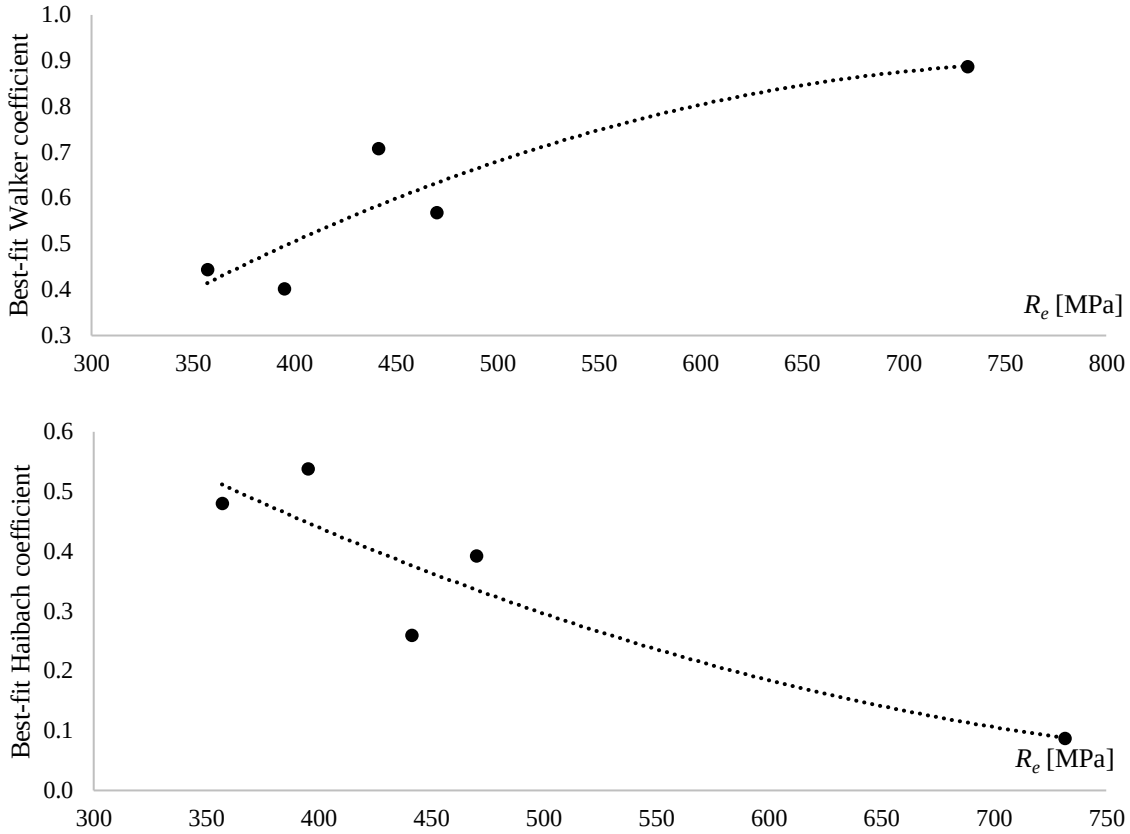

Figure 42 – fits of the coefficients of the Walker and Haibach models for bending type load data sets to the yield strength R_e

In Table 20, the results of the Kwofie model the $\tilde{\alpha}$ calculated using the ultimate tensile strength R_m via (60) are given in column Kwof.*, while the Kwof. column contains the results using the best-fit obtained via regression. The table also contains results of some of the unoptimized equivalent stress amplitude model, as these (except for the SWT model) only require the value of the ultimate tensile strength R_m in order to calculate the equivalent stress amplitude $\sigma_{a,eq}$, which makes them comparable to the Kwofie* model.

As the $\tilde{\alpha}(R_m)$ function has been found for tensile load type data sets, all bending type data set results are removed from Table 20.

A nice feature of the Kwofie* model is that the values of standard deviation of Δ_{FL} did not become significantly higher compared to its best-fit coefficient counterpart, however, the mean values of Δ_{FL} have become more scattered. The results of the Kwofie* model can be considered above average of the unoptimized group of equivalent stress amplitude models (here comprised of SWT, Goodman, Gerber and Dietmann models), alas, its results overall tend to be slightly worse than those of the very easy-to-use SWT model.

Data information		Mean value of Δ_{FL}						Standard deviation of Δ_{FL}					
Set	Points	Kwof.	Kwof.*	SWT	Good.	Gerb.	Diet.	Kwof.	Kwof.*	SWT	Good.	Gerb.	Diet.
AIS	22	0.02	0.06	0.04	0.09	-0.07	-0.03	0.07	0.07	0.06	0.07	0.08	0.08
BEL	35	0.00	-0.03	0.03	0.12	-0.02	-0.01	0.03	0.04	0.04	0.13	0.06	0.04
BaB	22	0.01	0.09	0.08	0.39	-0.05	0.01	0.04	0.06	0.06	0.28	0.10	0.04
Bai	25	0.00	-0.05	0.04	0.25	-0.08	-0.02	0.07	0.09	0.08	0.21	0.10	0.06
FAD3	27	-0.01	0.01	0.01	0.10	-0.03	-0.05	0.03	0.04	0.02	0.17	0.12	0.06
FAD4	30	0.00	-0.01	-0.04	0.05	-0.14	-0.12	0.09	0.09	0.05	0.14	0.12	0.11
GBA	68	0.01	0.02	-0.01	0.06	-0.09	-0.07	0.05	0.05	0.05	0.07	0.08	0.07
GBB	58	0.00	-0.02	-0.02	0.06	-0.09	-0.08	0.06	0.06	0.05	0.12	0.09	0.08
GrN	26	-0.01	-0.02	-0.02	0.01	-0.09	-0.06	0.08	0.08	0.05	0.09	0.13	0.10
LaB01	17	0.01	0.02	-0.01	0.05	-0.11	-0.08	0.06	0.06	0.03	0.08	0.08	0.07
LaB02	17	0.00	0.00	-0.01	0.00	-0.05	-0.03	0.03	0.03	0.04	0.03	0.08	0.05
LaB03	20	0.00	-0.03	-0.01	-0.01	-0.07	-0.06	0.04	0.04	0.02	0.05	0.07	0.06
No40	12	0.00	0.03	0.03	0.06	0.00	0.01	0.02	0.03	0.04	0.08	0.03	0.02
Ra1	44	-0.01	-0.05	-0.05	-0.02	-0.15	-0.13	0.06	0.06	0.07	0.07	0.13	0.11
SCa	69	0.00	0.01	-0.01	0.02	-0.06	-0.04	0.04	0.04	0.04	0.06	0.07	0.05
Tra30	8	0.00	0.02	0.04	0.08	0.01	0.02	0.02	0.04	0.07	0.16	0.02	0.05
Mean		0.00	0.00	0.01	0.08	-0.07	-0.05	0.05	0.06	0.05	0.11	0.08	0.07
Max		0.02	0.09	0.08	0.39	0.01	0.02	0.09	0.09	0.08	0.28	0.13	0.11
Min		-0.01	-0.05	-0.05	-0.02	-0.15	-0.13	0.02	0.03	0.02	0.03	0.02	0.02
Stand. dev.		0.01	0.04	0.04	0.10	0.05	0.04	0.02	0.02	0.02	0.07	0.03	0.03

Table 20 – mean and standard deviation values of Δ_{FL} of several equivalent stress amplitude models for each available data set with tensile type loading

Reduced fatigue limit – optimized

As the optimized reduced fatigue limit approach still relies on the ultimate tensile strength R_m, see Figure 7, the Han set results are not available in this chapter, since some of the mean stresses σ_m present in Han are greater than R_m. Furthermore, there are some cases where FEMFAT shift from 1.8 could not have been applied to the predicted fatigue lives.

In (51), $N_{FL,red}$ cannot be calculated when $\sigma_{FL,red}$ is less than 1. This happened in the case of the Gerber model for the data set FAD3, for the point on the (R = 0.7) with the highest stress amplitude σ_a. Another occurrence of this happened for the Smith and Klubberg model with 3 points of the Fin data set. All of these points lie on the (σ_m = 448 MPa) curve.

Overall however, the FEMFAT shift, again, had a negligible impact on the mean and standard deviation values of Δ_{FL} (0.02 was the maximum for both, in most cases, less than 0.01), which is why the results are not shown in Table 21 and Table 22.

The mean values of Δ_{FL} in Table 21 tend to be on the conservative side, and generally close to zero. The Smith, Klubberg and Haibach models have the highest scatter in the means. Overall, some of the worst results come from the Klubberg model when the underlying data is of the bending type load, which is expectable from this model, as has been repeatedly explained.

In Table 22, the standard deviation values of Δ_{FL} for each data set are presented. Smith's model seems to achieve the lowest mean values of standard deviation of Δ_{FL}, with the lowest scatter (standard deviation of the standard deviation of Δ_{FL}) as well.

In general, the quality of the results of individual models seem to follow similar trends, in that better results are achieved for the same data sets universally. The same is true for the worse results.

It is also worth pointing out that the optimization process was problematic in some cases. For the Fin set, the Gerber coefficient tends to rise to numbers which are nowhere near typical values. This turns the Haigh diagram for Gerber into, essentially, a horizontal line. This happens regardless of the starting point of the regression.

For the same set, the Smith coefficient equals the maximum value of the mean stress σ_m present in the set. This constraint has to be set for the solver, otherwise, the model starts producing negative values of the reduced fatigue limit $\sigma_{FL,red}$. This is also the case of the Gerber model in the sets FAD3 and FAD4.

Data information					Mean value of Δ_{FL}						
Set	Points	Load	Material	σ_{FL-1} [MPa]	Good.	Gerb.	Smith	Berg.	Kwof.	Klubb.	Haib.
AIS	22	T	Al alloy	178	0.03	0.00	0.03	0.03	0.03	0.01	0.04
BEL	35	T	Steel	386	0.00	-0.03	0.01	0.01	0.01	0.00	0.02
BaB	22	T	Steel	318	0.12	0.04	0.13	0.13	0.13	0.04	0.16
Bai	25	T	Steel	409	0.02	0.00	0.02	0.02	0.02	0.02	0.03
FAD3	27	T	Al alloy	139	0.16	0.07	-0.10	-0.09	-0.09	0.13	0.26
FAD4	30	T	Al alloy	183	0.05	0.03	0.05	0.06	0.05	0.06	0.06
Fin	25	B	Al alloy	238	0.09	-0.15	0.31	0.10	0.10	0.33	0.13
GBA	68	T	Al alloy	195	0.02	0.01	0.02	0.02	0.02	0.03	0.03
GBB	58	T	Al alloy	194	-0.01	0.00	0.00	0.01	-0.02	0.05	0.04
GrN	26	T	Cast iron	304	0.01	0.02	0.01	0.01	0.01	0.01	0.01
Han	47	B	Steel	498	N/A	N/A	N/A	N/A	N/A	N/A	N/A
KLN	49	B	Al alloy	156	-0.01	-0.01	-0.01	-0.01	-0.01	-0.01	-0.01
LaB01	17	T	Al alloy	186	0.01	-0.03	0.01	0.02	0.02	0.01	0.03
LaB02	17	T	Al alloy	170	0.00	0.00	0.00	0.00	0.00	0.00	0.00
LaB03	20	T	Al alloy	149	0.00	-0.02	0.01	0.01	0.01	0.01	0.01
No40	12	T	Steel	187	0.01	0.00	0.01	0.01	0.01	-0.01	0.01
PRb	27	B	Steel	258	0.02	0.01	0.02	0.02	0.02	0.02	0.03
Ra1	44	T	Cast iron	177	-0.02	-0.05	-0.02	-0.01	-0.01	-0.02	-0.01
SCa	69	T	Al alloy	228	0.01	0.01	0.01	0.01	0.01	0.01	0.01
SaL	19	B	Al alloy	207	0.06	0.01	0.07	0.07	0.07	-0.42	0.09
Tra30	8	T	Steel	495	0.00	0.00	0.00	0.00	0.00	0.00	0.00
Mean					0.03	0.00	0.03	0.02	0.02	0.01	0.05
Max					0.16	0.07	0.31	0.13	0.13	0.33	0.26
Min					-0.02	-0.15	-0.10	-0.09	-0.09	-0.42	-0.01
Standard deviation					0.05	0.04	0.08	0.04	0.05	0.13	0.07

Table 21 – mean values of Δ_{FL} of the optimized reduced fatigue limit models for each available data set

Data information					Standard deviation of Δ_{FL}						
Set	Points	Load	Material	σ_{FL-1} [MPa]	Good.	Gerb.	Smith	Berg.	Kwof.	Klubb.	Haib.
AIS	22	T	Al alloy	178	0.06	0.03	0.07	0.08	0.07	0.05	0.09
BEL	35	T	Steel	386	0.07	0.10	0.07	0.07	0.07	0.14	0.07
BaB	22	T	Steel	318	0.22	0.24	0.22	0.23	0.22	0.25	0.24
Bai	25	T	Steel	409	0.07	0.10	0.07	0.07	0.07	0.11	0.08
FAD3	27	T	Al alloy	139	0.23	0.25	0.15	0.14	0.15	0.25	0.23
FAD4	30	T	Al alloy	183	0.18	0.23	0.17	0.16	0.16	0.18	0.14
Fin	25	B	Al alloy	238	0.57	0.47	0.23	0.51	0.52	0.25	0.46
GBA	68	T	Al alloy	195	0.09	0.11	0.09	0.09	0.09	0.10	0.09
GBB	58	T	Al alloy	194	0.14	0.20	0.13	0.13	0.50	0.17	0.11
GrN	26	T	Cast iron	304	0.10	0.12	0.09	0.09	0.09	0.10	0.08
Han	47	B	Steel	498	N/A	N/A	N/A	N/A	N/A	N/A	N/A
KLN	49	B	Al alloy	156	0.04	0.05	0.04	0.04	0.04	0.04	0.04
LaB01	17	T	Al alloy	186	0.07	0.10	0.07	0.07	0.07	0.08	0.07
LaB02	17	T	Al alloy	170	0.03	0.03	0.03	0.03	0.03	0.03	0.03
LaB03	20	T	Al alloy	149	0.06	0.08	0.06	0.05	0.05	0.06	0.04
No40	12	T	Steel	187	0.02	0.02	0.03	0.03	0.03	0.04	0.04
PRb	27	B	Steel	258	0.11	0.12	0.11	0.11	0.11	0.12	0.11
Ra1	44	T	Cast iron	177	0.07	0.12	0.06	0.06	0.06	0.07	0.06
SCa	69	T	Al alloy	228	0.07	0.08	0.07	0.07	0.07	0.07	0.07
SaL	19	B	Al alloy	207	0.17	0.20	0.17	0.17	0.17	0.74	0.17
Tra30	8	T	Steel	495	0.03	0.04	0.03	0.03	0.03	0.04	0.03
Mean					0.12	0.13	0.10	0.11	0.13	0.14	0.11
Max					0.57	0.47	0.23	0.51	0.52	0.74	0.46
Min					0.02	0.02	0.03	0.03	0.03	0.03	0.03
Standard deviation					0.12	0.11	0.06	0.11	0.14	0.16	0.10

Table 22 – standard deviation values of Δ_{FL} of the optimized reduced fatigue limit models for each available data set

All the minimum values of Δ_{FL} in Table 23 are negative, meaning that at least one fatigue life prediction per data set is unconservative. This is expectable, as the optimization tries to minimize the error in fatigue life prediction in the least squares sense, which should theoretically result in about half of the values being on the conservative and half on the unconservative side (assuming Gaussian distribution of the Δ_{FL} error). Again, the colors of the cells are not an indicator high-low accuracy of fatigue life prediction, as this cannot be judged based on the minimum values of Δ_{FL}.

Smith's model retains its feature from the unoptimized approach, where the minimum values of Δ_{FL} tend to be the closest to zero, while the standard deviation of the minimums is the lowest of all models.

The results with the FEMFAT shift applied, again, are not shown in this table. However, the largest change of the minimum value of Δ_{FL} is 0.01, and all the values stay negative.

Data information					Minimum values of Δ_{FL}						
Set	Points	Load	Material	$\sigma_{FL\text{-}1}$ [MPa]	Good.	Gerb.	Smith	Berg.	Kwof.	Klubb.	Haib.
AIS	22	T	Al alloy	178	-0.15	-0.06	-0.17	-0.18	-0.18	-0.14	-0.21
BEL	35	T	Steel	386	-0.14	-0.19	-0.14	-0.14	-0.14	-0.22	-0.13
BaB	22	T	Steel	318	-0.35	-0.29	-0.36	-0.37	-0.37	-0.29	-0.39
Bai	25	T	Steel	409	-0.08	-0.18	-0.09	-0.10	-0.09	-0.17	-0.15
FAD3	27	T	Al alloy	139	-0.05	-0.23	-0.39	-0.36	-0.38	-0.10	-0.01
FAD4	30	T	Al alloy	183	-0.30	-0.40	-0.27	-0.26	-0.27	-0.26	-0.24
Fin	25	B	Al alloy	238	-1.32	-1.55	-0.03	-1.22	-1.24	-0.03	-1.12
GBA	68	T	Al alloy	195	-0.15	-0.20	-0.15	-0.16	-0.16	-0.14	-0.17
GBB	58	T	Al alloy	194	-0.27	-0.33	-0.24	-0.22	-2.13	-0.18	-0.21
GrN	26	T	Cast iron	304	-0.11	-0.14	-0.10	-0.10	-0.10	-0.10	-0.08
Han	47	B	Steel	498	N/A	N/A	N/A	N/A	N/A	N/A	N/A
KLN	49	B	Al alloy	156	-0.09	-0.11	-0.08	-0.08	-0.08	-0.08	-0.09
LaB01	17	T	Al alloy	186	-0.11	-0.18	-0.09	-0.09	-0.09	-0.13	-0.08
LaB02	17	T	Al alloy	170	-0.07	-0.07	-0.07	-0.07	-0.07	-0.07	-0.07
LaB03	20	T	Al alloy	149	-0.12	-0.19	-0.10	-0.08	-0.09	-0.10	-0.06
No40	12	T	Steel	187	-0.04	-0.03	-0.04	-0.04	-0.04	-0.06	-0.05
PRb	27	B	Steel	258	-0.11	-0.14	-0.10	-0.10	-0.10	-0.11	-0.10
Ra1	44	T	Cast iron	177	-0.16	-0.23	-0.16	-0.16	-0.16	-0.16	-0.16
SCa	69	T	Al alloy	228	-0.15	-0.17	-0.15	-0.15	-0.15	-0.15	-0.15
SaL	19	B	Al alloy	207	-0.20	-0.38	-0.19	-0.19	-0.19	-2.32	-0.17
Tra30	8	T	Steel	495	-0.05	-0.06	-0.05	-0.05	-0.05	-0.06	-0.04
Mean					-0.20	-0.26	-0.15	-0.21	-0.30	-0.24	-0.18
Max					-0.04	-0.03	-0.03	-0.04	-0.04	-0.03	-0.01
Min					-1.32	-1.55	-0.39	-1.22	-2.13	-2.32	-1.12
Standard deviation					0.28	0.32	0.10	0.26	0.50	0.49	0.24

Table 23 – minimum values of Δ_{FL} of the optimized reduced fatigue limit models for each available data set

From Table 24, it can be seen that the standard deviation of Δ_{FL} is generally much higher for bending compared to tensile loads. For this reason, let us focus directly on the bottom half of the table.

There is a general trend, where with the increase of the stress ratio R, the standard deviation grows. The opposite seems to be true for the experimental fatigue life N. However, Kwofie's model has a spike of high standard deviation in the <50k; 200k> region. In terms of the R_e/R_m ratio, all the models struggle with the highest category.

The difference between the results for steels and aluminum alloys do not look significant, except for, again, Kwofie's model, which fairs dramatically worse for aluminum alloys. The table also suggests that all the optimized reduced fatigue limit models tend to work best for cast irons, however, as has been noted before, this is based on only 2 data sets.

Overall, it is obvious that Kwofie generally gives some of the least precise fatigue life predictions out of the models presented in this chapter.

Data information			Standard deviation of Δ_{FL}						
		Total points	Good.	Gerb.	Smith	Berg.	Kwof.	Klubb.	Haib.
	All	667	0.16	0.17	0.13	0.15	0.21	0.21	0.15
	Consistent	418	0.11	0.14	0.11	0.11	0.21	0.22	0.11
R	<-1;0>	460	0.12	0.12	0.09	0.11	0.11	0.09	0.11
	(-1;0>	242	0.16	0.15	0.11	0.14	0.15	0.12	0.14
	(0;1)	207	0.24	0.25	0.20	0.21	0.34	0.35	0.22
	(0;0.3>	108	0.24	0.24	0.18	0.22	0.24	0.23	0.21
	(0.3;1)	99	0.23	0.24	0.21	0.20	0.41	0.43	0.23
N	<50 000	223	0.21	0.19	0.14	0.19	0.22	0.15	0.18
	<50 000;200 000>	233	0.13	0.16	0.13	0.12	0.26	0.16	0.13
	>200 000	211	0.11	0.14	0.10	0.09	0.10	0.28	0.12
R_e/R_m	<0.7	92	0.09	0.09	0.09	0.09	0.09	0.09	0.09
	<0.7;0.8>	208	0.11	0.12	0.11	0.11	0.11	0.11	0.11
	<0.8;0.9>	138	0.10	0.12	0.10	0.10	0.10	0.39	0.10
	>0.9	229	0.23	0.23	0.17	0.20	0.32	0.19	0.20
Material type	Al alloy	421	0.18	0.18	0.14	0.16	0.24	0.24	0.16
	Cast iron	70	0.08	0.12	0.08	0.07	0.08	0.08	0.07
	Steel	176	0.12	0.13	0.12	0.12	0.12	0.15	0.13
Load type	Tensile	500	0.12	0.14	0.11	0.11	0.20	0.13	0.12
	Bending	167	0.27	0.24	0.18	0.25	0.25	0.39	0.23
Tensile type loads only									
	All	500	0.12	0.14	0.11	0.11	0.20	0.13	0.12
	Consistent	372	0.11	0.13	0.10	0.10	0.22	0.12	0.10
R	<-1;0>	330	0.07	0.08	0.07	0.07	0.07	0.07	0.08
	(-1;0>	165	0.09	0.11	0.09	0.09	0.09	0.09	0.09
	(0;1)	170	0.18	0.21	0.16	0.16	0.32	0.20	0.18
	(0;0.3>	77	0.13	0.15	0.12	0.12	0.15	0.13	0.11
	(0.3;1)	93	0.21	0.23	0.19	0.18	0.41	0.22	0.22
N	<50 000	207	0.12	0.14	0.12	0.12	0.16	0.13	0.12
	<50 000;200 000>	181	0.12	0.15	0.10	0.10	0.26	0.14	0.12
	>200 000	112	0.12	0.14	0.09	0.09	0.09	0.12	0.13
R_e/R_m	<0.7	65	0.07	0.08	0.07	0.08	0.07	0.07	0.08
	<0.7;0.8>	159	0.12	0.14	0.12	0.12	0.12	0.13	0.12
	<0.8;0.9>	72	0.07	0.09	0.07	0.06	0.07	0.11	0.06
	>0.9	204	0.15	0.17	0.12	0.12	0.28	0.15	0.15
Material type	Al alloy	328	0.13	0.15	0.11	0.11	0.23	0.13	0.13
	Cast iron	70	0.08	0.12	0.08	0.07	0.08	0.08	0.07
	Steel	102	0.13	0.13	0.13	0.13	0.13	0.15	0.14

Table 24 – standard deviation values of Δ_{FL} of the optimized reduced fatigue limit approach models for different categories of underlying experimental data

Like with the standard deviations, let us skip directly to the bottom half of Table 25, where the mean values of Δ_{FL} are presented. In terms of the stress ratio R, no strong trends are observable, and although some of the values for higher stress ratios are promisingly close to zero, the corresponding standard deviations from Table 26 are too large. The R_e/R_m category does not seem to host any strong trends either.

Except for the Klubberg and Haibach models, the mean values tend to move to the unconservative side as the fatigue life N increases.

Mean values tend to be closer to zero for aluminum alloys compared to steels. A slight increase in the quality of predictions for said material is also visible in Table 24.

Data information			Mean value of Δ_{FL}						
		Total points	Good.	Gerb.	Smith	Berg.	Kwof.	Klubb.	Haib.
	All	667	0.02	0.00	0.02	0.02	0.01	0.02	0.04
	Consistent	418	0.01	0.00	0.02	0.02	0.02	0.00	0.03
R	<-1;0>	460	0.02	-0.02	0.02	0.02	0.02	0.01	0.03
	(-1;0>	242	0.04	-0.03	0.04	0.05	0.04	0.02	0.07
	(0;1)	207	0.04	0.03	0.03	0.01	0.00	0.06	0.06
	(0;0.3>	108	0.00	-0.04	0.04	0.02	-0.01	0.02	0.05
	(0.3;1)	99	0.06	0.09	0.02	0.00	0.01	0.09	0.07
N	<50 000	223	0.06	0.03	0.06	0.06	0.06	0.07	0.07
	<50 000;200 000>	233	0.00	-0.02	0.01	0.00	0.00	0.03	0.02
	>200 000	211	0.01	-0.02	-0.01	-0.01	-0.01	-0.04	0.03
R_e/R_m	<0.7	92	0.02	0.01	0.02	0.02	0.02	0.01	0.02
	<0.7;0.8>	208	0.02	-0.01	0.02	0.02	0.02	0.01	0.03
	<0.8;0.9>	138	0.02	-0.02	0.02	0.02	0.02	-0.08	0.04
	>0.9	229	0.04	0.00	0.03	0.01	0.01	0.08	0.07
Material type	Al alloy	421	0.03	0.00	0.03	0.02	0.01	0.03	0.05
	Cast iron	70	-0.01	-0.03	-0.01	0.00	0.00	-0.01	0.00
	Steel	176	0.03	0.00	0.03	0.03	0.03	0.02	0.05
Load type	Tensile	500	0.02	0.00	0.01	0.01	0.01	0.03	0.04
	Bending	167	0.03	-0.03	0.08	0.04	0.04	0.01	0.04
Tensile type loads only									
	All	500	0.02	0.00	0.01	0.01	0.01	0.03	0.04
	Consistent	372	0.01	0.00	0.02	0.02	0.01	0.02	0.03
R	<-1;0>	330	0.01	-0.01	0.02	0.02	0.02	0.00	0.03
	(-1;0>	165	0.03	-0.02	0.03	0.04	0.03	0.00	0.07
	(0;1)	170	0.04	0.03	0.00	0.01	0.00	0.08	0.06
	(0;0.3>	77	-0.01	-0.05	0.00	0.00	-0.03	0.00	0.03
	(0.3;1)	93	0.08	0.10	0.01	0.01	0.02	0.14	0.08
N	<50 000	207	0.05	0.03	0.05	0.05	0.05	0.05	0.06
	<50 000;200 000>	181	0.00	-0.01	-0.01	0.00	0.00	0.02	0.02
	>200 000	112	0.01	-0.03	-0.03	-0.03	-0.03	0.00	0.04
R_e/R_m	<0.7	65	0.01	0.01	0.01	0.01	0.01	0.01	0.02
	<0.7;0.8>	159	0.02	0.00	0.03	0.03	0.03	0.01	0.04
	<0.8;0.9>	72	0.00	-0.02	0.01	0.01	0.01	0.01	0.02
	>0.9	204	0.03	0.02	0.00	0.00	-0.01	0.05	0.06
Material type	Al alloy	328	0.02	0.01	0.01	0.01	0.00	0.04	0.05
	Cast iron	70	-0.01	-0.03	-0.01	0.00	0.00	-0.01	0.00
	Steel	102	0.03	0.00	0.04	0.04	0.04	0.01	0.05

Table 25 – mean values of Δ_{FL} of the optimized reduced fatigue limit approach models for different categories of underlying experimental data

Overall, the results of the optimized reduced fatigue limit approach tend to be quite inconclusive in regard to observable trends. The only strong trend seems to be that the load type does have a large impact on the quality of predictions – better results are generally achieved for tensile loading.

Reduced fatigue limit – optimized, modified

The optimized, modified variant of the Reduced fatigue limit, in contrast to the original optimized version, is no longer dependent on the ultimate tensile strength R_m – see Figure 15. This dependency often caused problems in earlier chapters. These problems are expected to not be present in this chapter.

As for data points omitted from the results, there are none. The fact that the Han set (which was missing from the 3.1 – Reduced fatigue limit – optimized chapter), contains data points where the value of mean stress σ_m exceeded R_m is no longer problematic. The problems with the FEMFAT shift caused by reduced fatigue limits $\sigma_{FL,red}$ of values less than 1, also appearing in mentioned chapter, did not occur here either.

As will be shown in this chapter, the Gerber and Haibach models tend to produce weaker results in this variant of the reduced fatigue limit approach. In some cases, no local minimum of the objective function (50) was available within reasonable bounds of the optimization coefficient. The Haigh diagram turned into, essentially, a horizontal line, meaning that the coefficient of Gerber's reduced fatigue limit model tended to be extremely high, while the coefficient of the Haibach model became equal to the reduced fatigue limit σ_{FL-1} of the (R = -1) curve. A summary of cases where this has happened is available in Table 26.

Set	Gerber	Haibach
FAD3	x	x
FAD4	x	x
GBA	x	
GBB	x	x
LaB01	x	
Ra1	x	x

Table 26 – cases where the coefficients of the optimized, modified reduced fatigue limit approach models have not been reasonable

As has probably become expectable by now, the results from the application of the FEMFAT shift are not present in Table 27, as this, in the extremes, caused a change in the mean value of only 0.006, and 0.002 for the standard deviation of Δ_{FL}.

As is visible in Table 27, the Smith and Goodman model tend to generally have low values of standard deviation while also having the mean value of Δ_{FL} close to 0. The Gerber and Haibach models produce generally similar values of standard deviation of Δ_{FL}, while the means of the first model tend to be on the unconservative side.

Data information				Mean value of Δ_{FL}				Standard deviation of Δ_{FL}			
Set	Points	Load	Mat. Type	Good.	Gerb.	Smith	Haib.	Good.	Gerb.	Smith	Haib.
AIS	22	T	Al alloy	0.01	0.03	0.00	-0.01	0.06	0.12	0.06	0.12
BEL	35	T	Steel	0.01	0.00	0.00	0.01	0.05	0.11	0.03	0.08
BaB	22	T	Steel	-0.03	-0.05	-0.04	-0.01	0.09	0.10	0.12	0.08
Bai	25	T	Steel	-0.02	-0.01	-0.04	-0.01	0.09	0.07	0.13	0.08
FAD3	27	T	Al alloy	0.00	-0.15	0.00	-0.12	0.09	0.06	0.05	0.07
FAD4	30	T	Al alloy	-0.03	-0.21	-0.01	-0.19	0.16	0.09	0.09	0.11
Fin	25	B	Al alloy	-0.03	-0.10	-0.02	-0.03	0.09	0.17	0.06	0.11
GBA	68	T	Al alloy	0.00	-0.18	0.01	-0.02	0.11	0.08	0.07	0.16
GBB	58	T	Al alloy	-0.01	-0.19	0.00	-0.18	0.13	0.09	0.09	0.08
GrN	26	T	Cast iron	-0.03	-0.16	-0.01	-0.02	0.10	0.08	0.06	0.10
Han	47	B	Steel	-0.01	-0.02	-0.01	-0.01	0.04	0.04	0.04	0.04
KLN	49	B	Al alloy	-0.01	-0.11	0.00	-0.01	0.08	0.07	0.05	0.08
LaB01	17	T	Al alloy	0.00	-0.21	0.00	-0.06	0.11	0.11	0.05	0.16
LaB02	17	T	Al alloy	0.00	-0.02	0.00	0.00	0.05	0.08	0.03	0.05
LaB03	20	T	Al alloy	-0.06	-0.12	-0.02	-0.09	0.11	0.08	0.09	0.10
No40	12	T	Steel	0.01	-0.06	0.01	-0.02	0.05	0.06	0.04	0.07
PRb	27	B	Steel	0.00	-0.02	0.00	0.00	0.06	0.10	0.04	0.06
Ra1	44	T	Cast iron	0.01	-0.20	0.00	-0.19	0.10	0.11	0.06	0.12
SCa	69	T	Al alloy	-0.01	-0.07	0.00	-0.01	0.08	0.12	0.05	0.08
SaL	19	B	Al alloy	-0.01	0.00	-0.01	0.00	0.03	0.06	0.04	0.05
Tra30	8	T	Steel	-0.01	0.01	-0.02	-0.01	0.03	0.03	0.05	0.03
Mean				-0.01	-0.09	-0.01	-0.05	0.08	0.09	0.06	0.09
Max				0.01	0.03	0.01	0.01	0.16	0.17	0.13	0.16
Min				-0.06	-0.21	-0.04	-0.19	0.03	0.03	0.03	0.03
Standard deviation				0.02	0.08	0.01	0.07	0.03	0.03	0.03	0.03

Table 27 – mean and standard deviation values of Δ_{FL} of the optimized, modified reduced fatigue limit models for each available data set

Looking at Table 28, it is visible that again, all the minimum values of Δ_{FL} are negative, which is expectable from an optimized model, as has been explained. The FEMFAT shift affects the values only slightly, with a 0.01 increase in the minimum values being the largest change caused by it. The Smith model does seem to stand out compared to the other models in the table, as its minimum values of Δ_{FL} are generally closest to zero, and the standard deviation of these values is the lowest of the four models.

Data information				Minimum value of Δ_{FL}							
				Good.		Gerb.		Smith		Haib.	
Set	Points	Load	Mat. Type	Orig.	FEM.	Orig.	FEM.	Orig.	FEM.	Orig.	FEM.
AIS	22	T	Al alloy	-0.16	-0.15	-0.31	-0.30	-0.12	-0.11	-0.34	-0.34
BEL	35	T	Steel	-0.09	-0.09	-0.23	-0.23	-0.08	-0.08	-0.14	-0.13
BaB	22	T	Steel	-0.20	-0.20	-0.22	-0.22	-0.30	-0.30	-0.15	-0.15
Bai	25	T	Steel	-0.18	-0.18	-0.16	-0.16	-0.27	-0.27	-0.23	-0.22
FAD3	27	T	Al alloy	-0.21	-0.20	-0.29	-0.29	-0.12	-0.12	-0.26	-0.26
FAD4	30	T	Al alloy	-0.47	-0.46	-0.37	-0.37	-0.27	-0.27	-0.41	-0.41
Fin	25	B	Al alloy	-0.18	-0.18	-0.42	-0.42	-0.12	-0.11	-0.26	-0.26
GBA	68	T	Al alloy	-0.23	-0.22	-0.35	-0.35	-0.15	-0.14	-0.36	-0.36
GBB	58	T	Al alloy	-0.27	-0.27	-0.47	-0.47	-0.17	-0.16	-0.36	-0.36
GrN	26	T	Cast iron	-0.24	-0.23	-0.28	-0.28	-0.11	-0.10	-0.23	-0.23
Han	47	B	Steel	-0.14	-0.14	-0.18	-0.18	-0.12	-0.12	-0.14	-0.14
KLN	49	B	Al alloy	-0.15	-0.15	-0.24	-0.24	-0.10	-0.10	-0.15	-0.15
LaB01	17	T	Al alloy	-0.14	-0.13	-0.39	-0.39	-0.09	-0.09	-0.31	-0.31
LaB02	17	T	Al alloy	-0.08	-0.08	-0.15	-0.15	-0.06	-0.06	-0.08	-0.08
LaB03	20	T	Al alloy	-0.25	-0.25	-0.27	-0.27	-0.20	-0.20	-0.25	-0.25
No40	12	T	Steel	-0.12	-0.11	-0.19	-0.19	-0.08	-0.08	-0.19	-0.19
PRb	27	B	Steel	-0.10	-0.10	-0.14	-0.14	-0.10	-0.09	-0.09	-0.09
Ra1	44	T	Cast iron	-0.18	-0.17	-0.39	-0.39	-0.14	-0.14	-0.38	-0.38
SCa	69	T	Al alloy	-0.21	-0.20	-0.30	-0.30	-0.14	-0.14	-0.20	-0.20
SaL	19	B	Al alloy	-0.08	-0.08	-0.12	-0.12	-0.12	-0.12	-0.09	-0.08
Tra30	8	T	Steel	-0.07	-0.07	-0.05	-0.05	-0.10	-0.10	-0.06	-0.06
Mean				-0.18	-0.17	-0.26	-0.26	-0.14	-0.14	-0.22	-0.22
Max				-0.07	-0.07	-0.05	-0.05	-0.06	-0.06	-0.06	-0.06
Min				-0.47	-0.46	-0.47	-0.47	-0.30	-0.30	-0.41	-0.41
Standard deviation				0.09	0.09	0.11	0.11	0.07	0.07	0.11	0.11

Table 28 – minimum values of Δ_{FL} of the optimized, modified reduced fatigue limit models for each available data set

Table 29 confirms that the results of the Smith model are generally the best (accuracy-wise) of the four. First, focus on the standard deviation part of the table. Interestingly, the stress ratio R seems to have no impact on the standard deviations of the Smith model. For all models, there is a visible trend that the standard deviation decreases with the rise of the experimental fatigue lives N. No strong trends in regard to the R_e/R_m ratio are apparent. All the models seem to produce worse results for aluminum alloys compared to steels, except for Smith's model.

The mean values seem to generally shift to the unconservative side with the increase in the stress ratio R. Neither the experimental life N or the ratio R_e/R_m category seem to have any pronounced trends visible. The Haibach and Gerber models seem to be quite unconservative for aluminum alloys.

The most interesting phenomenon in this table seems to come from the categorization according to the load type. All of the models seem to produce better results for bending, which is unique to the optimized, modified reduced fatigue limit approach. The modified version has been devised with the bending type load in mind, as has been said in 1.8 - Reduced fatigue limit – optimized, modified.

Data information		Total points	Mean value of Δ_{FL}				Standard deviation of Δ_{FL}			
			Good.	Gerb.	Smith	Haib.	Good.	Gerb.	Smith	Haib.
	All	667	-0.01	-0.10	-0.01	-0.05	0.09	0.12	0.07	0.12
	Consistent	418	0.00	-0.11	-0.01	-0.05	0.09	0.12	0.07	0.13
R	<-1;0>	460	0.01	-0.08	0.00	-0.03	0.08	0.11	0.07	0.12
	(-1;0>	242	-0.01	-0.12	0.00	-0.05	0.09	0.10	0.07	0.12
	(0;1)	207	-0.05	-0.15	-0.02	-0.11	0.10	0.12	0.07	0.10
	(0;0.3>	108	-0.04	-0.13	-0.02	-0.07	0.09	0.13	0.07	0.10
	(0.3;1)	99	-0.06	-0.17	-0.03	-0.16	0.10	0.11	0.07	0.09
N	<50 000	223	0.02	-0.13	0.00	-0.06	0.10	0.15	0.09	0.16
	<50 000;200 000>	233	-0.02	-0.11	-0.01	-0.07	0.08	0.11	0.06	0.10
	>200 000	211	-0.03	-0.06	-0.01	-0.03	0.08	0.08	0.05	0.08
R_e/R_m	<0.7	92	-0.01	-0.05	0.00	-0.01	0.07	0.12	0.05	0.09
	<0.7;0.8>	208	0.00	-0.13	-0.01	-0.05	0.10	0.11	0.08	0.14
	<0.8;0.9>	138	-0.01	-0.05	-0.01	-0.02	0.07	0.11	0.05	0.09
	>0.9	229	-0.01	-0.13	0.00	-0.09	0.11	0.12	0.07	0.12
Material type	Al alloy	421	-0.01	-0.12	0.00	-0.06	0.10	0.12	0.07	0.13
	Cast iron	70	0.00	-0.18	-0.01	-0.13	0.10	0.10	0.06	0.14
	Steel	176	-0.01	-0.02	-0.01	0.00	0.06	0.08	0.07	0.07
Load type	Tensile	500	-0.01	-0.12	0.00	-0.07	0.10	0.12	0.07	0.13
	Bending	167	-0.01	-0.06	-0.01	-0.01	0.06	0.10	0.05	0.07
Tensile type loads only										
	All	500	-0.01	-0.12	0.00	-0.07	0.10	0.12	0.07	0.13
	Consistent	372	-0.01	-0.12	-0.01	-0.06	0.10	0.12	0.07	0.13
R	<-1;0>	330	0.02	-0.09	0.01	-0.04	0.09	0.12	0.07	0.13
	(-1;0>	165	0.00	-0.13	0.01	-0.06	0.10	0.11	0.07	0.13
	(0;1)	170	-0.06	-0.17	-0.03	-0.13	0.10	0.11	0.07	0.10
	(0;0.3>	77	-0.05	-0.16	-0.02	-0.09	0.09	0.11	0.07	0.10
	(0.3;1)	93	-0.06	-0.18	-0.03	-0.16	0.11	0.11	0.07	0.09
N	<50 000	207	0.02	-0.14	0.00	-0.07	0.10	0.15	0.09	0.16
	<50 000;200 000>	181	-0.02	-0.12	-0.01	-0.08	0.09	0.10	0.06	0.11
	>200 000	112	-0.04	-0.07	-0.01	-0.04	0.10	0.08	0.06	0.09
R_e/R_m	<0.7	65	-0.01	-0.06	-0.01	-0.01	0.08	0.13	0.05	0.10
	<0.7;0.8>	159	0.00	-0.14	-0.01	-0.07	0.10	0.12	0.09	0.15
	<0.8;0.9>	72	-0.01	-0.08	0.00	-0.03	0.09	0.13	0.06	0.12
	>0.9	204	-0.01	-0.13	0.00	-0.10	0.11	0.11	0.07	0.12
Material type	Al alloy	328	-0.01	-0.13	0.00	-0.08	0.11	0.12	0.07	0.13
	Cast iron	70	0.00	-0.18	-0.01	-0.13	0.10	0.10	0.06	0.14
	Steel	102	-0.01	-0.02	-0.02	0.00	0.07	0.09	0.09	0.08

Table 29 – mean and standard deviation values of Δ_{FL} of the optimized, modified reduced fatigue limit approach models for different categories of underlying experimental data

Comparison of the optimized approaches

Models with results that suggest generally high precision of fatigue life prediction have been chosen based on the previous chapters. These are the Walker, Kwofie, Bergmann and Haibach models from the optimized equivalent stress amplitude approach, the Goodman, Smith and Haibach models from the reduced fatigue limit – optimized approach, and the Goodman and Smith models from the reduced fatigue limit – optimized, modified approach. Note that the FEMFAT shift is not applied to the results of the reduced fatigue limit approach in this chapter, as it has been shown to have little impact on the results.

All the models in this chapter feature a single optimization parameter (not counting the C_{-1} and W_{-1} coefficients of the basic S-N curve), while the underlying approaches have similar input data requirements, hence, they can be considered comparable.

Consider Table 30. In each row, a value is highlighted, pointing out the model that had the lowest standard deviation of Δ_{FL} for each data set. It is obvious the equivalent stress amplitude dominates here, as the best results have been achieved for 17 out of the 21 data sets, and in the 4 cases where a model from the reduced fatigue limit approach fared better, the differences are quite small. Notably, in the three cases where the optimized, modified reduced fatigue limit approach had a better result, the loading was of the bending type.

Data information			Standard deviation of Δ_{FL}								
			Equivalent stress amplitude approach				Reduced fatigue limit approach				
			Optimized				Optimized			Opt., Mod.	
Set	Points	Load	Walker	Kwofie	Bergmann	Haibach	Goodman	Smith	Haibach	Goodman	Smith
AIS	22	T	0.07	0.07	0.06	0.08	0.06	0.07	0.09	0.06	**0.06**
BEL	35	T	0.03	0.03	0.03	**0.03**	0.07	0.07	0.07	0.05	0.03
BaB	22	T	0.05	**0.04**	0.05	0.07	0.22	0.22	0.24	0.09	0.12
Bai	25	T	0.09	**0.07**	0.09	0.09	0.07	0.07	0.08	0.09	0.13
FAD3	27	T	**0.02**	0.03	0.02	0.04	0.23	0.15	0.23	0.09	0.05
FAD4	30	T	**0.04**	0.09	0.04	0.05	0.18	0.17	0.14	0.16	0.09
Fin	25	B	0.06	0.09	**0.06**	0.07	0.57	0.23	0.46	0.09	0.06
GBA	68	T	**0.04**	0.05	0.04	0.05	0.09	0.09	0.09	0.11	0.07
GBB	58	T	**0.04**	0.06	0.04	0.05	0.14	0.13	0.11	0.13	0.09
GrN	26	T	**0.05**	0.08	0.05	0.05	0.10	0.09	0.08	0.10	0.06
Han	47	B	0.04	0.04	0.04	0.04	N/A	N/A	N/A	0.04	**0.04**
KLN	49	B	0.04	0.04	**0.04**	0.04	0.04	0.04	0.04	0.08	0.05
LaB01	17	T	**0.03**	0.06	0.03	0.04	0.07	0.07	0.07	0.11	0.05
LaB02	17	T	0.04	**0.03**	0.04	0.04	0.03	0.03	0.03	0.05	0.03
LaB03	20	T	0.02	0.04	0.02	**0.02**	0.06	0.06	0.04	0.11	0.09
No40	12	T	0.03	0.02	0.03	0.03	**0.02**	0.03	0.04	0.05	0.04
PRb	27	B	0.04	0.04	**0.04**	0.04	0.11	0.11	0.11	0.06	0.04
Ra1	44	T	0.06	0.06	**0.06**	0.06	0.07	0.06	0.06	0.10	0.06
SCa	69	T	0.04	0.04	0.04	**0.04**	0.07	0.07	0.07	0.08	0.05
SaL	19	B	0.03	0.03	0.03	0.03	0.17	0.17	0.17	**0.03**	0.04
Tra30	8	T	0.02	**0.02**	0.02	0.02	0.03	0.03	0.03	0.03	0.05
Mean			0.04	0.05	0.04	0.05	0.12	0.10	0.11	0.08	0.06
Max			0.09	0.09	0.09	0.09	0.57	0.23	0.46	0.16	0.13
Min			0.02	0.02	0.02	0.02	0.02	0.03	0.03	0.03	0.03
Standard deviation			0.02	0.02	0.02	0.02	0.12	0.06	0.10	0.03	0.03

Table 30 – standard deviation values of Δ_{FL} of selected models for each available data set

In Table 31, it can be seen that the mean values of Δ_{FL} for the equivalent stress amplitude approach are generally close to zero. For the optimized reduced fatigue limit approach, they tend to be either close to zero or on the conservative side, while the results of the modified approach are a mixed bag. Overall, the most unconservative values come from the reduced fatigue limit approach family of models, while also being subjected to the largest amount of scatter in the results.

Data information			Mean value of Δ_{FL}								
			Equivalent stress amplitude approach				Reduced fatigue limit approach				
			Optimized				Optimized			Opt., Mod.	
Set	Points	Load	Walker	Kwofie	Bergmann	Haibach	Goodman	Smith	Haibach	Goodman	Smith
AIS	22	T	0.01	0.02	0.01	0.01	0.03	0.03	0.04	0.01	0.00
BEL	35	T	0.00	0.00	0.00	0.00	0.00	0.01	0.02	0.01	0.00
BaB	22	T	0.00	0.01	0.00	0.01	0.12	0.13	0.16	-0.03	-0.04
Bai	25	T	-0.01	0.00	-0.01	-0.01	0.02	0.02	0.03	-0.02	-0.04
FAD3	27	T	0.00	-0.01	0.00	0.00	0.16	-0.10	0.26	0.00	0.00
FAD4	30	T	0.00	0.00	0.01	0.01	0.05	0.05	0.06	-0.03	-0.01
Fin	25	B	0.01	0.00	0.00	0.01	0.09	0.31	0.13	-0.03	-0.02
GBA	68	T	0.01	0.01	0.01	0.01	0.02	0.02	0.03	0.00	0.01
GBB	58	T	0.00	0.00	0.00	0.01	-0.01	0.00	0.04	-0.01	0.00
GrN	26	T	0.00	-0.01	0.00	0.00	0.01	0.01	0.01	-0.03	-0.01
Han	47	B	0.00	0.00	0.00	0.00	N/A	N/A	N/A	-0.01	-0.01
KLN	49	B	-0.01	-0.01	-0.01	-0.01	-0.01	-0.01	-0.01	-0.01	0.00
LaB01	17	T	0.00	0.01	0.00	0.01	0.01	0.01	0.03	0.00	0.00
LaB02	17	T	0.00	0.00	0.00	0.00	0.00	0.00	0.00	0.00	0.00
LaB03	20	T	0.00	0.00	0.00	0.00	0.00	0.01	0.01	-0.06	-0.02
No40	12	T	0.00	0.00	0.00	0.00	0.01	0.01	0.01	0.01	0.01
PRb	27	B	-0.01	-0.01	-0.01	-0.01	0.02	0.02	0.03	0.00	0.00
Ra1	44	T	-0.02	-0.01	-0.01	-0.01	-0.02	-0.02	-0.01	0.01	0.00
SCa	69	T	0.00	0.00	0.00	0.00	0.01	0.01	0.01	-0.01	0.00
SaL	19	B	0.00	0.00	0.00	0.01	0.06	0.07	0.09	-0.01	-0.01
Tra30	8	T	0.00	0.00	0.00	0.00	0.00	0.00	0.00	-0.01	-0.02
Mean			0.00	0.00	0.00	0.00	0.03	0.03	0.05	-0.01	-0.01
Max			0.01	0.02	0.01	0.01	0.16	0.31	0.26	0.01	0.01
Min			-0.02	-0.01	-0.01	-0.01	-0.02	-0.10	-0.01	-0.06	-0.04
Standard deviation			0.01	0.01	0.01	0.01	0.05	0.08	0.07	0.02	0.01

Table 31 – mean values of Δ_{FL} of selected models of the optimized approaches for each available data set

Equivalent stress amplitude – 3 degrees of feedom

As has been described in 1.8, results of fatigue life prediction obtained through the equivalent stress amplitude – 3 degrees of freedom (referred to as 3D in this chapter) approach do not have as much direct, practical usage as, for example, the equivalent stress amplitude – 1(2) degree of freedom (referred to as 1D in this chapter) approach. However, it does give hints on whether the 1D models have a potential to improve with some tweaks of the core equivalent stress amplitude approach described in 1.3.

For this reason, in this chapter, the focus lies on the differences between the results of the 1D and 3D approaches, rather than directly examining the results of the 3D approach. This means that the results for the Klubberg model are not available when considering the Han set, since they are not available for the 1D approach.

When quantifying the amount of change in the S-N curves coefficients, the σ_f' and b coefficients of the Basquin S-N curve model (2) will be used rather than the C and W constants of the power law model which appear throughout this thesis. The reason for this is that the Basquin constants have a more direct geometrical meaning. σ_f' is the stress amplitude value which corresponds to a fatigue life of one half-cycle, while b dictates the slope of the S-N curve, see Figure 43. Note that b is generally a negative number.

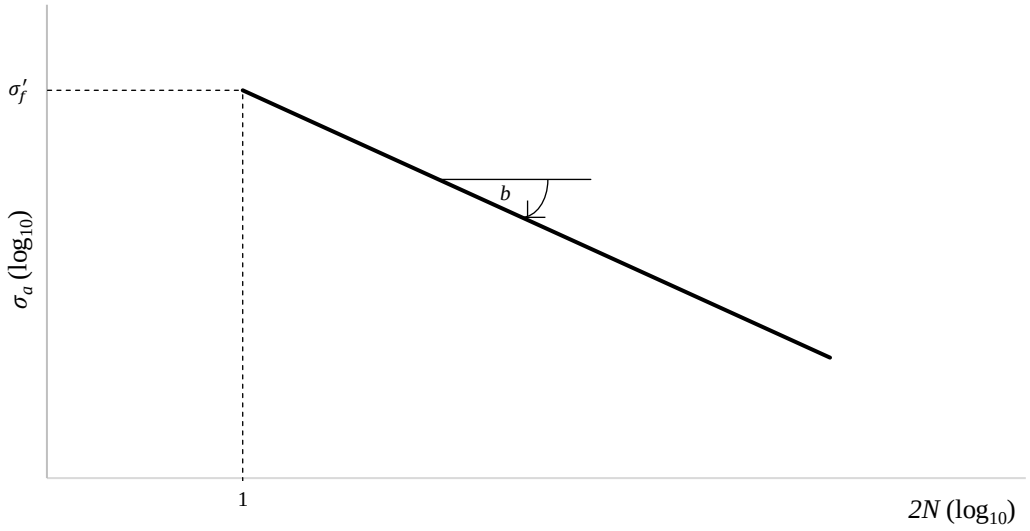

Figure 43 – geometrical interpretation of the Basquin curve constants

As the power law and Basquin curve models are equivalent, the two constants in the models can be calculated from one another via (62).

$$C = \frac{1}{2}\left(\sigma_f'\right)^{-\frac{1}{b}}$$

$$W = -\frac{1}{b}$$

(62)

Now, consider Table 32. It shows the difference between the mean square errors of fatigue lives (see 1.9). All the values are positive, meaning that the mean square error is always lower in the 3D variant compared to the 1D variant. This makes sense, as the mean square error is directly tied to the objective

function (50) of the optimizations, so the error should never increase when more parameters are optimized.

Looking at the mean value of the improvements, Walker, Bergmann, Haibach and Kwofie (order corresponds to amount of improvement) models tend to stay true to their original results. Note that these have already been highlighted before for providing some of the best results of the optimized equivalent stress amplitude models. The results of the other 4 models (which faired visibly worse in the chapter dedicated to the optimized equivalent stress approach) tend to improve a lot more. Also, calculating the mean improvement of each row, the data sets Fin, FAD4 and FAD3 generate the largest improvement of the fits.

Data information			Improvement in mean square error							
Set	Points	Load	Walk.	Kwof.	Berg.	Lin.	Diett.	Gerb.	Klubb.	Haib.
AIS	22	T	0.03	0.04	0.01	0.03	0.02	0.00	0.00	0.05
BEL	35	T	0.00	0.00	0.00	0.00	0.01	0.05	0.05	0.00
BaB	22	T	0.01	0.01	0.01	0.00	0.00	0.09	0.02	0.01
Bai	25	T	0.02	0.01	0.02	0.01	0.01	0.01	0.01	0.02
FAD3	27	T	0.00	0.02	0.00	0.06	0.15	0.28	0.32	0.02
FAD4	30	T	0.02	0.18	0.02	0.26	0.47	0.80	0.35	0.04
Fin	25	B	0.05	0.15	0.05	0.17	0.20	0.40	1.76	0.07
GBA	68	T	0.01	0.03	0.01	0.03	0.06	0.14	0.04	0.01
GBB	58	T	0.01	0.05	0.01	0.08	0.15	0.30	0.14	0.01
GrN	26	T	0.02	0.08	0.02	0.10	0.14	0.25	0.11	0.02
Han	47	B	0.01	0.02	0.01	0.02	0.02	0.02	N/A	0.01
KLN	49	B	0.00	0.01	0.00	0.01	0.01	0.04	0.01	0.00
LaB01	17	T	0.01	0.06	0.01	0.05	0.08	0.19	0.06	0.02
LaB02	17	T	0.00	0.00	0.00	0.00	0.00	0.00	0.00	0.00
LaB03	20	T	0.00	0.03	0.00	0.04	0.05	0.09	0.04	0.00
No40	12	T	0.00	0.00	0.00	0.00	0.00	0.00	0.00	0.00
PRb	27	B	0.00	0.01	0.00	0.01	0.02	0.05	0.02	0.00
Ra1	44	T	0.01	0.01	0.01	0.03	0.10	0.24	0.02	0.00
SCa	69	T	0.00	0.01	0.00	0.01	0.01	0.03	0.01	0.00
SaL	19	B	0.00	0.01	0.00	0.01	0.00	0.03	0.27	0.01
Tra30	8	T	0.00	0.00	0.00	0.00	0.00	0.00	0.00	0.00
Mean			0.01	0.03	0.01	0.04	0.07	0.14	0.16	0.01
Max			0.05	0.18	0.05	0.26	0.47	0.80	1.76	0.07
Min			0.00	0.00	0.00	0.00	0.00	0.00	0.00	0.00
Standard deviation			0.01	0.05	0.01	0.06	0.11	0.19	0.39	0.02

Table 32 – improvements in the mean square errors of individual data sets between the 3D and 1D equivalent stress approaches

Now, for the sake of clarity, let us focus directly on the models which have been found to provide some of the better results of the models explored in this thesis. Consider Table 33, where the standard deviations of Δ_{FL} are presented. Note that the relationship between the mean square error and standard deviation of Δ_{FL} is not linear, and in some rare cases (the numbers highlighted in bold in the 'Difference' columns of the table) the standard deviation has actually increased in the 3D variant, albeit, very slightly (the largest difference in these cases was $5 \cdot 10^{-4}$). The improvements are overall quite negligible, with the most notable ones present in the case of the Kwofie model.

Data information			3D – stand. dev. of Δ_{FL}				1D – stand. dev. of Δ_{FL}				Difference			
Set	Points	Load	Walk.	Kwof.	Berg.	Haib.	Walk.	Kwof.	Berg.	Haib.	Walk.	Kwof.	Berg.	Haib.
AIS	22	T	0.06	0.06	0.06	0.07	0.07	0.07	0.06	0.08	0.00	0.01	0.00	0.01
BEL	35	T	0.03	0.03	0.03	0.03	0.03	0.03	0.03	0.03	0.00	0.00	0.00	0.00
BaB	22	T	0.04	0.04	0.04	0.07	0.05	0.04	0.05	0.07	0.00	0.00	0.01	**0.00**
Bai	25	T	0.08	0.06	0.08	0.09	0.09	0.07	0.09	0.09	0.01	0.01	0.01	0.01
FAD3	27	T	0.02	0.02	0.02	0.03	0.02	0.03	0.02	0.04	0.00	0.01	0.00	0.01
FAD4	30	T	0.03	0.03	0.03	0.03	0.04	0.09	0.04	0.05	0.01	0.05	0.01	0.02
Fin	25	B	0.03	0.04	0.03	0.03	0.06	0.09	0.06	0.07	0.03	0.06	0.03	0.03
GBA	68	T	0.04	0.04	0.04	0.04	0.04	0.05	0.04	0.05	0.00	0.01	0.00	0.01
GBB	58	T	0.04	0.04	0.04	0.04	0.04	0.06	0.04	0.05	0.00	0.02	0.00	0.01
GrN	26	T	0.04	0.05	0.04	0.04	0.05	0.08	0.05	0.05	0.01	0.03	0.01	0.01
Han	47	B	0.03	0.03	0.03	0.03	0.04	0.04	0.04	0.04	0.01	0.01	0.01	0.01
KLN	49	B	0.04	0.04	0.04	0.04	0.04	0.04	0.04	0.04	0.00	0.00	0.00	0.00
LaB01	17	T	0.02	0.02	0.02	0.02	0.03	0.06	0.03	0.04	0.01	0.03	0.01	0.01
LaB02	17	T	0.04	0.03	0.04	0.04	0.04	0.03	0.04	0.04	0.00	**0.00**	0.00	0.00
LaB03	20	T	0.02	0.03	0.02	0.02	0.02	0.04	0.02	0.02	0.00	0.02	0.00	0.00
No40	12	T	0.03	0.02	0.03	0.03	0.03	0.02	0.03	0.03	0.00	0.00	0.00	0.00
PRb	27	B	0.04	0.04	0.04	0.04	0.04	0.04	0.04	0.04	0.00	0.00	0.00	0.00
Ra1	44	T	0.06	0.05	0.06	0.06	0.06	0.06	0.06	0.06	0.00	0.00	0.00	0.00
SCa	69	T	0.04	0.04	0.04	0.04	0.04	0.04	0.04	0.04	**0.00**	0.00	**0.00**	**0.00**
SaL	19	B	0.03	0.03	0.03	0.03	0.03	0.03	0.03	0.03	0.00	0.00	0.00	0.00
Tra30	8	T	0.02	0.02	0.02	0.02	0.02	0.02	0.02	0.02	0.00	0.00	0.00	0.00
Mean			0.04	0.04	0.04	0.04	0.04	0.05	0.04	0.05	0.00	0.01	0.00	0.01
Max			0.08	0.06	0.08	0.09	0.09	0.09	0.09	0.09	0.03	0.06	0.03	0.03
Min			0.02	0.02	0.02	0.02	0.02	0.02	0.02	0.02	0.00	0.00	0.00	0.00
Standard deviation			0.01	0.01	0.01	0.02	0.02	0.02	0.02	0.02	0.01	0.02	0.01	0.01

Table 33 – standard deviation of Δ_{FL} of individual data sets for the 3D and 1D equivalent stress approaches

It is also worth looking at how the individual coefficients change between the 1D and 3D approaches. This is quantified via (63), where the index *original* refers to the parameters of the original, existing (R = -1) curve, *1D* to the coefficient obtained via the equivalent stress amplitude – 1(2) degrees of freedom approach, and *3D* to the equivalent stress amplitude – 3 degrees of freedom approach.

Understand the MSE (mean stress effect) coefficient as the coefficient appearing directly in the equivalent stress amplitude models, for example, the γ coefficient of the Walker model.

$$Change\ in\ \sigma_f' = \frac{\sigma_{f\ original}' - \sigma_{f\ 3D}'}{\sigma_{f\ original}'}$$

$$Change\ in\ b = \frac{b_{original} - b_{3D}}{b_{original}}$$

$$Change\ in\ MSE\ coefficient = \frac{MSE\ coefficient_{1D} - MSE\ coefficient_{3D}}{MSE\ coefficient_{1D}}$$

(63)

Now, consider Table 34. For the S-N curve parameters σ_f' and b, there seems to be a general trend, in that they both decrease (move in the direction of -∞). This results in the S-N curve moving vertically lower, while increasing the slope, in other words, increasing the sensitivity of the fatigue life N to an increase of the stress amplitude σ_a. In fact, these two coefficients tend to move in the same direction, in other words, they either both decrease (most common) or both increase. There is a single case that breaks this rule, with the Bergmann model and the SaL set, however, the change in parameters is quite small in this case. Out of the 21 data sets, in 15 cases, the direction of change of the two parameters is common for all 4 models in the table.

This could imply that the models could benefit from relating the equivalent stress amplitude to a different curve than (R = -1). This would, however, require a reformulation of the underlying expressions for the equivalent stress amplitude $\sigma_{a,eq}$, since, for example, the $\sigma_{a,eq}$ values of the (R = -1) curve would, in the current form, be equal to the experimental stress amplitudes σ_a, and obtaining fatigue life predictions from a different curve than the (R = -1) curve via such stress amplitudes does not make sense.

An attempt was made to relate common direction of change of the σ_f' and b coefficients to the experimental coefficients of the (R = -1) and (R = 0) curves. However, this was unsuccessful, as out of the 19 data sets that contain the actual experimental (R = 0) curve or at least its approximation available, only in 3 cases (FAD4, GBB, LaB01), the direction of change of the σ_f' and b coefficient was identical.

Data information			Change in σ_f' [%]				Change in b [%]				Change in the MSE coefficient [%]			
Set	Points	Load	Walk.	Kwof.	Berg.	Haib.	Walk.	Kwof.	Berg.	Haib.	Walk.	Kwof.	Berg.	Haib.
AIS	22	T	-27.3	-56.4	-20.7	-69.1	-14.3	-29.1	-11.4	-35.4	10.6	-17.7	-15.7	-19.0
BEL	35	T	18.4	-26.3	19.6	16.7	10.9	-11.5	11.4	10.4	3.2	0.6	-6.0	-8.9
BaB	22	T	5.3	-6.2	7.1	-8.5	9.8	-6.1	11.5	-8.8	3.8	-4.0	-5.3	-5.2
Bai	25	T	13.7	10.5	14.0	11.8	19.8	15.4	20.1	17.0	1.4	-2.2	-2.2	-2.4
FAD3	27	T	4.1	-117.4	6.9	-167.3	0.9	-34.1	2.3	-40.3	-2.4	9.8	3.9	3.2
FAD4	30	T	-56.4	-334.3	-61.7	-106.5	-28.7	-95.6	-30.3	-44.6	-3.1	7.7	1.5	-2.0
Fin	25	B	-115.2	-267.7	-112.8	-138.3	-60.3	-104.5	-59.8	-67.5	4.2	-5.7	-6.3	-11.3
GBA	68	T	-53.0	-149.9	-56.9	-80.5	-21.1	-47.2	-22.2	-29.3	7.2	-7.5	-12.2	-11.0
GBB	58	T	-60.9	-408.0	-61.9	-94.8	-20.7	-75.0	-20.3	-27.9	7.8	-7.1	-16.0	-16.2
GrN	26	T	-41.8	-105.5	-41.8	-41.8	-32.6	-67.4	-32.6	-32.6	-14.5	19.6	13.9	11.8
Han	47	B	-123.5	-159.8	-115.4	-127.9	-43.9	-52.3	-42.0	-44.9	2.2	-23.2	-14.3	-20.1
KLN	49	B	-9.7	-32.6	-8.9	-11.8	-6.2	-16.8	-5.7	-7.4	-12.9	10.5	10.4	11.1
LaB01	17	T	-30.1	-80.6	-30.2	-40.1	-18.0	-39.0	-17.7	-21.6	-4.0	2.2	3.9	-0.2
LaB02	17	T	9.0	2.6	9.0	9.0	6.1	1.8	6.1	6.1	-1.6	0.4	1.7	1.5
LaB03	20	T	-18.1	-169.0	-19.0	-26.7	-6.5	-34.9	-6.5	-8.3	-6.0	3.3	5.3	2.2
No40	12	T	3.0	1.9	11.8	-36.7	1.7	1.3	4.7	-10.1	2.7	-5.5	-5.8	-4.6
PRb	27	B	4.0	-6.3	1.4	-1.9	0.8	-4.7	-0.3	-2.4	-10.6	8.8	9.3	10.3
Ra1	44	T	8.4	-26.0	7.2	-13.6	2.9	-16.7	2.5	-9.5	-8.9	6.3	9.3	5.5
SCa	69	T	-10.1	-40.8	-10.5	-8.5	-5.3	-18.9	-5.5	-4.7	-0.1	-1.8	0.0	1.2
SaL	19	B	-17.2	-30.2	-9.9	-28.5	-10.4	-18.3	-6.4	-16.9	1.1	-0.2	-1.0	-2.9
Tra30	8	T	1.9	0.9	1.9	1.9	1.6	0.8	1.6	1.6	0.0	-0.1	-0.1	-0.1
Mean			-23.6	-95.3	-22.4	-45.9	-10.2	-31.1	-9.5	-18.0	-0.9	-0.3	-1.2	-2.7
Max			18.4	10.5	19.6	16.7	19.8	15.4	20.1	17.0	10.6	19.6	13.9	11.8
Min			-123.5	-408.0	-115.4	-167.3	-60.3	-104.5	-59.8	-67.5	-14.5	-23.2	-16.0	-20.1
Standard deviation			39.7	117.4	39.4	53.9	19.4	32.7	19.6	21.2	6.7	9.6	8.7	9.2

Table 34 - change of values of optimized parameters of individual data sets for the 3D and 1D equivalent stress approaches

As for the changes of the values of the MSE coefficients, they are quite insignificant compared to the changes of the S-N curve coefficients σ_f' and b. Note that it does not matter whether we use the coefficient from (29) or (30) for quantifying the change of the MSE coefficients of Kwofie's model, as $\tilde{\alpha} = \alpha / R_m$, and the outcome of (63) does not change between these two formulations.

The best-fit $\tilde{\alpha}$ coefficient obtained via the 3D equivalent stress amplitude approach can be fit on to the ultimate tensile strength R_m in a similarly accurate way to what has been shown in Figure 40. The coefficient of determination R^2 is now 0.87 (0.03 higher than in the 1D variant). This new fit is represented by the black dotted line in Figure 44, the nearly identical green dotted line is the original fit of the coefficients obtained via the 1D approach. The equation of the new fit is given by (64).

$$\tilde{\alpha}_{3D}(R_m) = 5.83 \cdot 10^{-9} \cdot {R_m}^2 - 1.22 \cdot 10^{-5} \cdot R_m + 6.94 \cdot 10^{-3} \quad \textbf{(64)}$$

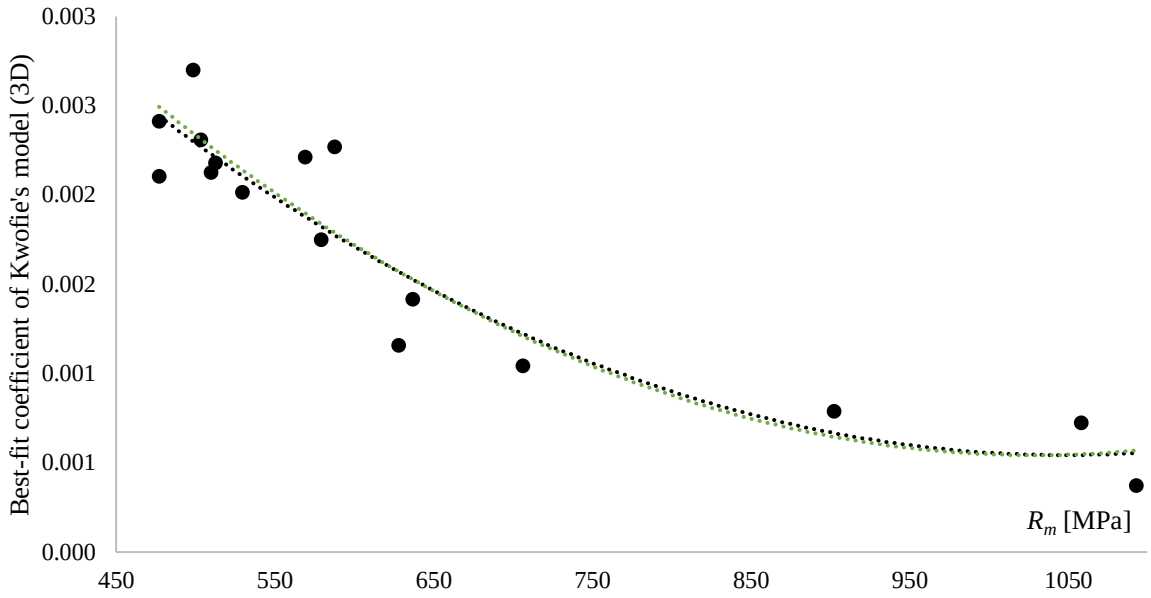

Figure 44 – best fit values of the $\tilde{\alpha}$ coefficient of Kwofie's model obtained via equivalent stress amplitude – 3 degrees of freedom approach, green dotted line shows fit of the original 1 degree of freedom equivalent stress amplitude model

Since the idea that using an S-N curve different from (R = -1) as the core of the equivalent stress approach has been touched on, it seems unfair to not look at the results of the 4 models that have been mostly left out in this chapter. The results of these models could theoretically benefit the most from this (as has been confirmed in Table 32).

Data information			3D – stand. dev. of Δ_{FL}				1D – stand. dev. of Δ_{FL}				Difference			
Set	Points	Load	Lin.	Diett.	Gerb.	Klubb.	Lin.	Diett.	Gerb.	Klubb.	Lin.	Diett.	Gerb.	Klubb.
AIS	22	T	0.05	0.03	0.02	0.04	0.06	0.04	0.02	0.04	0.01	0.00	0.00	0.00
BEL	35	T	0.04	0.04	0.04	0.05	0.04	0.04	0.06	0.06	0.00	0.00	0.01	0.01
BaB	22	T	0.03	0.04	0.08	0.09	0.03	0.04	0.10	0.10	0.00	0.00	0.02	0.00
Bai	25	T	0.06	0.05	0.07	0.06	0.06	0.06	0.08	0.06	0.01	0.01	0.00	0.00
FAD3	27	T	0.03	0.04	0.04	0.06	0.05	0.07	0.09	0.12	0.02	0.03	0.05	0.06
FAD4	30	T	0.04	0.04	0.05	0.05	0.10	0.12	0.15	0.12	0.06	0.08	0.10	0.08
Fin	25	B	0.04	0.04	0.05	0.08	0.10	0.10	0.12	0.29	0.06	0.06	0.07	0.21
GBA	68	T	0.04	0.04	0.05	0.04	0.05	0.06	0.08	0.06	0.01	0.02	0.04	0.02
GBB	58	T	0.04	0.05	0.05	0.05	0.07	0.08	0.10	0.09	0.03	0.04	0.05	0.04
GrN	26	T	0.05	0.05	0.06	0.05	0.08	0.09	0.11	0.09	0.03	0.04	0.06	0.03
Han	47	B	0.03	0.03	0.03	N/A	0.04	0.04	0.04	N/A	0.01	0.01	0.01	N/A
KLN	49	B	0.04	0.04	0.04	0.04	0.04	0.04	0.05	0.04	0.00	0.00	0.01	0.00
LaB01	17	T	0.03	0.03	0.05	0.04	0.05	0.06	0.08	0.06	0.03	0.03	0.03	0.02
LaB02	17	T	0.03	0.03	0.04	0.03	0.03	0.03	0.04	0.03	0.00	0.00	0.00	0.00
LaB03	20	T	0.03	0.03	0.04	0.03	0.05	0.05	0.06	0.05	0.02	0.02	0.02	0.02
No40	12	T	0.02	0.02	0.02	0.02	0.02	0.02	0.02	0.03	0.00	0.00	0.00	0.00
PRb	27	B	0.04	0.04	0.05	0.05	0.04	0.05	0.06	0.05	0.00	0.00	0.01	0.01
Ra1	44	T	0.06	0.07	0.08	0.06	0.07	0.09	0.12	0.07	0.01	0.02	0.03	0.01
SCa	69	T	0.04	0.04	0.05	0.04	0.04	0.05	0.06	0.05	0.00	0.00	0.01	0.00
SaL	19	B	0.03	0.03	0.03	0.07	0.03	0.03	0.04	0.11	0.00	0.00	0.01	0.04
Tra30	8	T	0.02	0.02	0.02	0.02	0.02	0.02	0.02	0.02	0.00	0.00	0.00	0.00
Mean			0.04	0.04	0.05	0.05	0.05	0.06	0.07	0.08	0.01	0.02	0.02	0.03
Max			0.06	0.07	0.08	0.09	0.10	0.12	0.15	0.29	0.06	0.08	0.10	0.21
Min			0.02	0.02	0.02	0.02	0.02	0.02	0.02	0.02	0.00	0.00	0.00	0.00
Standard deviation			0.01	0.01	0.02	0.02	0.02	0.03	0.04	0.06	0.02	0.02	0.03	0.05

Table 35 - standard deviation of Δ_{FL} of individual data sets for the 3D and 1D equivalent stress approaches

Indeed, in the 3D section of Table 35 , the summarizing values in the bottom are on par with the corresponding values in Table 33. This implies that the potential of tweaking, say, the Linear or Dietmann model in order to achieve more accurate fatigue life prediction results is quite high. This is, however, contrary to the information extractable from Table 36.

The change in the S-N curve constants σ_f' and b are generally a lot more drastic compared to what has been previously shown in Table 34. The scatter of these changes, quantified by the standard deviation in the bottom of Table 36, is also quite high. This lowers the potential that these models would provide better results than the ones highlighted previously if a tweaked version of the equivalent stress approach utilizing a different core S-N would be used.

It is worth noting that the trend of the common direction of change of the two S-N curve parameters is confirmed for these four models as well, with a shift towards lower values being again dominant, and with no case where the shift happened in opposite directions being present.

Data information			Change in σ_f' [%]				Change in b [%]				Change in coefficient [%]			
Set	Points	Load	Lin.	Diett.	Gerb.	Klubb.	Lin.	Diett.	Gerb.	Klubb.	Lin.	Diett.	Gerb.	Klubb.
AIS	22	T	-29	-10	3	-8	-15	-4	1	-4	10	5	-1	-14
BEL	35	T	-48	-101	-501	-2199	-20	-37	-95	-162	-5	-9	-17	799
BaB	22	T	-1	2	-2	-7	-1	1	-13	-15	2	-1	-8	161
Bai	25	T	11	11	5	7	15	15	3	9	1	0	-3	5
FAD3	27	T	-238	-484	-1349	-63341	-55	-80	-120	-275	-15	-12	-17	922
FAD4	30	T	-407	-545	-880	-696	-109	-128	-159	-139	-11	-9	-11	44
Fin	25	B	-272	-282	-391	-568406	-108	-112	-137	-695	-1	-5	-9	52
GBA	68	T	-163	-225	-417	-215	-52	-65	-94	-62	1	-2	-5	1
GBB	58	T	-572	-859	-2005	-1832	-92	-112	-152	-141	-2	-4	-5	8
GrN	26	T	-122	-141	-225	-136	-75	-83	-111	-80	-21	-18	-15	32
Han	47	B	-159	-159	-156	N/A	-52	-52	-52	N/A	17	16	2	N/A
KLN	49	B	-38	-43	-89	-35	-19	-21	-38	-18	-11	-11	-11	11
LaB01	17	T	-71	-71	-87	-71	-38	-40	-50	-38	-7	-8	-11	21
LaB02	17	T	2	1	-5	2	1	1	-4	1	0	0	0	0
LaB03	20	T	-171	-181	-232	-182	-36	-39	-46	-37	-7	-6	-8	9
No40	12	T	12	16	-1	-10	5	6	-1	-4	4	2	-2	-271
PRb	27	B	-10	-14	-59	-56	-7	-9	-28	-25	-9	-9	-6	13
Ra1	44	T	-37	-88	-293	-41	-24	-46	-95	-25	-8	-7	-11	14
SCa	69	T	-44	-49	-74	-48	-20	-23	-33	-22	0	-1	-2	0
SaL	19	B	-25	-23	-35	-1745	-16	-15	-24	-215	-1	-3	-8	-108
Tra30	8	T	1	1	-1	-1	1	1	-1	-1	0	0	0	0
Mean			-113	-155	-323	-31951	-34	-40	-59	-97	-3	-4	-7	85
Max			12	16	5	7	15	15	3	9	17	16	2	922
Min			-572	-859	-2005	-568406	-109	-128	-159	-695	-21	-18	-17	-271
Standard deviation			152	224	511	127050	37	42	54	162	8	7	6	277

Table 36 - change of values of optimized parameters of individual data sets for the 3D and 1D equivalent stress approaches

3.2 Conclusions

The goal of this thesis was to analyze the fatigue life prediction accuracy of various approaches in regard to the influence of the mean stress effect. The area of concern is restricted to positive values of mean stress σ_m, unnotched specimens, strictly metal materials (aluminum alloys, steels, cast irons), and two types of loading – tensile and bending. These limitations are mostly in place for two reasons.

The first is the size of the pool of available data. This means that for example, due to an insufficient amount of torsion type load data sets, torsion has not been analyzed in this thesis at all.

The second reason is to have as few factors outside the mean stress effect influencing the fatigue life. This, for example, results in only experimental data based on unnotched specimens to be accepted for analysis.

No experimental campaign with the goal to directly support this thesis has been realized. All the used experimental data has been taken from elsewhere. The data acceptance criteria and the individual data sets used have been described. In total, these amounted to 21 data sets, consisting of 667 total used experimental points. Most of these data sets are of the tensile load type.

The approaches incorporating mean stress effect into the fatigue life prediction that have been analyzed in this thesis can be split into two categories, the equivalent stress amplitude (ESA) and the reduced fatigue limit (RFL) approach. These can be further divided, for example, into the unoptimized and optimized category. Optimized approaches are, in this thesis, generally understood as approaches that incorporate a reduced fatigue limit or equivalent stress amplitude model that requires a coefficient that is fit onto experimental data via an optimization algorithm in order to calculate $\sigma_{FL,red}$ or $\sigma_{a,eq}$, respectively.

As has been said, the focus of this thesis was to judge the accuracy of the results achieved via various means. This does not mean that the fatigue life predictions are readily useable in practice. On the contrary, the optimized approaches, which are tuned to have the lowest error in terms of fatigue life often give unconservative results in regard to experimental data. The parameter Δ_{FL} has been used to quantify fatigue life prediction errors. For a group of experimental data points, the main focus was on the mean and standard deviation value of this error. Accuracy in this thesis is viewed as 'better' if both the mean value of Δ_{FL} and its standard deviation are close to zero.

The fatigue data has been categorized according to different filters in order for trends to be observable. This means that not only were the results stemming from individual data sets examined, but also the mixed data from these sets, for example, according the type of the used material or the stress ratio R of the load cycle.

Six different unoptimized models of the equivalent stress amplitude approach were tested. Two of these (the unoptimized Linear and Walker model) are based on previously proposed models but the way they are realized in this category ("unoptimized") is unique to this thesis. Out of the six models, the SWT model proved to have some of the most accurate results. This can be seen as surprising, as the model features no material parameters, and the resulting equivalent stress amplitude $\sigma_{a,eq}$ is only a function of the stress amplitude σ_a and mean stress σ_m of the load cycle. A big advantage of the SWT model is that it was the only one of the unoptimized models to be useable for every single data point used for this thesis. Some other models in this category, for example, the Goodman model, rely on the ultimate tensile strength value R_m. This often caused problems for the bending type load data, as the assumption that an immediate break occurs when R_m is exceeded does not apply to bending.

The results of the unoptimized Walker and Linear equivalent stress amplitude approaches, which are unique to this thesis, produced mixed results. These are based on the properties of the (R = -1) and (R = 0) curves. The generally good results were often degraded by spikes of high standard deviations of Δ_{FL} in certain data sets. A possible link between this value and the ratio of parameters of the (R = -1) and (R = 0) has been proposed.

When analyzing the fatigue life prediction results of the unoptimized reduced fatigue limit approach, it has been found out that bending type loads are generally quite problematic. This has been explained via the fact that not only are many of the individual models based on the ultimate tensile strength R_m, but so is the core principle of the approach itself, without even considering any of the reduced fatigue limit models like that of Goodman or Smith, for example. Overall, the two mentioned models showed the highest fatigue life prediction accuracy out of the six analyzed in this category.

Additional results were obtained from the unoptimized fatigue result based on the 'FEMFAT shift', which in short, further reduces the predicted fatigue lives based on the ratios of the fatigue limit of the (R = -1) curve and the reduced fatigue limit $\sigma_{FL,red}$ of the non-zero mean stress curve. These was shown to not affect the achieved results in a major way.

As the unoptimized equivalent stress amplitude and reduced fatigue limit approaches have similar input-data requirements, the results achieved by them have been compared. Overall, the predicted fatigue life accuracy (based on the criteria described earlier) of the equivalent stress approach models was notably higher.

The optimized, so called 1(2) degree of freedom equivalent stress amplitude is based around models that feature a coefficient(s) that determines the influence of the mean stress on the predicted achieved life and is found through an optimization algorithm. The Exponential model features two such coefficients, the other eight analyzed models, one. Of the 9 different models, five were shown to provide quite similar, and relatively speaking, accurate fatigue life predictions. These are the Walker, Kwofie, Bergmann, Exponential and Haibach models. To further distinguish them, an attempt was made to see if the best-fit coefficients of these models could be predicted based on various static and fatigue material properties and their ratios. The Exponential model was left out of this analysis, as it does contain two parameters rather than one, making them less predictable. The best fit for tensile load type was found for the coefficient of Kwofie's model when the ultimate tensile strength R_m is chosen as the independent variable. Bending type data was examined in a similar way, and some promising fits were found the Walker and Haibach coefficients when the yield strength R_e was used as the independent variable, however, more data sets would be desirable to confirm the quality of these fits.

Results of the tensile load type fatigue predictions using the Kwofie coefficient calculated via the R_m fit were examined. When using Kwofie's model in this way, the input data requirements are the same as for the unoptimized equivalent stress amplitude approach, thus, the results were put in comparison. The results of the now "unoptimized" Kwofie model were shown to be highly comparable with those of the SWT model, which, as has been said, can be considered the highlight of this category.

The optimized reduced fatigue limit drops the dependency on the ultimate tensile strength R_m from most of the individual models, however, R_m is still rooted in the basis of approach. This led to similar problems with bending type loads as with the unoptimized counterpart of this approach. From the 7 models analyzed in this category, the Goodman, Smith and Haibach models stood out in terms of fatigue life prediction accuracy. The FEMFAT shift was, again, shown to have little influence on the overall results in this category.

A modified version of the optimized reduced fatigue limit approach was devised. This approach completely removes any dependency on the ultimate tensile strength value R_m, with the main motivation for this being the inaccurate, or in some cases unobtainable fatigue life predictions for bending type loads. This led to all data being useable in this category, unlike in the previously described reduced fatigue limit procedures. The results of this approach show a rare occurrence in this thesis – the fatigue life predictions are of higher accuracy for bending than for tensile type loads. In this category, four different reduced fatigue limit models were tested, with the Goodman and Smith model being highlighted as those of higher potential in terms of fatigue life prediction accuracy. Again, the FEMFAT shift has not affected the results in a major way.

The promising models of the three optimized approach categories (optimized equivalent stress amplitude, optimized reduced fatigue limit and its modified version) have been compared. Like when this was done for the unoptimized approaches, the equivalent stress approach results were shown to be superior. The modified version of the optimized reduced fatigue limit approach shows some promise for bending type loads (albeit with only little improvement over equivalent stress amplitude, where improvement was present), though, more such data sets would be desirable in order to make any conclusive judgements on this.

Finally, the results of the so-called equivalent stress amplitude – 3 degrees of freedom (3D) category were analyzed. These results do not hold as much potential practical usability as, say, the 1(2) degree of freedom equivalent stress (1D) approach, however, they hold other qualities. This approach is derived from the 1D variant. Instead of only finding the best fit coefficients of the mean stress effect quantifying model, the coefficients of the (R = -1) curve, which serve as a basis for all approaches explored in this thesis are fine-tuned in order to minimize the sum of squares of fatigue life errors as well. This makes this approach inconsistent with some of the basic principles of the general mean stress effect theory. However, it can reveal potential improvements of the 1D approach. Eight models (same as the ones that appeared in the 1D approach) were tested this way. From the results, a conclusion was made, that the Walker, Kwofie, Bergmann and Linear models (all of which were previously shown to produce relatively accurate results) could potentially benefit by being tweaked in order to be able to use a different curve than the (R = -1) curve as a basis for fatigue life predictions.

Potential topics for future research based on the conclusions made in this thesis will now be proposed:

- The relation of the equivalent stress amplitude to a curve different curve than (R = -1) could potentially improve the fatigue life predictions, especially for higher values of mean stress.

- Different formulation of the basic S-N curve for use with the equivalent stress amplitude could hold new qualities compared to the linear Basquin/power law model. Experiments with such approach (using the Kohout-Věchet formulation for example) were started during preparation of the MATLAB scripts needed for obtaining the various results, however, this ultimately showed to be out of scope of this work.

- The Walker and Linear models of the unoptimized equivalent stress amplitude approach showed some promising results. Further exploration of these models, and perhaps new models altered in a similar fashion, could potentially provide interesting results. Also, basing these models on different curves than (R = -1) and (R = 0) is possible, and further generalization of these models could extend their area of usability.

- It is desirable for more equivalent stress amplitude approach models to be tested.

- From a practical standpoint, it is important to explore ways to incorporate a safety factor that would strike balance between reliability and over dimensioning when considering the mean stress effect while making fatigue life predictions.

REFERENCES

[1] Sochava, A. I.: Approximating the diagram of limiting amplitudes taking into consideration the area of medium compressive stresses. Strength of Materials Vol. 9, No. 10; ISBN/ISSN:1573-9325, 1977, pp. 1169-1173. DOI: 10.1007/BF01528902. (link: https://doi.org/10.1007/BF01528902)

[2] Bell, W. J.: The effect of stress-concentrations and local plastic deformation on the fatigue properties of stainless steel sheet. [PhD thesis]. London, Imperial College London 1961. (link: https://spiral.imperial.ac.uk/handle/10044/1/13480)

[3] Baier, F.: Zeit- und Dauerfestigkeit bei überlagerter statischer und schwingender Zug-Druck- und Torsionbeanspruchung. [PhD thesis]. Stuttgart, Universität Stuttgart 1970.

[4] Papuga, J.; Fojtík, F.; Vargas, M.; Hodr, A.; Karolczuk, A.; Fusek, M.; Halama, R.: Summary of experiments on 2124-T851 realized within FADOFF project. [Technical report FAD/14/001]. Prague, CTU in Prague 2014.

[5] Findley, W. N.: Combined-stress fatigue strength of 76S-T61 aluminum alloy with superimposed mean stresses and corrections for yielding. [Technical report NACA TN-2924]. Washington, NACA 1953. (link: http://ntrs.nasa.gov/archive/nasa/casi.ntrs.nasa.gov/19930083649_1993083649.pdf)

[6] Grover, H. J.; Bishop, S. M.; Jackson, L. R.: Fatigue strengths of aircraft materials: Axial-load fatigue tests on unnotched sheet specimens of 24S-T3 and 75S-T6 aluminum alloys and of SAE 4130 steel. [Technical report NACA TN 2324]. Washington, NACA 1951. (link: http://ntrs.nasa.gov/archive/nasa/casi.ntrs.nasa.gov/19930083007_1993083007.pdf)

[7] Grubisic, V.; Neugebauer, J.: Festigkeitsverhalten von Guseisen mit Kugelgraphit unter mehrachsiger Schwingbeanspruchung. Giessereiforschung Vol. 31, No. 4, 1979, pp. 123-128.

[8] Hanley, B. C.: The effect of range of stress and state of stress on the fatigue strength of SAE 4340 steel. [Technical report]. Urbana, Illinois, Dept. of Theoretical and Applied Mechanics, University of Illinois 1951.

[9] Niesłony, A.; Łagoda, T.; Walat, K.; Kurek, M.: Multiaxial fatigue behaviour of AA6068 and AA2017A aluminium alloys under in-phase bending with torsion loading condition. Materialwissenschaft und Werkstofftechnik Vol. 45, No. 10; ISBN/ISSN:1521-4052, 2014, pp. 947-952. (link: http://dx.doi.org/10.1002/mawe.201400214)

[10] Blatherwick, A. A.; Lazan, B. J.: Fatigue properties of aluminium alloys at various diret stress ratios, Part I - Rolled Alloys. [Technical report WADC Technical Report 52-307, Part I]. Ohio, Wright Air Development Center, Air Research and Development Command, US Air Force 1952. (link: http://contrails.iit.edu/files/original/WADCTR52-307part01.pdf)

[11] Data sheets on fatigue properties for butt welded joints of SPV50 steel plate for pressure vessels, Effect of stress ratio. [Technical report NRIM Fatigue Data Sheet No. 40]. Tokyo, Japan, National Research Institute for Metals 1984.

[12] Rausch, T.: Zum Schwingfestigkeitsverhalten von Gusseisenwerkstoffen unter einachsiger und mehrachsiger Beanspruchung am Beispiel von EN-GJV-450. [PhD thesis]. Aachen, Shaker Verlag 2011.

[13] Smith, C. R.: S-N characteristics of notched specimens Final report. [Technical report NASA-CR-54503]. United States, NATIONAL AERONAUTICS AND SPACE ADMINISTRATION 1966. (link: https://ntrs.nasa.gov/search.jsp?R=19660019791)

[14] Sauer, J. A.; Lemmon, D. C.: Effect of Steady Stress on Fatigue Behavior of Aluminum. Transactions of the American Society for Metals Vol. 42, 1950, pp. 559-576.

[15] Trapp, W. J.: Elevated Temperature Fatigue Properties of SAE 4340 Steel. [Technical report WADC Technical Report 52-325, Part I]. Ohio, Wright Air Development Center, Air Research and Development Command, US Air Force 1952. (link: www.dtic.mil/get-tr-doc/pdf?AD=AD0008716)

[16] Pawliczek, R.; Rozumek, Dariusz: The Effect of Mean Load for S355J0 Steel with Increased Strength. Metals 10(2), 209, 2020, pp. -. (link: https://www.mdpi.com/2075-4701/10/2/209?type=check_update&version=1)

[17] Pook, L. P. Metal fatigue : what it is, why it matters. Dordrecht London: Springer, 2007. Print.

[18] Růžička, M., Hanke, M., & Rost, M. (1993). Dynamická pevnost a životnost. Praha, Czech republic: Čes. vys. učení techn.

[19] Multiphysics Cyclopedia. (2016, March 15). Retrieved July 12, 2020, from https://www.comsol.com/multiphysics/material-fatigue

[20] Papuga, J. & Vízková, Ivona & Lutovinov, Maxim & Nesládek, Martin. (2018). Mean stress effect in stress-life fatigue prediction re-evaluated. MATEC Web of Conferences. 165. 10018. 10.1051/matecconf/201816510018.

[21] FEMFAT 4.7 BASIC Theorie manual. (n.d.). MAGNA POWERTRAIN.

[22] N. Dowling, C. Calhoun, A. Arcari, Fat & Fract of Engng Maters & Structs. 32, 163-179 (2009)

[23] S. Kwofie, Int Jnl of Fatigue. 23, 829-836 (2001)

[24] Pallarés-Santasmartas, L.; Albizuri, J.; Avilés, A.; Avilés, R. Mean Stress Effect on the Axial Fatigue Strength of DIN 34CrNiMo6 Quenched and Tempered Steel. Metals 2018, 8, 213.

[25] Nihei, M., Heuler, P., Boller, C., & Seeger, T. (1986). Evaluation of mean stress effect on fatigue life by use of damage parameters. International Journal of Fatigue, 8(3), 119-126. doi:10.1016/0142-1123(86)90002-2

[26] VÍZKOVÁ, Ivona. Vliv středního napětí na dynamickou pevnost a životnost. Praha, 2017. Bakalářská práce. České vysoké učení technické v Praze, Fakulta strojní, Ústav mechaniky, biomechaniky a mechatroniky. Vedoucí práce Ing. Jan Papuga, Ph.D

[27] Klubberg, F., Broeckmann, C., & Beiss, P. (2012). Festigkeitskennwerte und mehrachsige Schwingfestigkeit von lamellarem Gusseisen. Materials Testing, 54(9), 569-577. doi:10.3139/120.110367

[28] Haibach, E. (2006). Betriebsfestigkeit: Verhahren und Daten zur Bauteilberechnung. Berlin, Germany: Springer.

[29] Smith, J. O. (1942). The effect of range of stress on the fatigue strength of metals. University of Illinois. Engineering Experiment Station., 39(26), university of illinois bulletin.

[30] Pomp, A.; Hempel, M.: Über das Verhalten von Gusseisen und Temperguss unter wechselnder Beanspruchung. Mitteilungen aus dem Kaiser-Wilhelm-Institut für Eisenforschung zu Düsseldorf, Verl. Stahleisen Band XXII, Lieferung 11, Abhandlung 402, 1940, pp. 169-181.

[31] Kohout, J., & Věchet, S. (2001). A new function for fatigue curves characterization and its multiple merits. International Journal of Fatigue, 23(2), 175-183. doi:10.1016/s0142-1123(00)00082-7

[32] Rohatgi, A. (n.d.). WebPlotDigitizer. Retrieved August 05, 2020, from https://apps.automeris.io/wpd/